Title	Spatial and Temporal Equalization Methods for High-Speed Wireless Communications
Author(s)	Hayashi, Kazunori
Citation	大阪大学, 2002, 博士論文
Version Type	VoR
URL	https://hdl.handle.net/11094/2071
rights	
Note	

Spatial and Temporal Equalization Methods for High-Speed Wireless Communications Systems

KAZUNORI HAYASHI

OSAKA UNIVERSITY

Department of Electronic, Information Systems
and Energy Engineering
Graduate School of Engineering

January 2002

Preface

This dissertation treats spatial and temporal equalization methods for high-speed wireless communications systems, which are based on the research carried out by the author during Ph. D. course at the Department of Electronic, Information Systems and Energy Engineering, Graduate School of Engineering, Osaka University. The dissertation is organized as follows:

Chapter 1 is a general introduction, where the background and purpose of the study are presented from the viewpoints of demand for wireless communications systems and of progress of digital signal processing devices.

Chapter 2 presents fundamentals of array signal processing in wireless communications systems. Implementation of a temporal filter requires processing of signals collected over temporal aperture. Similarly, implementing a spatial filter requires signals collected over a spatial antenna. In this sense, an adaptive antenna array has a capability of spatial filtering, which is essential for realization of spatial and temporal equalization. Herein, three basic and important applications of antenna array are introduced; beamforming, direction of arrival (DoA) estimation, and pilot-free channel identification. The matters presented in this chapter will be the groundwork for the systems in subsequent chapters.

Chapter 3 deals with spatial equalization methods, in other words, beamforming methods. Taking into account the extension to spatial and temporal equalization, we propose a spatial equalization method based on estimated channel responses, which gives us some degrees of freedom in beamforming. As for the channel estimation, two different approaches are given for the spatial equalization; a pilot-assisted approach and a pilot-free identification approach. As a pilot-assisted approach, we utilize suppressed spread spectrum (SS) pilot signal, which is coherently added to data signal, and whose power is suppressed enough before the addition. With the SS pilot signal, the receiver can handle only the pilot channel, independent of the data channel, and this separation in the array signal processing makes it independent of employed modulation scheme. In addition, the SS technique makes it possible to work in low carrier to noise power ratio (CNR) environments. On the other hand, as a pilot-free identification approach, we employ a second-order statistics-based pilot-free channel identification method and discuss applicability of the pilot-free channel identification to practical wireless communications systems.

Chapter 4 proposes a spatial and temporal equalization method with reduced number of weights, utilizing a cascade configuration of an adaptive antenna array and a decision feedback equalizer (DFE). Taking advantage of different features of the adaptive antenna array and the DFE, the equalization functionality should be split into spatial processing and temporal processing, such that 'incoming signals with larger time delays (beyond the filter length of the DFE) are cancelled at the adaptive antenna array.' This makes it possible to reduce the num-

ber of weights in the DFE. The weights of both the adaptive antenna array and the DFE are separately calculated using estimated channel impulse response at each sensor. We show the performance of the proposed system in multipath fading channels observed in indoor wireless environments, and discuss the attainable bit error rate (BER), antenna patterns, and computational complexity in comparison with those of other equalization methods, such as spatial equalization and temporal equalization.

Chapter 5 proposes a spatial and temporal equalization method, which is versatile for various kinds of DoA patterns. So far, among conventional spatial and temporal equalization methods, only an adaptive tapped-delay-line (TDL) array has such a robustness. However, it requires huge number of weights, and hence, extremely high computational complexity. In order to reduce the complexity, the proposed equalizer utilizes the same configuration as in chapter 4. Though the cascade configuration has a problem that the cost function in the minimum mean-squared-error (MMSE) based algorithm sometimes have two local minima, the proposed equalizer can avoid the problem by introducing beamforming criterion selectability. The proposed equalizer selects a path or paths to capture with the adaptive antenna array depending on estimated channel conditions, therefore, it can achieve good performance even in the channel models where DoAs of incoming waves are randomly determined. The BER performance of the proposed equalizer is investigated in various kinds of channel models, which are based on measurement reports, in comparison with the performance of the adaptive TDL arrays. Furthermore, we discuss the operability of the selection algorithm from the viewpoint of antenna beam patterns, and evaluate the computational complexity in terms of the number of multiplications in the weights calculation algorithm.

Chapter 6 summarizes all the results.

All the results described in the thesis were or will be published in IEICE Transactions on Communication, IEEE Transactions on Vehicular Technology, Proceedings of the First International Symposium on Wireless Personal Multimedia Communications, Proceedings of the 10th International Symposium on Personal, Indoor and Mobile Radio Communications, Proceedings of IEEE Vehicular Technology Conference 2000-Spring, Proceedings of the 7th Asia-Pacific Conference on Communications, Proceedings of the 12th International Symposium on Personal, Indoor and Mobile Radio Communications, Proceedings of IEEE Vehicular Technology Conference 2001-Fall, Technical Reports of the IEICE, and Proceedings of the IEICE Conference.

Kazunori Hayashi

Osaka, Japan

January 2002

Acknowledgments

The present research has been carried out during my tenure of doctoral course at the Department of Electronic, Information Systems and Energy Engineering, Graduate School of Engineering, Osaka University, under the guidance of Prof. Ken-ichi Kitayama.

I would like to express my deep sense of appreciation to Prof. Ken-ichi Kitayama, who is also the chief examiner of my thesis, for his guidance, support, and advice for this research. Acknowledgments also go to Prof. Kenji Taniguchi and Associate Prof. Shinsuke Hara of Electronic, Information Systems and Energy Engineering Department, and Prof. Shozo Komaki of Communications Engineering Department for their valuable discussions and careful review on this thesis.

I am also greatly indebted to Prof. Fumio Kishino and Prof. Tetsuzo Tanino of Electronic, Information Systems and Energy Engineering Department, and Prof. Norihiko Morinaga, Prof. Toshiyuki Shiozawa, Prof. Zen-ichiro Kawasaki, the late Prof. Hajime Maeda of Communications Engineering Department, Prof. Hiroshi Motoda of Intelligent Systems Science Division, Prof. Akira Hasegawa of Himeji Dokkyo University, Prof. Hiromasa Ikeda of Tokyo University of Information Sciences, Prof. Yuji Kodama of Ohio State University, U.S.A., Emeritus Prof. Sadao Kurazono of Communications Engineering Department, and all academic lecturers at the Department of Electronic, Information Systems and Energy Engineering, and the Department of Communications Engineering, Graduate School of Engineering, Osaka University for their giving me sufficient basic backgrounds for this thesis.

I wish to express my sincere thanks to Prof. Ramjee Prasad, who is in the Center for PersonKommunikation, Aalborg University, Denmark, for his guidance during my short visit to Aalborg, constant encouragement, and his hearty hospitality. The three months I spent in Aalborg developed not only my research ability but also my cosmopolitan outlook.

I particularly appreciate Assistant Prof. Akihiro Maruta of Electronic, Information Systems and Energy Engineering Department, Associate Prof. Masayuki Matsumoto, Assistant Prof. Hiroyuki Toda, Dr. Takahiro Matsuda, and Dr. Akimasa Hirata of Communications Engineering Department for various helpful discussions and advice.

I express my gratitude to all the past and present colleagues in the Research Group of Advanced Communications Engineering in the Department of Electronic, Information Systems and Energy Engineering and the Research Group of Fundamentals of Communications Engineering in the Department of Communications Engineering. Especially, I thank Dr. Hiroyuki Yomo for a number of fruitful discussions and his deep friendship ever since my undergraduate years. Also, I heartily thank Dr. Hiroto Sugahara, Dr. Toshihiko Hirooka, Dr. Takashi Inoue, Mr. Itaru Nishioka, Mr. Montree Budsabathon, Mr. Toyokazu Kitano, Mr. Hitoshi Masutani, Mr. Daniele Alzetta, Mr. Maoki Suzuki, Mr. Tomotada Kamisaka, Mr. Shigehiko Tsumura, Mr.

Contents

Chapter 1

Introduction

1.1 Introduction

The information and communication technology (IT) revolution, unfolding at a dizzying speed over the past several years, has generated particularly strong interest in Japan. Capital-I Internet, which is an internet that spans the globe, has been without doubt a principal driving force of the revolution. According to the White Paper [1] published by Ministry of Public Management, Home Affairs, Posts and Telecommunications, Japan, in 2001, the Internet usage in Japan has been increasing with the number of users reaching an estimated 47.08 million at the end of 2000, up 74.0% year over year. Some 37.23 million of these users access the Internet via personal computer (PC), while 23.64 million gain access via cell phones. The latter figure indicates that cell phones have been already a prime factor in the surge in overall Internet usership since access via cell phone first became possible in February 1999, although only limited number of services are available via cell phone at present. One of the reasons for the great success of Internet access via cell phone could be that the transmission rate has been almost equivalent to the connections using ordinary phone, which have been used by half of residential PC Internet users. However, considering the rapid penetration of broadband access services, such as digital subscriber line (DSL) service, cable Internet service, and Fiber to the Home (FTTH, testing service only) to the PC Internet connections, it is hardly possible for wireless communications systems to satisfy the users with such a limited way of Internet access and the low transmission rate. Now, wireless communications systems are required to be portions of Internet in a true sense and to achieve high-speed communications.

Clearly positioning IT as an important strategic issue, the Japanese government is undertaking various programs to ensure its advance in the name of *e-Japan Priority Policy Program*. A part of the roles of wireless communications systems in the program is as follows:

> By realizing the fourth-generation wireless communications (4G) system which enables a most advanced high-speed wireless Internet environment and seamless communications service, the world's most advanced mobile IT environment will be achieved. For this purpose, world-leading technological development will be further promoted, based on world-class IT and industrial accumulation, and international contribution will be also aggressively progressed in international standardization activities. With these measures, the government aims at establishing necessary basic

technologies by 2005 and at putting them into practical use by 2010.

Thus, realization of the wireless communications systems, which can achieve seamless access to the Internet and high-speed communications, by 2010 is one of the most important goals in this field.

1.2   Obstacles to High-Speed Wireless Communications Systems

1.2.1   Wireless Channel Aspects

Channels of wireless communications can be characterized by a time-varying multipath channel [2]. This means that the received signal consists of several incoming signals, which have experienced different paths during the propagation from transmission antenna to receiving antenna, and that the paths vary with time because of the movement of the terminals or something around the channel. Basically, the higher transmission rate becomes, the shorter one symbol time becomes, therefore, in wireless communications systems, high-speed transmission results in large delay spread measured by means of the symbol time. If the order of the delay spread becomes equivalent to the symbol time, the neighboring symbols in the time domain interfere with each other. This phenomenon is called inter-symbol interference (ISI), and is the most serious limiting factor for wireless communications systems of speeding up the transmission rate. In the frequency domain, we can observe the phenomenon as a random fluctuation of the spectrum of the received signal without keeping original shape of the spectrum, therefore, it is also called frequency selective fading. It has been reported that indoor wireless channels become frequency selective if the signal bandwidth exceeds several dozens of MHz [3], even when 60 GHz band is employed, where there is a specific attenuation characteristic due to atmospheric oxygen of about 15 dB/km [4], [5]. In order to achieve the transmission rate of over 100 Mbit/sec, some countermeasures have to be taken to cope with the frequency selective fading. Therefore, equalization, which is one of the most effective anti-frequency selective fading techniques, will be a key issue in the realization of high-speed wireless communications systems.

1.2.2   Frequency Bands Aspects

In wireless communications, unlike fiber-optic communications, all the users and all the systems have to share the same medium of space for the transmission of signals. In order to keep orthogonalities among the systems, a radio frequency band is assigned to each system. Although wireless communications system of over 100 Mbit/sec requires on the order of 100 MHz spectral space, such a broad spectral space is not available in the conventional frequency bands for mobile communications. Uncongested bandwidths of this order are only available at higher radio frequencies. The employment of the higher frequencies means a decrease in antenna size, and hence, antenna gain, however, increasing demands for data communications and for seamless connection with wired communications systems require higher signal to noise power ratio (SNR) than conventional voice communications. An adaptive antenna array, which is composed of multiple sensors, can be a silver bullet for the problem. Utilization of adaptive antenna array not only increases the received signal power but also brings about a signal processing in a new domain, namely, spatial signal processing. So far, space resource has not been made good use

Figure 1.1: Processing Speed of DSP and its Roadmap.

of in wireless communications systems, therefore, its efficient use has a dramatic potential to break through the system performance.

1.2.3 Digital Signal Processing Aspects

Looking at the history of the development of wireless communications systems, it can be said that it's a history of "digitalization" of the systems. Digital signal processing plays important roles in present wireless communications systems, such as voice compression/decompression, modulation/demodulation, echo cancellation, forward error correction, tone generation, and so on. Due to the rapid progress of digital signal processing devices, the digital processing of signals in not only baseband but also intermediate frequency (IF) or even radio frequency (RF) band has become a real possibility. With the digitalization up to IF or RF signal, wireless communications systems can change the communication functionality by replacing the software, therefore, such a wireless communications system is called "software radio" or "software-defined radio".

Since the digital signal processing is an inextricable part of wireless communications systems now, we cannot forget the processing speed of digital signal processing devices when we talk about speeding up the transmission rate of the systems. Concretely, the processing speed could be one of the limiting factors of high-speed wireless communications systems. According to the roadmap of digital signal processor (DSP), which has been announced by TEXAS INSTRU-MENTS, Inc. (Dec. 6, 1999), the company will develop DSP's performance to beyond 1,000,000 MIPS (million instructions per second) and even up to 3,000,000 MIPS by 2010. Fig. 1.1 shows the change of processing speed of the company's DSP in terms of MIPS and its roadmap. The

upper and the lower bounds of Moore's Law [1] are also shown in the same figure. From the figure, we can expect that the processing speed of DSP in 2010 will be around 1,000,000 MIPS.

1.3   Overview of the Thesis

Based on the backgrounds and the discussions described above, this thesis investigates spatial and temporal equalization methods, which mean equalization methods utilizing both spatial and temporal information on the received signal, for high-speed wireless communications systems. All the systems presented in this thesis can be realized with the estimated performance of DSP in 2010, i.e., 1,000,000 MIPS, while achieving the transmission rate of over 100 Mbit/sec.

Chapter 2 presents fundamentals of array signal processing in wireless communications systems. Implementation of a temporal filter requires processing of signals collected over temporal aperture. Similarly, implementing a spatial filter requires signals collected over a spatial aperture. In this sense, an adaptive antenna array has a capability of spatial filtering, which is essential for realization of the spatial and temporal equalization. Herein, we introduce three basic and important applications of antenna array; beamforming, direction of arrival (DoA) estimation, and pilot-free channel identification. The matters presented in this chapter will be the groundwork for the systems in subsequent chapters.

Chapter 3 deals with spatial equalization methods, in other words, beamforming methods. Taking into account the extension to spatial and temporal equalization, we propose a spatial equalization method based on estimated channel responses, which gives us some degrees of freedom in beamforming. As for the channel estimation, two different approaches are given for the spatial equalization; a pilot-assisted approach and a pilot-free identification approach. As a pilot-assisted approach, we utilize suppressed spread spectrum (SS) pilot signal, which is coherently added to data signal, and whose power is suppressed enough before the addition. With the SS pilot signal, the receiver can handle only the pilot channel, independent of the data channel, and this separation of the array signal processing makes it independent of employed modulation scheme. In addition, the SS technique can work in low carrier to noise power ratio (CNR) environments. On the other hand, as a pilot-free identification approach, we employ a second-order statistics-based pilot-free channel identification method and discuss applicability of the pilot-free channel identification to practical wireless communications systems.

Chapter 4 proposes a spatial and temporal equalization method with reduced number of weights, utilizing a cascade configuration of an adaptive antenna array and a decision feedback equalizer (DFE). Taking advantage of different features of the adaptive antenna array and the DFE, the equalization functionality should be split into spatial processing and temporal processing, such that 'incoming signals with larger time delays (beyond the filter length of the DFE) are cancelled at the adaptive antenna array.' This makes it possible to reduce the number of weights in the DFE. The weights of both the adaptive antenna array and the DFE are

---

[1] The observation that the logic density of silicon integrated circuits has closely followed the curve (bits per square inch) $= 2^{(t-1962)}$ where t is time in years; that is, the amount of information storable on a given amount of silicon has roughly doubled every year since the technology was invented. This relation, first uttered in 1964 by semiconductor engineer Gordon Moore (who co-founded Intel four years later) held until the late 1970s, at which point the doubling period slowed to 18 months. The doubling period remained at that value through time of writing (late 1999). Moore's Law is known for its capability of prediction about not only the logic density of integrated circuits but also any number which shows exponential growth.

separately calculated using estimated channel impulse response at each sensor. We show the performance of the proposed system in multipath fading channels observed in indoor wireless environments, and discuss the attainable bit error rate (BER), antenna patterns, and computational complexity in comparison with those of other equalization methods, such as spatial equalization and temporal equalization.

Chapter 5 proposes a spatial and temporal equalization method, which is versatile for various kinds of DoA patterns. So far, among conventional spatial and temporal equalization methods, only an adaptive tapped-delay-line (TDL) array has such a robustness. However, it requires huge number of weights, and hence, extremely high computational complexity. In order to reduce the complexity, the proposed equalizer utilizes the same configuration as in chapter 4. Though the cascade configuration has a problem that the cost function in the minimum mean-squared-error (MMSE) based algorithm sometimes have two local minima, the proposed equalizer can avoid the problem by introducing beamforming criterion selectability. The proposed equalizer selects a path or paths to capture with the adaptive antenna array depending on estimated channel conditions, therefore, it can achieve good performance even in the channel models where DoAs of incoming waves are randomly determined. The BER performance of the proposed equalizer is investigated in various kinds of channel models, which are based on measurement reports, in comparison with the performance of the adaptive TDL arrays. Furthermore, we discuss the operation of the selection algorithm from the viewpoint of antenna beam patterns, and evaluate the computational complexity in terms of the number of multiplications in the weights calculation algorithm.

Chapter 6 summarizes all the results.

Chapter 2

Fundamentals of Array Signal Processing

2.1 Introduction

Chapter 2 presents fundamentals of array signal processing in wireless communications systems. Implementation of a temporal filter requires processing of signals collected over temporal aperture. Similarly, implementing a spatial filter requires signals collected over a spatial aperture [6]. In this sense, an adaptive antenna array has a capability of spatial filtering, which is essential for the realization of the spatial and temporal equalization. Herein, we introduce three basic and important applications of the antenna array; beamforming, DoA estimation, and pilot-free channel identification. The matters presented in this chapter will be the groundwork for the systems in subsequent chapters.

2.2 Direction-of-Arrival Estimation

The temporal problem of "estimating the frequencies of complex sinusoids in additive receiver noise", and the spatial problem of "estimating DoAs of incident plane waves with additive sensor noise", which arise in entirely different application areas, can be considered the same problem from a mathematical point of view [7], [8]. Although a lot of algorithms [9]- [14], which can estimate DoAs of incoming signals with high accuracy, here, we introduce only the principle of DoA estimation.

In the temporal processing, consider a received signal $u(i)$ that consists of L complex sinusoids whose complex amplitudes are $\alpha_1, \alpha_2, \cdots, \alpha_L$ and whose angular frequencies are $\omega_1, \omega_2, \cdots, \omega_L$, respectively. A sample $u(i)$ of the received signal is written as

$$u(i) = \sum_{l=1}^{L} \alpha_l e^{j\omega_l i} + v(i), \quad i = 0, 1, \cdots, N - 1 \tag{2.1}$$

where $v(i)$ is a sample of complex additive noise, and N is the total data length. In order to process the received signal $u(i)$ in the temporal domain, we assume to use a transversal filter of length M as shown in Fig. 2.1. The output of the filter $y(i)$ can be written as

$$y(i) = \sum_{m=0}^{M-1} \sum_{l=1}^{L} w_m^* \alpha_l e^{j\omega_l (i-m)} + \sum_{m=0}^{M-1} w_m^* v(i - m). \tag{2.2}$$

Figure 2.1: Transversal Filter for Temporal Processing.

Figure 2.2: Linear Antenna Array for Spatial Processing.

Given the time series of Eq. (2.1), the problem then is to estimate the unknown amplitudes and unknown frequencies contained in the time series.

On the other hand, Fig. 2.2 depicts a linear adaptive antenna array for the spatial processing. The number of antenna elements is M and they are uniformly spaced. The separation between adjacent sensors of the antenna array is d. A set of L incoming waves which originate from incoherent sources are incident on the antenna array. Assume that these waves come from far field of the antenna array, therefore, at the antenna array, these incident waves are plane waves. In the figure, we show a single plane wave impinging on the antenna array at an angle of incidence θ. We further assume that the incoming wave is narrow-band signal, namely, it is characterized by a single frequency f_0. In other words, the signal envelope does not change

during the time the incident plane wave interacts with the array. Here, note that the narrow-band assumption can be applied even to multi-carrier system, such as orthogonal frequency division multiplexing (OFDM), as long as the total bandwidth is much smaller than the carrier frequency f_0. Correspondingly, the wavelength of the incoming signal is

$$\lambda = \frac{c}{f_0}, \tag{2.3}$$

where c is the speed of propagation. In Fig. 2.2, we can see that the wavefront of the incident plane wave reaches sensor 0 before sensor 1 by a distance equal to $d \sin \theta$, therefore, corresponding phase difference ϕ between sensor 0 and 1 becomes

$$\phi = 2\pi \frac{d \sin \theta}{\lambda}. \tag{2.4}$$

In Eq. (2.4), ϕ is called electrical angle of the incident wave. Eq. (2.4) also holds good in phase difference between every other pair of adjacent sensors. Then, the baseband model of the received signal at the ith sensor of the antenna array in Fig. 2.2 and at time k can be written as

$$u(i, k) = \sum_{l=1}^{L} \alpha_l e^{j\phi_l i} + v(i, k), \tag{2.5}$$

where α_l and ϕ_l represent the complex amplitude and electrical angle of the lth incident plane wave, respectively, and $v(i, k)$ is the additive noise of the sensor. L denotes the number of incident plane waves. Note that in the baseband model of Eq. (2.5), it is assumed that the incident plane waves are all narrow-band and their center frequencies are all f_0. The output of the linear adaptive antenna array at time k will be

$$y(i, k) = \sum_{m=0}^{M-1} \sum_{l=1}^{L} w_m^* \alpha_l e^{j\phi_l(i-m)} + \sum_{m=0}^{M-1} w_m^* v(i - m, k). \tag{2.6}$$

By comparing the temporal model of Eq. (2.1) and the spatial model of Eq. (2.5), we can see that the temporal problem of estimating ω_l is the same as the spatial problem of estimating ϕ_l.

Since the sampling duration T in the temporal processing corresponds to sensor spacing d in the spatial processing, sensor spacing d has a limitation like the temporal version of the sampling theorem that if the sampling rate $1/T$ is less than twice the highest frequency component of a bandlimited signal, then aliasing occurs [2]; it is then impossible to distinguish between frequencies that lie outside the interval $(-\pi/T, \pi/T)$ from those that lie inside this interval [15]. Hence, in the spatial processing problem depicted in Fig. 2.2, the distance d between adjacent sensors in the array must be chosen less than $\lambda/2$. As far as d satisfies the condition, we can have the one-to-one correspondence between ϕ and θ in Eq. (2.4), therefore, it is possible to estimate the DoA θ from the phase difference ϕ, which is calculated from the received signal. Furthermore, we can regard "estimating the frequencies ω_l of complex sinusoids in additive receiver noise" and "estimating the DoA θ_l of waves with additive sensor noise" as the same problem.

However, there is one basic difference between the temporal processing and spatial processing. Time series of Eq. (2.1) is serial in nature which continues for a total observation interval N. On the other hand, the space series of Eq. (2.5) is based snapshot of the incident waves, with each snapshot corresponding to a particular instant of time. Therefore, in the temporal model
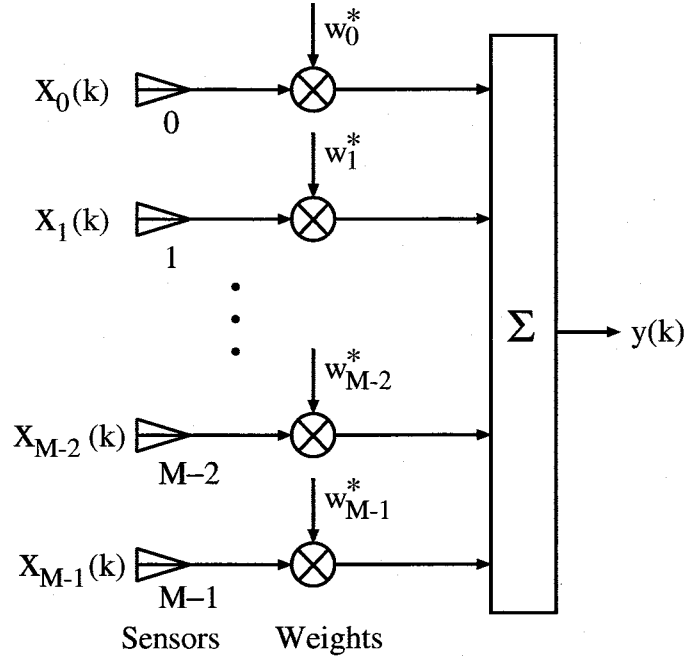
Figure 2.3: Generic Adaptive Beamformer.

of Fig. 2.1 the data evolve in time one sample after another, and in the spatial model of Fig. 2.2 the data evolve in time one snapshot after another. Clearly, if we perform block processing of the received signal, this difference between the temporal processing and spatial processing will be trivial.

2.3 Beamforming

Beamforming is a technique which tries to capture only desired signals and to cancel undesired signals, employing an adaptive antenna array, therefore, it is the name given to a wide variety of array signal processing algorithms that focuses the antenna array's signal-capturing abilities in a particular direction [16]- [19]. The adaptive antenna array consists of several sensors each having a weight of complex value, which can be adaptively changed in order to control the antenna beam patterns with a signal processing. Because of the changeability of the antenna beam pattern by software, the adaptive antenna array is also called "smart antenna" or "software antenna". Considering to apply wireless communications system, the changeability of the antenna beam pattern can be exploited for ISI or co-channel interference (CCI) cancellation. Since the adaptive antenna array can separate desired signals from the interferences, as far as they have different DoAs, even if the desired signal and the interferences occupy the same temporal frequency band.

Fig. 2.3 depicts a generic adaptive beamforming system. The output $y(k)$ at time k is given by a linear combination of the received signal at the M sensors at time k;

$$y(k) = \sum_{m=0}^{M-1} w_m^* x_m(k) \qquad (2.7)$$

where $(\cdot)^*$ and w_m^* represent complex conjugate and the weight of the adaptive antenna array, respectively. By defining a weight vector $w^H = [w_0^*, w_1^*, \ldots, w_{M-1}^*]$, where the superscript H

denotes Hermitian transpose, and a received signal vector $\mathbf{x}(k) = [x_0(k), x_1(k), \ldots, x_{M-1}(k)]$, we can express the output signal $y(k)$ as

$$y(k) = \mathbf{w}^H \mathbf{x}(k) \tag{2.8}$$

The frequency response of a transversal filter with tap weights w_p^* ($0 \leq p \leq M-1$) and a tap delay of T seconds is given by

$$r(\omega) = \sum_{p=0}^{M-1} w_p^* e^{-j\omega T p}. \tag{2.9}$$

Alternatively,

$$r(\omega) = \mathbf{w}^H \mathbf{d}(\omega) \tag{2.10}$$

where $\mathbf{w}^H = [w_0^*, \ldots, w_{M-1}^*]$ and $\mathbf{d}(\omega) = [1, e^{j\omega T}, \ldots, e^{j(M-1)\omega T}]$. $r(\omega)$ represents the response of the filter to complex sinusoid of frequency ω and $\mathbf{d}(\omega)$ is a vector describing the phase of the complex sinusoid at each tap in the transversal filter relative to the tap associated with w_0.

Similarly, beamformer response is defined as the amplitude and phase presented to a complex plane wave as a function of location and frequency. Location is in general a three dimensional quantity, but we are only concerned with one or two dimensional DoA. Assume that the signal is a complex plane wave with DoA θ and frequency ω. For convenience let the phase be zero at the first sensor. This implies $x_0(k) = e^{j\omega k}$ and $x_m(k) = e^{j\omega[k-\Delta_m(\theta)]}$, $1 \leq m \leq M-1$. $\Delta_m(\theta)$ denotes the time delay, due to propagation from the first to the mth sensor. Using these expressions, the output of the adaptive antenna array can be written as

$$y(k) = e^{j\omega k} \sum_{m=0}^{M-1} w_m^* e^{-j\omega \Delta_m(\theta)} = e^{j\omega k} r(\theta, \omega), \tag{2.11}$$

where $\Delta_0(\theta) = 0$. $r(\theta, \omega)$ is the beamformer response and can be expressed in vector form as

$$r(\theta, \omega) = \mathbf{w}^H \mathbf{d}(\theta, \omega). \tag{2.12}$$

The elements of $\mathbf{d}(\theta, \omega)$ correspond to the complex exponentials $e^{-j\omega \Delta_m(\theta)}$. $\mathbf{d}(\theta, \omega)$ is termed the array response vector, or the steering vector. Since the antenna beam pattern of the adaptive antenna array is defined as the magnitude squared of $r(\theta, \omega)$, we can see from Eq. (2.12) that the beam pattern can be controlled by changing $\mathbf{w}$, i.e., the weights of the adaptive antenna array.

2.4 Pilot-Free Channel Identification

By pilot-free channel identification, in other words, blind channel identification, we mean that the channel impulse response is identified without knowing its input [20]. At first glance, the problem seems to be ill posed, however, it turns out that this apparently intractable problem can have elegant solutions with efficient algorithms [21]. The idea of pilot-free channel identification in M-ary pulse amplitude modulation (PAM) systems dates back to the work of Sato [22], which is classified in Bussgang algorithm [20]. After this, quite a few number of pilot-free identification algorithms were proposed, however, the algorithms were not employed in the practical wireless communications systems. This is because they have a common drawback,

namely, the slow rate of convergence, since they all exploited higher-order statistics (HOS) of the received signal implicitly or explicitly. It was not until the 1990s that it was shown the pilot-free identification of the nonminimum-phase channel is possible from the second-order statistics [23,24] by exploiting the cyclostationary characteristics [25], which can be observed in the oversampled signal or in the signal received by multiple sensors, i.e., the antenna array. After this, quite a few number of pilot-free identification algorithms, which utilize the second-order statistics, have been proposed [26]- [31].

In this section, the pilot-free channel identification capability is discussed from a view point of the zeros of a channel transfer function.

2.4.1 Problem Formulation

Consider a discrete-time model for a baseband communications system with signaling

$$
\begin{aligned}
x(t) &= \sum_{\alpha} h(\alpha)u(t - \alpha), \\
u(t) &= \sum_{k} s_k \delta(t - kT),
\end{aligned}
\tag{2.13}
$$

where $x(\cdot)$ is the received signal, $h(\cdot)$ is the channel impulse response, $\{s_k\}$ the information symbols, $1/T$ the symbol rate, $\delta(\cdot)$ the discrete-time impulse function, The sampling rate is normalized to 1. For the simplicity of the analysis, we consider a noiseless case.

The following conditions are assumed in this section.

Assumption

1. The symbol interval T is a known integer.

2. The channel has a finite impulse response (FIR).

3. $\{s_k\}$ is zero mean, and $E[s_k s_l^*] = \delta(k - l)$, where $E[\cdot]$ denotes the operation of ensemble average.

2.4.2 Pilot-Free Identification Capability of SISO System

Here, we consider the pilot-free identification capability of a single-input single-output (SISO) system. Letting $T = 1$ in Eq. (2.13), we obtain such a SISO system. In this case, the received signal will be a wide-sense stationary sequence. Define the autocorrelation function of the received signal $x(t)$ and its discrete-time Fourier transform by
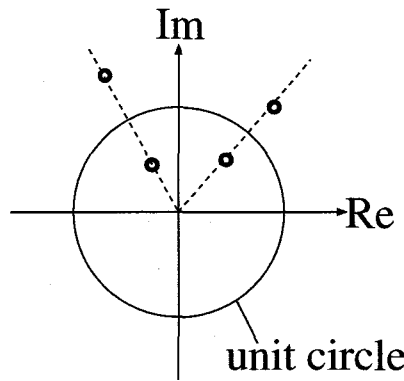
$$
R_x(\tau) = E[x(t)x^*(t - \tau)],
\tag{2.14}
$$

$$
S(\nu) = \sum_{k} R_x(k)e^{-j\nu k}.
\tag{2.15}
$$

Under the Assumption 1-3, it can be shown that

$$
S(\nu) = H(\nu)H^*(\nu),
\tag{2.16}
$$

where $H(\nu)$ is the discrete-time Fourier transform of $h(\cdot)$ defined by

$$
H(\nu) = \sum_{k} h(k)e^{-j\nu k},
\tag{2.17}
$$

Figure 2.4: Zeros of $H(z)H^*(\frac{1}{z})$.

or in z-domain, $h(\cdot)$ by

$$S(z) = H(z)H^*(\frac{1}{z}), \tag{2.18}$$

where $H(z)$ is the z-transform of $h(\cdot)$ defined by

$$H(z) = \sum_k h(k)z^{-k}. \tag{2.19}$$

The problem here is whether it is possible, or not, to uniquely identify $H(z)$ from the second-order statistics, in other word, the power spectrum $S(z)$ of the received signal. Note that the zeros of $H^*(\frac{1}{z})$ are reciprocals of the zeros of $H(z)$ with respect to a unit circle in the z-plane [32] as shown in Fig. 2.4. Then, it is impossible to uniquely determine the zeros of $H(z)$ from the zeros of the product $H(z)H^*(\frac{1}{z})$, unless $H(z)$ is minimum-phase, which means all the zeros of $H(z)$ are inside the unit circle. Since we can have the amplitude $|H(\nu)|$, all we have shown is that phase information cannot be recovered from stationary second-order statistics, such as the power spectrum.

2.4.3 Pilot-Free Identification Capability of SIMO System (1-input 2-output)

We discuss the identification Capability of single-input multiple-output (SIMO) system. As an example of the SIMO system, we consider a communications system, where the received signal is oversampled $(T > 1)$. Wireless communications systems with adaptive antenna array in the receiver are also classified in the SIMO system. In this case, the oversampled received signal becomes a wide-sense cyclostationary sequence [25]. To obtain the relation between the output (cyclostationary) statistics and the channel transfer function, define the autocorrelation function $R_x(t, \tau)$ of $x(\cdot)$ and its Fourier transform $S_x(t, \nu)$ by

$$
\begin{aligned}
R_x(t, \tau) &= E[\, x(t)x^*(t - \tau)\,] \\
S_x(t, \nu) &= \sum_\tau r_x(t, \tau)e^{-j\nu\tau}.
\end{aligned}
\tag{2.20}
$$

The autocorrelation functions (Fourier transforms of the autocorrelations) of $u(\cdot)$ and $n(\cdot)$ are denoted by $R_u(t, \tau)$ $(S_u(t, \nu))$ and $R_n(t, \tau)$ $(S_n(t, \nu))$, respectively. Under the Assumption 1-4,

it can be shown that

$$S_x(t,\nu) = (\ \sum_\alpha h(\alpha)e^{-j\nu\alpha} S_u(t-\alpha,\nu)\ )H^*(\nu) + S_n(t,\nu) \tag{2.21}$$

$$S_u(t,\nu) = \sum_{k=-\infty}^{\infty} \delta(t-kT) \tag{2.22}$$

where $H(\nu)$ is the discrete-time Fourier transform of $h(\cdot)$. Since $S_u(t,\tau)$ is a periodic function of t with the period T, $S_x(t,\tau)$ is also periodic in t with period T when the noise process is wide-sense stationary. (That's why it's called *cyclostationary* sequence!) Let $\Gamma_x^{(k)}(\nu)$ be the kth Fourier coefficient of $S_x(t,\tau)$, referred to as the kth *cyclic spectrum*, given by

$$\Gamma_x^{(k)}(\nu) = \sum_{t=0}^{T-1} S_x(t,\nu)e^{-jk(2\pi/T)t}, \quad k = 0,\ \ldots,T-1. \tag{2.23}$$

In order to facilitate the analytical treatment, we first consider the case of $T = 2$, namely, two times oversampling. The $0th$ and $1st$ cyclic spectra of $S_x(t,\tau)$ are given by

$$\begin{aligned}
\Gamma_x^{(0)}(\nu) &= \sum_{t=0}^{1} S_x(t,\nu)\\
&= S_x(0,\tau) + S_x(1,\nu)\\
&= \{\ \sum_\alpha h(\alpha)e^{-j\nu\alpha} S_u(-\alpha,\nu)\ \}H^*(\nu)\ +\ \{\ \sum_\alpha h(\alpha)e^{-j\nu\alpha} S_u(1-\alpha,\nu)\ \}H^*(\nu)\\
&= [\ \sum_\alpha h(\alpha)e^{-j\nu\alpha}\{\ S_u(-\alpha,\nu) + S_u(1-\alpha,\nu)\ \}]H^*(\nu)\\
&= H(\nu)H^*(\nu),
\end{aligned} \tag{2.24}$$

and

$$\begin{aligned}
\Gamma_x^{(1)}(\nu) &= \sum_{t=0}^{1} S_x(t,\nu)e^{-j\pi t}\\
&= S_x(0,\tau) + S_x(1,\nu)e^{-j\pi}\\
&= \{\ \sum_\alpha h(\alpha)e^{-j\nu\alpha} S_u(-\alpha,\nu)\ \}H^*(\nu)\ -\ \{\ \sum_\alpha h(\alpha)e^{-j\nu\alpha} S_u(1-\alpha,\nu)\ \}H^*(\nu)\\
&= [\ \sum_\alpha h(\alpha)e^{-j(\nu+\pi)\alpha}\{\ S_u(-\alpha,\nu)\ -\ S_u(1-\alpha,\nu)\ \}]e^{-j\pi\alpha}H^*(\nu)\\
&= H(\nu+\pi)H^*(\nu),
\end{aligned} \tag{2.25}$$

respectively. For notational convenience, let $\nu = \omega$ in Eq. (2.24), and $\nu + \pi = \omega$ in Eq. (2.25), then we have

$$\Gamma_x^{(0)}(\omega) = H(\omega)H^*(\omega) \tag{2.26}$$

$$\Gamma_x^{(1)}(\omega) = H(\omega)H^*(\omega - \pi) \tag{2.27}$$

Furthermore, we can describe the equations in z-domain as

$$\Gamma_x^{(0)}(z) = H(z)H^*(\frac{1}{z^*}) \tag{2.28}$$

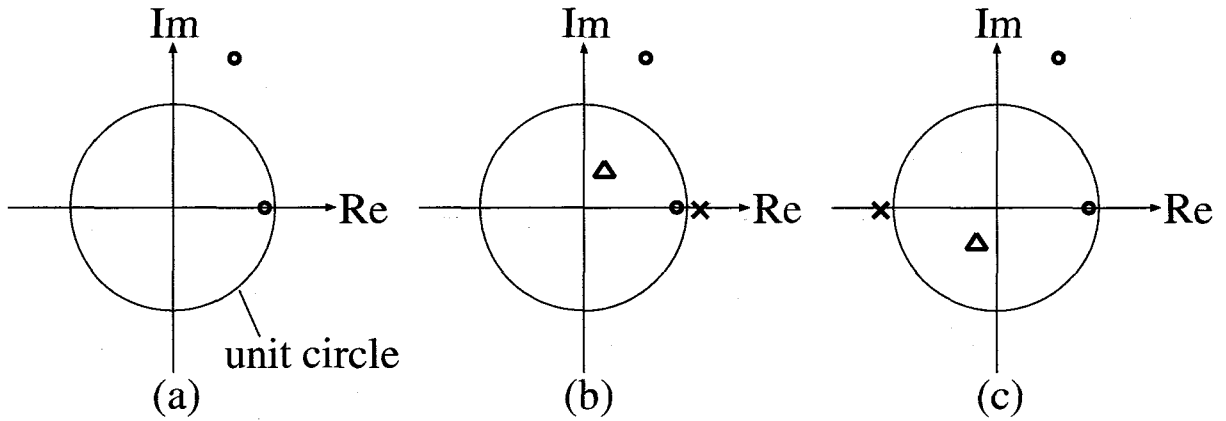$$\Gamma_x^{(1)}(z) = H(z)H^*(e^{-j\pi}\frac{1}{z^*}) \tag{2.29}$$

Figure 2.5: Identifiable Channel: (a)The Zeros of $H(z)$ (b)The Zeros of $\Gamma_x^{(0)}(z) = H(z)H^*(\frac{1}{z^*})$ (c)The Zeros of $\Gamma_x^{(1)}(z) = H(z)H^*(e^{-j\pi}\frac{1}{z^*})$.

Denoting a set of zeros of $G(z)$ by $\mathcal{ZERO}[G(z)]$, if $H(\cdot)$ satisfies

$$\mathcal{ZERO}[H^*(\frac{1}{z^*})] \bigcap \mathcal{ZERO}[H^*(e^{-j\pi}\frac{1}{z^*})] = \emptyset, \tag{2.30}$$

namely, if all the zeros of $H^*(\frac{1}{z^*})$ and $H^*(e^{-j\pi}\frac{1}{z^*})$ are distinct, we can uniquely determine the zeros of $H(z)$ from $\Gamma_x^{(0)}(z)$, and $\Gamma_x^{(1)}(z)$. This is because

$$\mathcal{ZERO}[\Gamma_x^{(0)}(z)] \bigcap \mathcal{ZERO}[\Gamma_x^{(1)}(z)]$$

$$= \mathcal{ZERO}[H(z)] \bigcap \mathcal{ZERO}[H^*(\frac{1}{z^*})] \bigcap \mathcal{ZERO}[H^*(e^{-j\pi}\frac{1}{z^*})]$$

$$= \mathcal{ZERO}[H(z)]. \tag{2.31}$$

If we define the cyclic autocorrelation function of the received signal as

$$\eta_\tau^0 = \sum_{t=0}^{1} R_x(t,\tau) \quad , \quad \eta_\tau^1 = \sum_{t=0}^{1} R_x(t,\tau)e^{-j\pi t}, \tag{2.32}$$

the coefficients γ_τ^k of z^τ in $\Gamma_x^{(k)}(z)(k = 0, 1)$ are given by

$$\gamma_\tau^0 = \eta_\tau^0 \quad , \quad \gamma_\tau^1 = \eta_\tau^1 e^{j\pi\tau}. \tag{2.33}$$

It is noted that, once $R_x(t,\tau)$ is obtained, γ_τ^k can be computed by applying the fast Fourier transform (FFT) to $R_x(t,\tau)$. In other words, we can uniquely identify the channel impulse response up to a multiplicative constant (inherent to the problem).

Let's discuss the pilot-free identification capability from a viewpoint of zero diagrams in z plane. Fig. 2.5 (a) shows an example of the zero diagram of $H(z)$. The zeros of $H^*(e^{-jk\theta}\frac{1}{z^*})$ are reciprocals of the zeros of $H(z)$ rotated counterclockwise by $k\theta$, therefore, the zeros of $\Gamma_x^{(0)}(z) = H(z)H^*(\frac{1}{z^*})$ can be shown as in Fig. 2.5(b), and $\Gamma_x^{(1)}(z) = H(z)H^*(e^{-j\pi}\frac{1}{z^*})$ in Fig. 2.5(c). In the figures, o denotes the zeros of $H(z)$, $\triangle$ the zeros of $H^*(\frac{1}{z^*})$, and $\times$ the zeros of $H^*(e^{-j\pi}\frac{1}{z^*})$. In this case, it is clear that the zeros of the channel $H(z)$ can be obtained from the intersection of the zeros of the observation spectra.
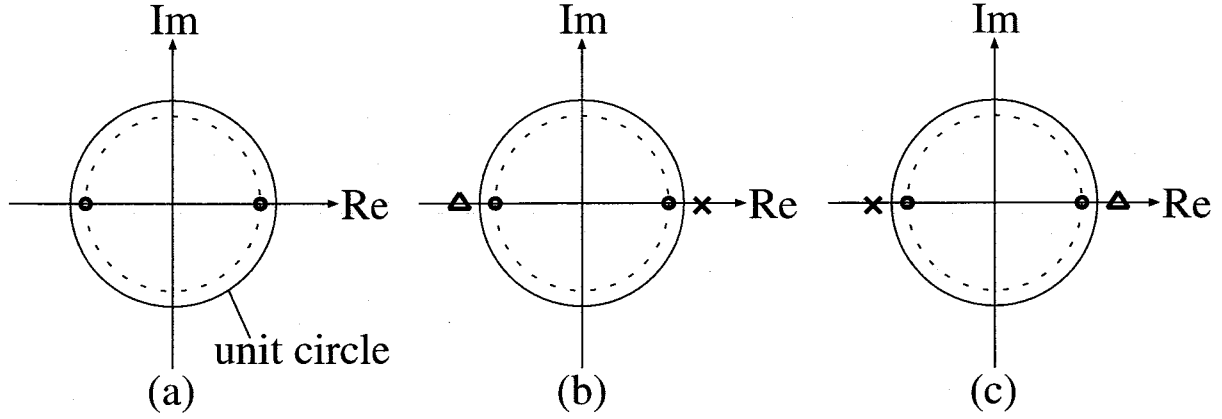
Figure 2.6: Unidentifialbe Channel: (a)The Zeros of $H(z)$ (b)The Zeros of $\Gamma_x^{(0)}(z) = H(z)H^*(\frac{1}{z^*})$ (c)The Zeros of $\Gamma_x^{(1)}(z) = H(z)H^*(e^{-j\pi}\frac{1}{z^*})$.

On the other hand, if $H(z)$ has the zeros as shown in Fig. 2.6(a), it is impossible to uniquely determine the zeros of $H(z)$ from the intersection of the zeros in Fig. 2.6(b) and (c).

Based on the discussions above, we can have the following theorem on the channel identification capability when the received signal is oversampled at 2 times the symbol rate;

Theorem 1:

An linear time-invariant FIR channel $H(z)$ is identifiable from $\Gamma^k(z), k = 0, 1$ if and only if $H(z)$ does not have zeros on a concentric circle with angular spacing π. Moreover, if the channel is identifiable, the zeros of $H(z)$ are the common zeros of the $\Gamma^k(z), k = 0, 1$, i.e.,

$$\mathcal{ZERO}[H(z)] = \bigcap_k \mathcal{ZERO}[\Gamma_x^{(k)}(z)], k = 0, 1. \tag{2.34}$$

Proof of Theorem 1:

-*necessary condition*: The most obvious case is when the two zeros are on a concentric circle with angular spacing π. It is then impossible to identify the zeros of $H(z)$ from $\mathcal{ZERO}[\Gamma_x^{(k)}(z)]$ since one cannot determine if a zero of $H(z)$ is inside or outside the unit circle.

-*sufficient condition*: Suppose that $H(z)$ does not have zeros on a concentric circle with π-space, and that

$$z_0 \in \mathcal{ZERO}[H^*(\frac{1}{z^*})] \bigcap \mathcal{ZERO}[H^*(e^{-j\pi}\frac{1}{z^*})].$$

Then

$$z_0, z_0e^{-j\pi} \in \mathcal{ZERO}[H^*(\frac{1}{z^*})].$$

Therefore $z_0, z_0e^{-j\pi}$ is a set of zeros on a concentric circle with π-space. Hence $H(z)$ has zeros on a concentric circle with angular spacing π. This is a contradiction.

□

2.4.4 Pilot-Free Identification Capability of SIMO System (1-input m-output)

Then, we consider a general case, i.e., 1-input m-output system ($T = m, m > 1$), such as cases when the received signal m times oversampled, or the signal is received by m sensors of an antenna array. The cyclic spectrum of the received signal $x(t)$ in z-domain is given by

$$\Gamma_x^{(k)}(z) = H(z)H^*(e^{-jk(2\pi/T)}\frac{1}{z^*}), \quad k = 0, 1, \ldots, T - 1 \tag{2.35}$$

Also, the cyclic autocorrelation function η_τ^k and the coefficient γ_τ^k of $z^{-\tau}$ in $\Gamma_x^{(k)}(z)$ ($k = 0, 1, \ldots T - 1$) are expressed as

$$\eta_\tau^k = \sum_{t=0}^{T-1} R_x(t, \tau)e^{-jk(2\pi/T)t}, \quad k = 0, 1, \ldots, T - 1, \tag{2.36}$$

$$\gamma_\tau^k = \begin{cases} \eta_\tau^{(0)} - \sigma^2 T\delta(\tau), & k = 0, \\ \eta_\tau^{(k)}e^{jk(2\pi/T)\tau}, & k \neq 0. \end{cases} \tag{2.37}$$

Since γ_τ^k can be calculated from $R_x(t, \tau)$, which can be estimated from the received signal $x(t)$, the problem of channel identification is now equivalent to identifying $H(z)$ given $\Gamma_x^{(k)}(z)$ ($k = 0, 1, \ldots T - 1$).

The necessary condition of the pilot-free identification capability is given by

$$\bigcap_{k=0}^{T-1} \mathcal{ZERO}[\Gamma_x^{(k)}(z)] = \emptyset. \tag{2.38}$$

This is because, if Eq. (2.38) is satisfied, then we obtain

$$\begin{aligned} \bigcap_{k=0}^{T-1} \mathcal{ZERO}[\Gamma_x^{(k)}(z)] &= \bigcap_{k=0}^{T-1} \mathcal{ZERO}[H(z)H^*(e^{-jk(2\pi/T)}\frac{1}{z^*})] \\ &= \mathcal{ZERO}[H(z)] \bigcup \{\bigcap_{k=0}^{T-1} \mathcal{ZERO}[H^*(e^{-jk(2\pi/T)}\frac{1}{z^*})]\} \\ &= \mathcal{ZERO}[H(z)] \end{aligned}$$
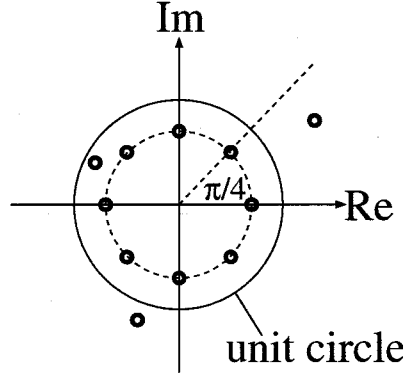
from Eq. (2.35).

The identification capability condition on $H(z)$ in the case of 1-input m-output system relates to a notation of uniformly spaced zeros. $H(z)$ is said to have uniformly θ-spaced zeros [33] if a subset of zeros of $H(z)$ is uniformly spaced on a circle of the z-plane with angular spacing θ, as shown in Fig. 2.7. Such a set of zeros have to have the form { $re^{j\phi+\theta}, re^{j\phi+2\theta}, \ldots, re^{j\phi+K\theta} = re^{j\phi}$ }.

Finally, we have the theorem on channel identification capability of general SIMO systems.

Theorem 2:

A linear time-invariant FIR channel is identifiable from $\Gamma_x^{(k)}(z)$, $k = 0, \ldots, T - 1$ if and only if $H(z)$ does not have uniformly $(2\pi/T)$-spaced zeros. Moreover, if the channel is identifiable, the zeros of $H(z)$ are the common zeros of the $\Gamma_x^{(k)}(z)$, $k = 0, \ldots, T - 1$, i.e.,

$$\mathcal{ZERO}[H(z)] = \bigcap_k \mathcal{ZERO}[\Gamma_x^{(k)}(z)], k = 0, \ldots, T - 1. \tag{2.39}$$

Figure 2.7: A Channel with Uniformly $(\pi/4)$-Spaced Zeros.

Proof of Theorem 2:

When all the zeros of $H(z)$ are uniformly $(2\pi/T)$-spaced, we have

$$\mathcal{ZERO}[\Gamma_x^{(k)}(z)] = \mathcal{ZERO}[\Gamma_x^{(0)}(z)], \quad \forall k. \tag{2.40}$$

It is then impossible to identify the zeros of $H(z)$ from $\Gamma_x^{(k)}(z)$ since one cannot determine if a zero of $H(z)$ is inside or outside the unit circle. When a subset of $\mathcal{ZERO}[H(z)]$ is uniformly $(2\pi/T)$-spaced, this subset cannot be identified.

Suppose now that $H(z)$ does not have uniformly $(2\pi/T)$-spaced zeros. We have

$$\bigcap_k \mathcal{ZERO}[\Gamma_x^{(k)}(z)] = \mathcal{ZERO}[H(z)] \bigcup \bigcap_k \mathcal{ZERO}[H^*(e^{-jk(2\pi/T)}\frac{1}{z^*})]. \tag{2.41}$$

Then we show that

$$\bigcap_k \mathcal{ZERO}[H^*(e^{-jk(2\pi/T)}\frac{1}{z^*})] = \emptyset. \tag{2.42}$$

Suppose that

$$z_0 \in \bigcap_k \mathcal{ZERO}[H^*(e^{-jk(2\pi/T)}\frac{1}{z^*})]. \tag{2.43}$$

Then

$$z_0 e^{-jk(2\pi/T)} \in \mathcal{ZERO}[H^*(\frac{1}{z^*})], \forall k. \tag{2.44}$$

Therefore, $\{z_0, z_0 e^{-j(2\pi/T)}, \ldots, z_0 e^{-j(T-1)(2\pi/T)}\}$ is a set of uniformly $(2\pi/T)$-spaced zeros of $H^*(1/z^*)$. Hence, $H(z)$ has uniformly $(2\pi/T)$-spaced zeros. This is a contradiction.

$\square$

The key issue here is that it is possible to identify a nonminimum phase channel in a pilot-free manner from a second-order statistics of the received signal, as far as the channel can be considered as a SIMO system.

2.5 Summary

This chapter has presented fundamentals of array signal processing by showing three applications of the array processing; DoA estimation, Beamforming, and pilot-free channel identification. Array signal processing is defined as a processing of spatially sampled signals. In wireless communications systems, the spatial sampling can be performed by antenna array. Although array signal processing, in other words, spatial signal processing, and conventional temporal signal processing arise in entirely different application areas, there is analogy between them. In the following chapter, by utilizing the adaptive antenna array, we propose a spatial equalization method, which can be easily extend to a spatial and temporal equalization. Also, the feasibility of a second-order statistics based pilot-free channel identification method will be discussed.

Chapter 3

Spatial Equalization Methods Based on Estimated Channel Impulse Response

3.1 Introduction

In this chapter, spatial equalization methods, which utilize the spatial filtering capability of the adaptive antenna array, are discussed. Taking into account the extension to the spatial and temporal equalization, we propose spatial equalization methods based on estimated channel responses, which gives us some degrees of freedom in the beamforming. As for the channel estimation, two different approaches are given for the spatial equalization; a pilot-assisted approach and a pilot-free identification approach. As a pilot-assisted approach, we utilize suppressed SS pilot signal, which is coherently added to data signal, and whose power is sufficiently suppressed before the addition. With the SS pilot signal, the receiver can handle only the pilot channel, independent of the data channel, and this separation of the array signal processing makes it independent of employed modulation scheme. In addition, the SS technique gives workability in low CN ratio environments. On the other hand, as a pilot-free identification approach, we employ a second-order statistics-based pilot-free channel identification method [26] and discuss the applicability of the pilot-free channel identification to practical wireless communications systems.

3.2 Design Criteria

Array signal processing contains many applications such as DoA estimation and beamforming, and there are a lot of algorithms [9]- [19] for them. Such algorithms can be applied to the spatial equalizer, however, it becomes a problem that the determination of the weights of adaptive antenna array could require both DoA estimation and beamforming procedures, in other words, the spatial equalization could be made in two steps, with different characteristics of processing. In order to avoid the two-step approach, we consider the spatial equalization method, where the equalizer calculates and adjusts the weights of the adaptive antenna array using only an estimated channel impulse response [34], [35]. Here, taking into account that the estimated

channel impulse response can be also used for the temporal equalization, it is quite natural that we can easily extend the idea of 'impulse response estimation-based control' in the spatial equalization to a basic strategy in spatial and temporal equalization.

There are basically two different kinds of strategies for channel impulse response estimation, such as a pilot-assisted approach and a pilot-free approach. For pilot-assisted approach, transmitter classically inserts known pilot signal at the top end of signal frame [36], and at receiver end, equalizer adjusts its weights every frame timing. In such a system, the weight calculation time must be shorter than a period of one frame, otherwise, it is impossible to process. However, even in high-speed wireless communications using short length frame, variation speed of fading does not depend on data transmission speed and hence it is not necessary to update the weights for each frame timing, or rather say, it is sufficient to update the weights slowly enough to follow the fading. Therefore, we consider the pilot signal, which consists of pseudo noise (PN) sequence and has the same bandwidth as the data signal, is superimposed on the data signal. In addition, the power of the pilot signal is sufficiently suppressed before the addition. Though the pilot signal and data signal are not orthogonal in frequency and time domains, we can extract the pilot signal by correlation (despreading). The usage of such a suppressed SS pilot signal brings about some attractive features. The main advantage is that we can independently handle the data demodulation process and the spatial/temporal control process. This means that we can separate the weight calculation, which often requires high computational complexity, from the data signal processing, therefore, high speed demodulation processing can be achieved. It will be also the reason why the proposed scheme is suited for high speed communications that all the time slots can be used for user data. In addition, since the weights are calculated from the estimated channel response, there is no limitation in the modulation format of the data signal. However, on the other hand, the proposed system has a disadvantage that the pilot signal gives interference to the data signal. Therefore, to suppress the power enough, keeping good estimation and equalization performance, is also a key issue. On the other hand, pilot-free channel identification methods, which are based only on calculation of second-order statistics of received signal, recently have been proposed. A lot of discussions have been made from mathematical point of view [23]- [31], however, the applicability and feasibility have never been fully discussed in wireless communications applications. Among the many second-order statistics based pilot-free identification methods, we have picked the subspace decomposition method described in [26], and discuss the advantage, disadvantage, applicability, and feasibility of the pilot-free signal processing in practical wireless communications systems.

3.3   Pilot-Assisted Spatial Equalizer

3.3.1   System Configuration

Assume that the proposed spatial equalizer is applied to the down link of a wireless local area network (LAN) system, where a base station with an omnidirectional antenna communicates with n terminals each having an adaptive antenna array. Fig. 3.1 shows the transmitter/receiver structure. In the proposed method, two types of channels are prepared; a traffic channel and a pilot channel. The traffic channel is used to convey information signals, and the pilot channel to estimate channel impulse response for weights calculation.
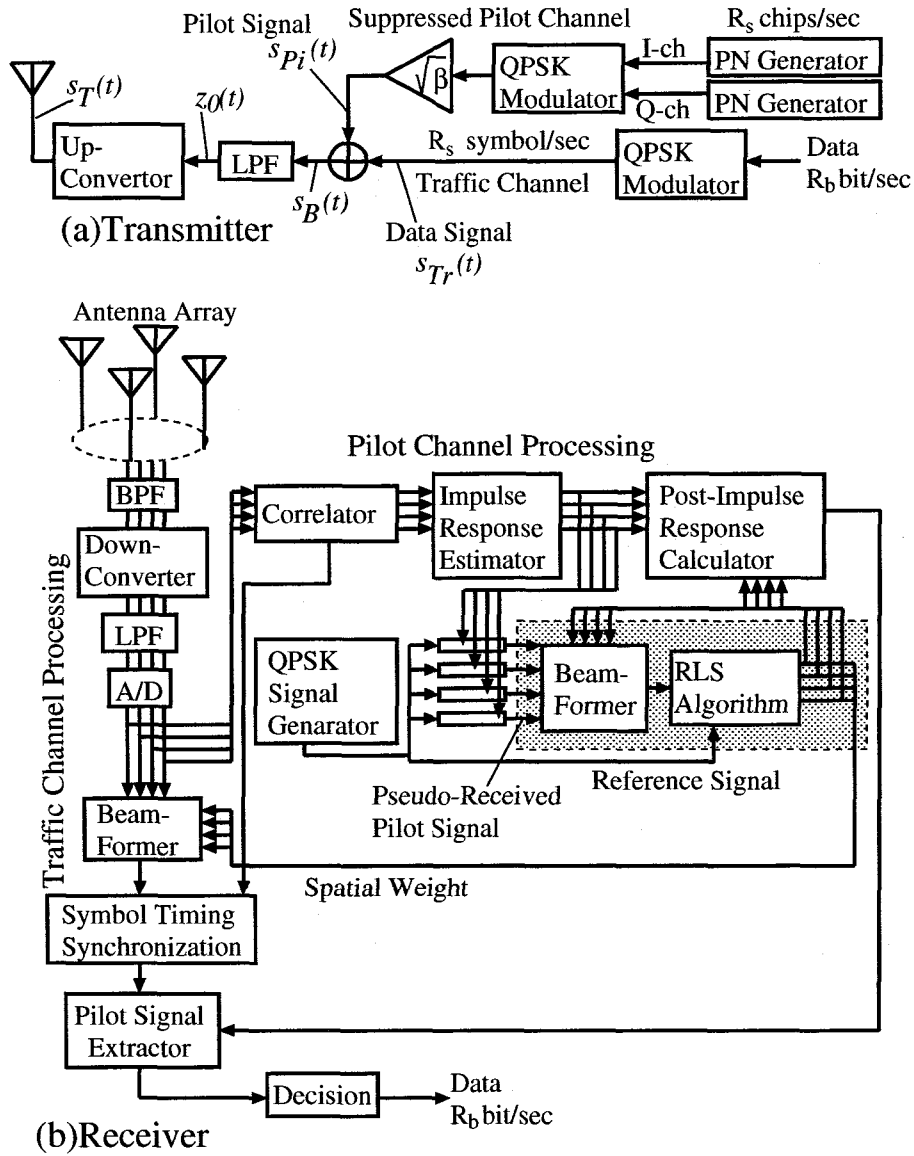
Figure 3.1: Transmitter/Receiver Structure.

In the transmitter, data sequence (R_b bit/sec) is first converted into quadrature phase shift keying (QPSK) waveform ($R_s(=R_b/2)$ symbol/sec) for the traffic channel, on the other hand, known pilot signal is generated by the PN sequence generator for the pilot channel, which has the same frequency band width as the traffic channel. Note that PN sequence generators generate two different PN sequences, which are respectively used for inphase and quadrature pilot channels (I and Q-ch) after QPSK modulation. In addition, the power of the pilot signal is sufficiently suppressed before the addition to the data signal. If we use a S_{pn}-stage maximum length shift resister (M-) sequence as a PN sequence, the period of the PN sequence becomes $P (= 2^{S_{pn}} - 1)$ symbols long.

Let $s_B(t)$, $s_{Tr}(t)$, and $s_{Pi}(t)$ denote the baseband transmitted signal, the data signal, and the pilot signal, respectively. They can be written as

$$s_B(t) = s_{Tr}(t) + \sqrt{\beta} \cdot s_{Pi}(t), \tag{3.1}$$

$$s_{Tr}(t) = \sum_{k=-\infty}^{\infty} d_k \delta(t - kT_s), \tag{3.2}$$

$$s_{Pi}(t) = \sum_{l=-\infty}^{\infty} \sum_{k=0}^{P-1} m_k \delta(t - (lP + k)T_s), \tag{3.3}$$

$$d_k = d_{I_k} + j d_{Q_k}, \tag{3.4}$$

$$m_k = m_{I_k} + j m_{Q_k}, \tag{3.5}$$

where d_{I_k} and d_{Q_k} denote the kth symbol of the inphase and quadrature components in the data signal, respectively. T_s, β, and $\delta(y)$ denote the time duration of one symbol, the power suppression ratio of the pilot channel, and the Dirac's delta function, respectively. Moreover, m_{I_k} and m_{Q_k} express the inphase and quadrature components of the pilot signal at the kth symbol, respectively.

The baseband signal passes through the low pass filter (LPF), i.e., emission filter, and then is transmitted from the omnidirectional antenna after up-conversion. The transmitted signal $s_T(t)$ will be

$$s_T(t) = Re[z_0(t) \exp(j2\pi f_c t)], \tag{3.6}$$

$$z_0(t) = s_B(t) * h_B(t), \tag{3.7}$$

where $h_B(t)$, f_c, and $z_0(t)$ denote the impulse response of the LPF, the carrier frequency, and the band-limited baseband signal, respectively.

In the receiver, the incoming signal is received by the antenna array which consists of M sensors, where the sensor spacing is the half of carrier wavelength. After then, the received signal undergoes the band pass filter (BPF), down-converter, LPF (matched filter), and analog-to-digital (A/D) converter. The BPF is used for the suppression of the adjacent channel interference and noise as well as for the extraction of the spectrum around the desired signal. Moreover, the A/D converter operates with the sampling rate of N_{smp} times the symbol rate. After the A/D conversion, the received signal is processed in the traffic channel processing and in the pilot channel processing independently.

In the traffic channel processing, the outputs from the matched filters are multiplied by the weights of the adaptive antenna array which are calculated in the pilot channel processing. After symbol timing synchronization and equalization with DFE which has N_{ftap} taps in the feedforward filter and N_{btap} taps in the feedback filter, the data are recovered.

In the pilot channel processing, the complex instantaneous channel impulse response at each antenna element is first estimated by correlating the received pilot signal. And then, a QPSK signal (reference signal) is generated in the receiver and is fed into the filter whose tap coefficients are the same as the estimated channel impulse response, and as a result, the output of the filter becomes a pseudo-received pilot signal (without data signal). Note that, in our approach, the pilot signal is sent as a PN code which is superposed on the data signal, therefore, the received pilot signal itself can not be obtained as a training signal for weight calculation. Using the pseudo-received pilot signal, the weights of the adaptive antenna array are calculated the recursive least square (RLS) algorithm [20].
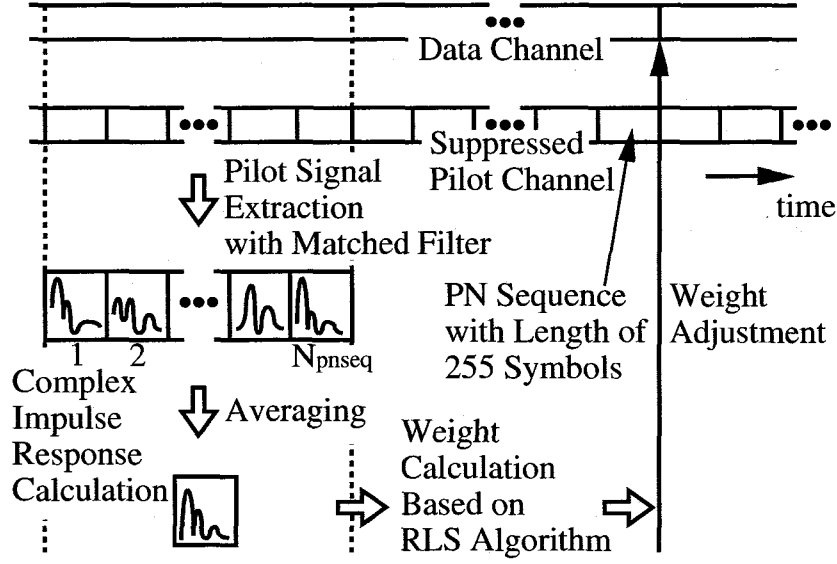
Figure 3.2: Signal Frame Structure.

3.3.2 Pilot-Assisted Channel Identification

Fig. 3.2 shows the signal frame structure of the proposed system. The length of one frame is P (the period of the PN sequence in the pilot channel) times N_{pnseq} symbols. The complex instantaneous channel impulse response at each sensor is estimated using the received pilot signals of the frame. To be concrete, the received signals first pass through the matched filter for the pilot channel, and the outputs will be N_{pnseq} complex instantaneous impulse responses, which are still distorted by the traffic channel. Furthermore, the N_{pnseq} estimated channel responses are coherently added. By means of this procedure, we can obtain a channel response, where the power of the traffic channel is sufficiently suppressed. Then in the next frame, using the estimated channel response, the reference signal generation and the calculation of the weights of the adaptive antenna array are performed by the RLS algorithm. At the end of the frame, the weights are updated and used for the processing of the traffic channel.

In the channel response estimation, the processing gain of the pilot channel G_p is given by

$$G_p = P \times N_{pnseq}. \tag{3.8}$$

However, since the power ratio of the pilot channel to the traffic channel in the transmitted signal is equal to β, the effective processing gain G_{total}, namely, the power ratio of the pilot channel to the traffic channel at the pilot channel processing in the receiver, is given by

$$G_{total} = G_p \beta = P \times N_{pnseq} \beta. \tag{3.9}$$

3.3.3 Spatial Equalization Method

In the pilot channel processing, we first estimate the channel impulse response. Let $g_l(t)$ denotes the output of the matched filter at the lth antenna element. In the proposed system, since the observation window width of the channel impulse response is equal to P symbols, the
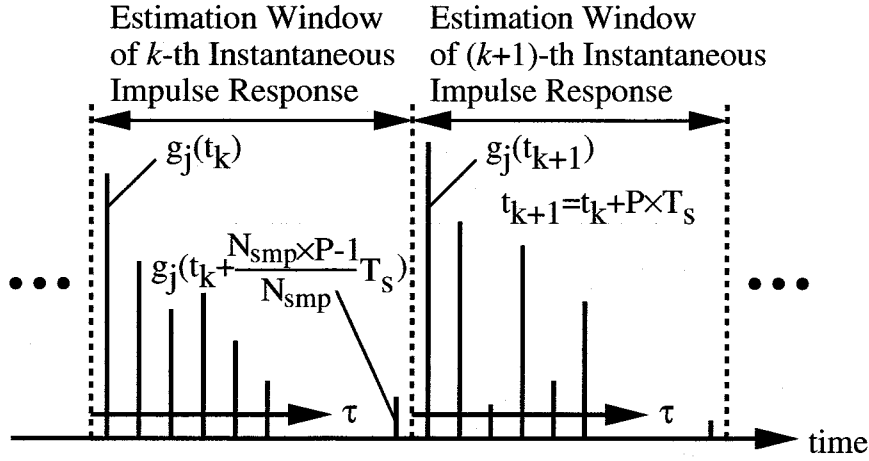
Figure 3.3: Estimated Instantaneous Impulse Response.

estimated channel impulse response at the kth estimation window can be written as

$$\hat{h}_l^k(\tau) = \sum_{i=0}^{N_{smp} \times P-1} g_l\left(t_k + i\frac{T_s}{N_{smp}}\right)\delta\left(\tau - i\frac{T_s}{N_{smp}}\right), \quad (0 \le \tau \le P \times T_s) \tag{3.10}$$

where $\hat{(\cdot)}$ denotes the estimation of $(\cdot)$.

Fig. 3.3 shows an example of the estimated impulse response. As we mentioned above, the channel impulse response is estimated using $P \times N_{pnseq}$ received pilot signals, therefore, the estimated channel impulse response at the lth antenna element $\hat{h}_l$ will be obtained by averaging out $\hat{h}_l^k(\tau)$, namely,

$$\hat{h}_l(\tau) = \frac{1}{N_{pnseq}} \sum_{k=1}^{N_{pnseq}} \hat{h}_l^k(\tau). \tag{3.11}$$

Next, we search for a path with the maximum power. In other words, defining

$$\sigma(\tau) = \sum_{l=1}^{M} |\hat{h}_l(\tau)|^2, \tag{3.12}$$

as the total power at τ, we search for $\tau = \tau_{max}$ such that $\sigma(\tau)$ is maximal. Using τ_{max}, we can estimate the channel impulse response at the lth antenna element including the path with the maximum power as

$$f_l(k) = \hat{h}_l(\tau_{max} + kT), \quad (1 \le l \le N_{ary}). \tag{3.13}$$

which has a non-zero value for k satisfying $0 \le \tau_{max} + kT_s \le P \times T_s$ and zeros otherwise.

The impulse response $f_l(k)$ is used to generate the pseudo-received pilot signal at the lth antenna element $x_l'(k)$:

$$x_l'(k) = d'(k) * f_l(k) + n_l'(k), \tag{3.14}$$

where $*$ denotes the convolution, $d'(k)$ is the QPSK (pilot) signal generated in the receiver, and $n_l'(k)$ is also the generated white Gaussian noise, whose power is equal to that of the noise in the

channel. Since the noise has all kinds of phase components and hence all DoA components, the excess beam which only captures the noise can be suppressed by the addition of the noise. The important point to note is that the proposed system requires not the accurate knowledge on noise power but the spatial whiteness of the noise for the noise suppression. This is because, unlike in the case of temporal filters, adaptive array can eliminate the delayed signals without giving large gain to any spatial frequency components. As a result, the performance of the proposed system is not sensitive to the noise power in the pseudo-received pilot signal, and we can fix the ratio of the energy per symbol to the noise power density (E_s/N_0) of the pseudo-received pilot signal, for instance, 20 dB, in advance.

As far as the weight calculation algorithm is concerned, various MMSE based algorithms are available. However, least mean square (LMS) algorithm, which is often used in constant modulus algorithm (CMA) [37], has the shortages of the slow rate of convergence and the difficulty in the selection of the step size. Attaching greater importance to the rate of convergence, we have adopted the RLS algorithm [20]. The details of the algorithm are as follows:

1. initial condition
   $w(0) = 0$
   $P(0) = p^{-1}I$ (p : minute positive number, I : $N_{ary} \times N_{ary}$ identity matrix)

2. RLS algorithm

   (a) $k = 1$

   (b) calculation of kalman gain

   $$K(k) = \frac{P(k-1)x'(k)}{\mu + x'^{*T}P(k-1)x'(k)}$$

   (c) $y(k) = x'^T w(k-1)$

   (d) calculation of error

   $$\epsilon(k) = y(k) - d'(k)$$

   (e) renewal of the weights

   $$w(k) = w(k-1) - K^*(k)\epsilon(k)$$

   (f) renewal of inverse covariance matrix

   $$P(k) = \frac{1}{\mu}P(k-1) - K(k)x'^{*T}(k)P(k-1)$$

Table 3.1: System Parameters.

# of sensors N_{ary}	4
Symbol rate R_s	100 Msymbol/sec
Mod./Demod. Scheme	QPSK
Oversampling factor N_{smp}	4
Carrier frequency f_c	60 GHz
Roll-off factor α	0.5
Period of the M-sequence P	255 symbols
Repetitions of the RLS algorithm	50

(g) $k = k + 1$, return to (b)

where μ denotes the forgetting factor.

3.3.4   Computer Simulation

Computer simulations are conducted to evaluate the performance of the proposed spatial equalizer. Parameters used in all the simulations are summarized in Table 3.1. Considering indoor wireless environments, DoAs of incoming signals will be distributed from 0° to 360°, therefore, we adopted not a linear array, whose beamforming ability significantly degrades for a particular direction, i.e., parallel to the linear array, but a circular array (with 4 elements), which can achieve almost uniform beamforming performance for all directions. Also, we adopt a root Nyquist filter with roll-off factor α of 0.5 as the LPF in the transmitter and receiver, the symbol rate R_s of 100 Msymbol/sec, the oversampling factor N_{smp} of 4, the period of M-sequence P of 255 symbols, and the carrier frequency f_c of 60 GHz. The number of repetitions of the RLS algorithm is chosen to be 50.

The indoor channel can be modeled by a frequency selective fading channel [38]. Fig. 3.4 shows the frequency selective fading channel models when the direct wave is scattered by obstacles around the receiver and the delayed waves are reflected by the wall surface. In the models, there are four primary waves and two 4-symbol delayed waves. On the other hand, Fig. 3.5 shows channel models, where one primary wave and two delayed waves with 2- and 4-symbol delays exist, to discuss the performance of the propose equalizer comparing with that of the CMA method. In all the channel models, taking account of an indoor environment and assuming the speed of human walk around the receiver to be 2.7 km/h, we have used the Doppler spectrum of flat and the maximum Doppler shift of 150 Hz.

Since the data signal and the pilot signal in the proposed system are not orthogonal, in other words, the pilot signal can be considered to be a co-channel interference, the performance depends on the power suppression ratio β of the pilot channel and the number of coherent additions N_{pnseq} after the correlation. Thus, we discuss these values first. In the proposed system, it is found from Eq. (3.9) that if β or N_{pnseq} increases, the measurement accuracy of the channel impulse response is improved. However, it is more efficient to make β smaller and N_{pnseq} larger from the viewpoint of power efficiency, whereas it is preferable to make β larger and
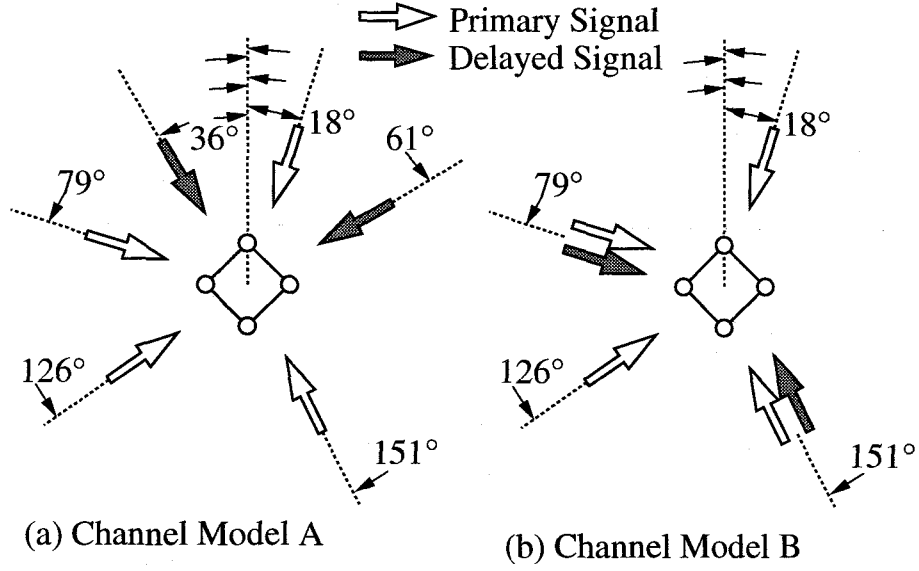
Figure 3.4: Channel Model A and B.

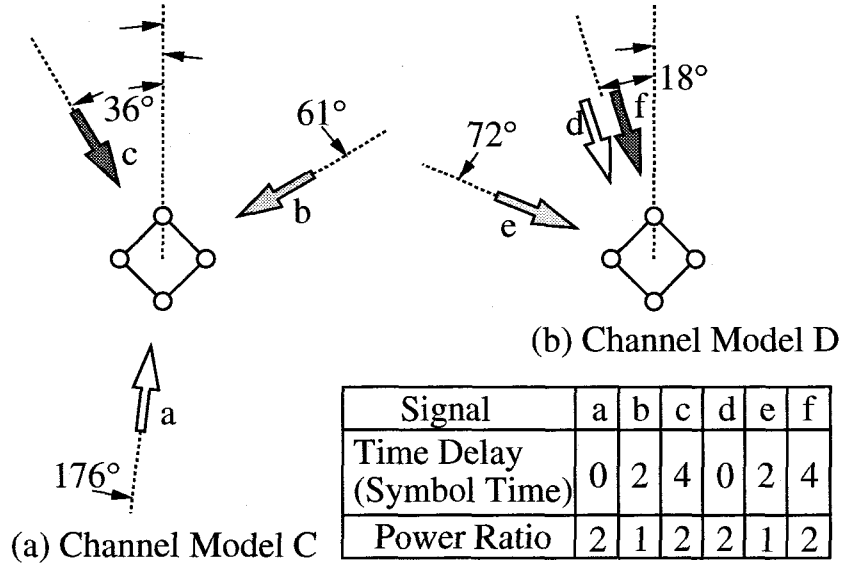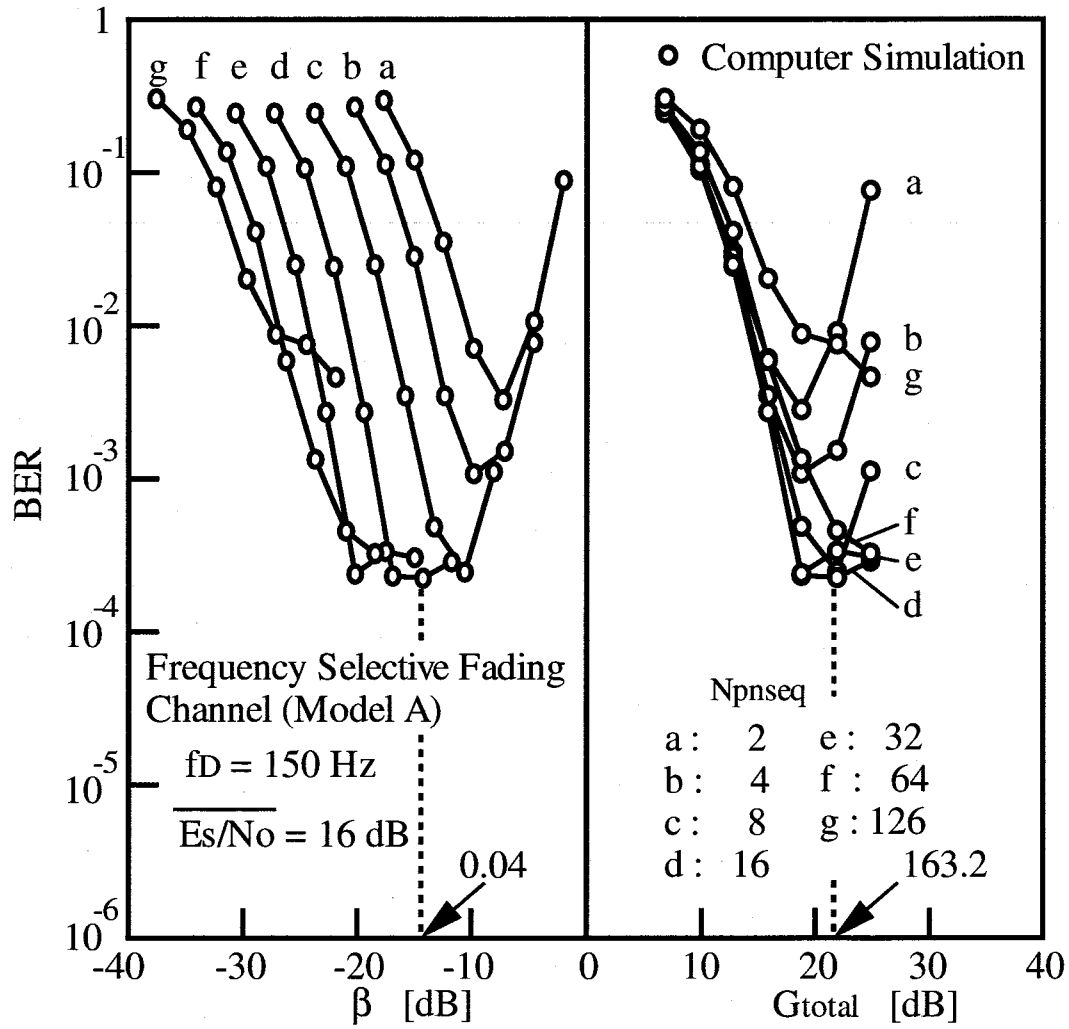| Signal	a	b	c	d	e	f
Time Delay (Symbol Time)	0	2	4	0	2	4
Power Ratio	2	1	2	2	1	2

Figure 3.5: Channel Model C and D.

N_{pnseq} smaller from the viewpoint of tracking of fading variations. Therefore, it is considered that there is an optimum point in β and N_{pnseq} to maximize the performance. Fig. 3.6 shows the BER versus β and G_{total} for several values of N_{pnseq}, when we assume the channel model A with $\overline{E_s/N_0}$=16 dB, where $\overline{(\cdot)}$ denotes the average of $(\cdot)$. Here, note that E_s includes both the user signal and the pilot signal unlike the theoretical equation (Eqs. (3.15)-(3.17)). Hereafter, we use this new definition of E_s. The performance is poor for large β, because the power assigned to the traffic channel becomes smaller, whereas the BER degrades for smaller β, because the measurement accuracy of the channel impulse response becomes poor. From this figure, we have selected N_{pnseq}=16 and β=0.04 as the optimum values, which correspond to G_p=4,080

Figure 3.6: BER vs. β and G_{total}.

and $G_{total}=163.2$.

When the BER characteristics are evaluated, it is considered effective to compare the results with the theoretical BER of diversity reception, or to confirm how many branches as diversity gain the results correspond to. Assuming the average power of each signal is the same and the envelope follows a Rayleigh distribution, the BER of QPSK in the case of the L branch maximum ratio combining diversity is given [2],

$$BER = \left(\frac{1-\mu}{2}\right)^L \sum_{k=0}^{L-1} {}_{L-1+k}C_k \left(\frac{1+\mu}{2}\right)^k, \qquad (3.15)$$

$$\mu = \sqrt{\frac{\overline{\gamma_s}/2}{1+\overline{\gamma_s}/2}}, \qquad (3.16)$$

where $\overline{\gamma_s}$ is E_s/N_0. On the other hand, the BER in an additive white Gaussian noise (AWGN) channel is given by the following [2],

$$BER = \frac{1}{2}erfc\left(\sqrt{N_{ary} \cdot \gamma_s/2}\right), \qquad (3.17)$$
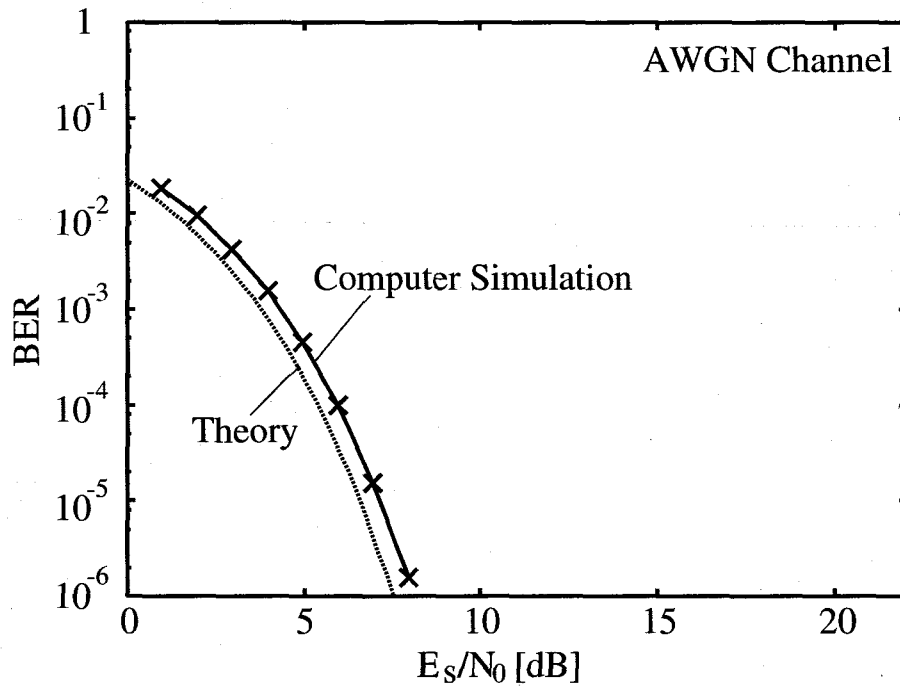
Figure 3.7: BER Performance in AWGN Channel.

where $erfc(\cdot)$ is the complementary error function. Note that γ_s is multiplied by the number of sensor.

Fig. 3.7 shows the BER versus E_s/N_0 in the AWGN channel. We can recognize about 1 dB degradation from the theoretical line. This may be because of the insertion of the pilot channel, and the error in the channel impulse response estimation or in the spatial and temporal weights calculation. The effect of the four times over sampling also may be the cause of the degradation. However, as we can see from Fig. 3.6, both of the first two degradation sources, i.e., the insertion of the pilot channel and the error in the channel identification, severely affect the BER performance.

In Fig. 3.8, the BER performances of the proposed system, the CMA method, and the receiver without an antenna array are shown for the channel model A. For reference, the theoretical BER of the 4-branch maximum ratio combining diversity is shown in the same figure. The CMA method is capable of pilot-free beamforming (beamforming without known pilot signal), however, in order to compare the performance with that of the proposed equalizer, the same pseudo received pilot signal as the proposed equalizer is used for the weights calculation. Also, though the CMA method often utilizes the LMS algorithm for the weights calculation, the RLS algorithm, where the cost function is referred to [37] ($p = 1$, $q = 2$), is employed. From the figure, it is found that the BER performance is significantly degraded by the frequency selective fading channel if no adaptive antenna array is employed while an excellent BER of 4 in terms of the number of diversity branches is obtained in the proposed equalizer. Furthermore, the proposed equalizer outperforms the CMA method. This is because the CMA method can not always combine the received signal as to be the maximum ratio combining, while the proposed equalizer can form the beam in such a way that the received signal power is always maximized.
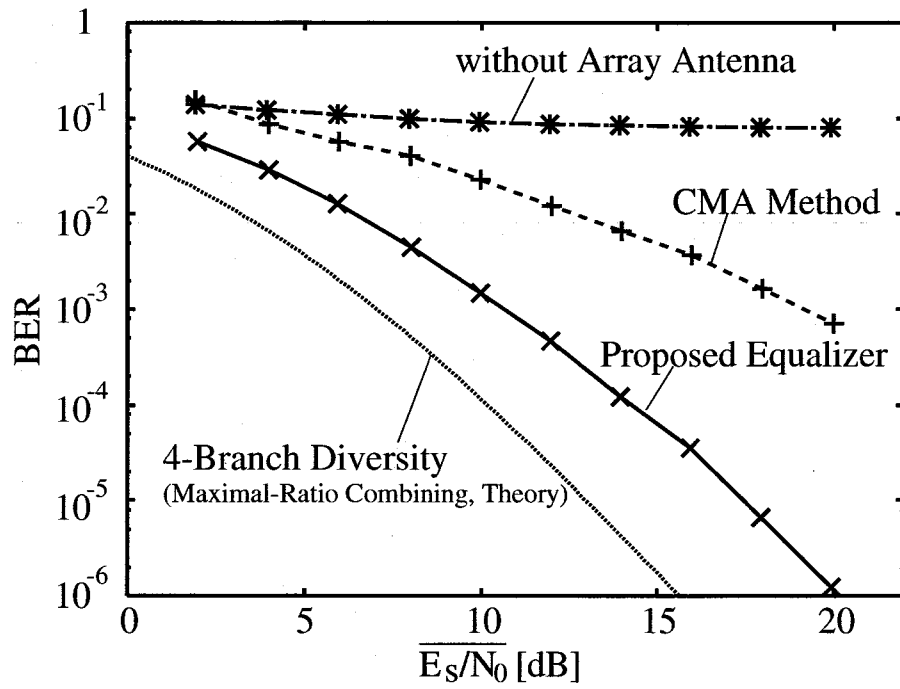
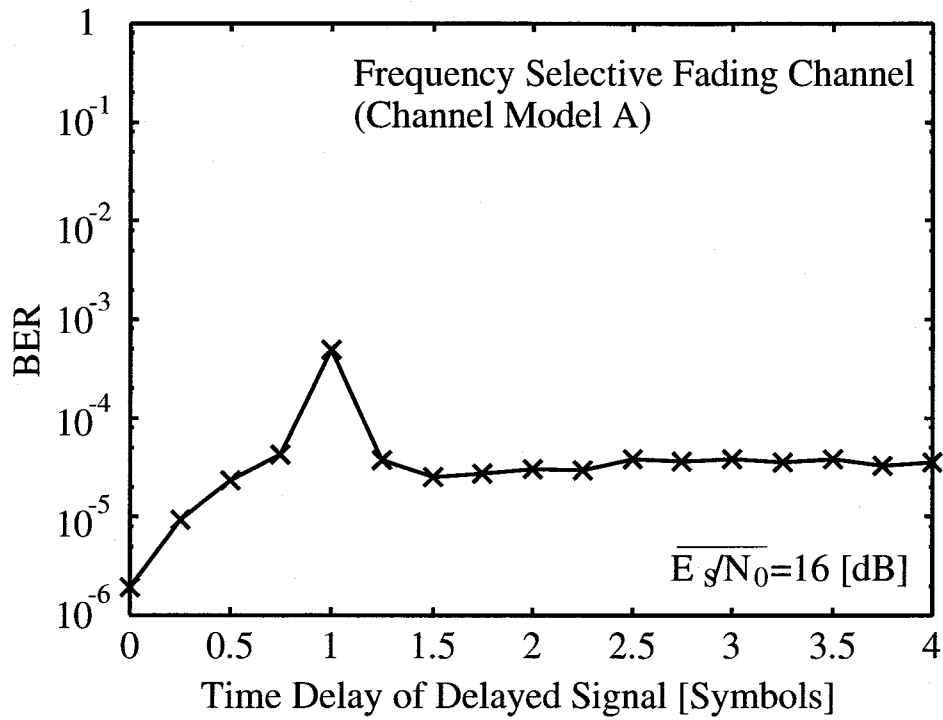Figure 3.8: BER Performance in Channel Model A.

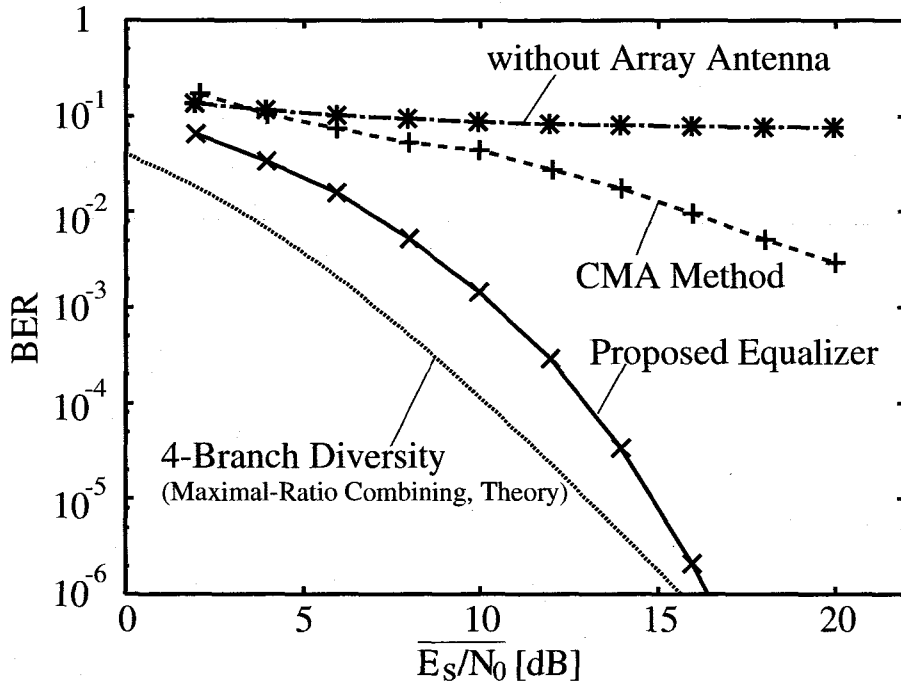Figure 3.9: BER vs. Time Delay of Delayed Signal.

Figure 3.10: BER Performance in Channel Model B.

Fig. 3.9 shows the BER of the proposed equalizer versus the time delay of the delayed waves for the channel model A when the $\overline{E_s/N_0}$ is fixed to 16 dB. From the figure, we can see that the BER does not depend on the time delay. This proves that the adaptive antenna array is suited for high-speed communications systems.

The BER performances in the channel model B are shown in Fig. 3.10. The channel model B is almost the same as the channel model A except for the DoAs of the delayed waves. In the channel model B, the delayed waves have the same DoAs as the primary waves, therefore, it is expected that the BER performance is poorer than the one in the channel model A. However, in practice, the proposed equalizer achieves an excellent BER with about 4 in terms of the diversity branches. This is because the delayed signal components are eliminated by canceling each other in the combining instead of pointing nulls toward the delayed signals if there are several signals arriving with the same time delay.

Let us discuss the difference of the operation between the proposed spatial equalization method and the CMA method by using the channel models C and D. Fig. 3.11 shows the BER performances corresponding to the channel models. Here, note that the methods can equalize up to a four-wave model basically, since the adaptive antenna arrays have four sensors, and a good performance should be obtained for a three-wave model. In the channel model C, where three waves are arriving from various directions, both the proposed equalizer and the CMA method can obtain a good performance. Especially, the proposed equalizer can achieve a diversity gain of 4 in terms of the number of branches. On the other hand, in the channel model D, which is also a three-wave model, the performance of the proposed equalizer is significantly degraded while the CMA method can achieve a good performance. In the channel model, the primary wave d and the delayed wave f are arriving from the same direction, and the composite
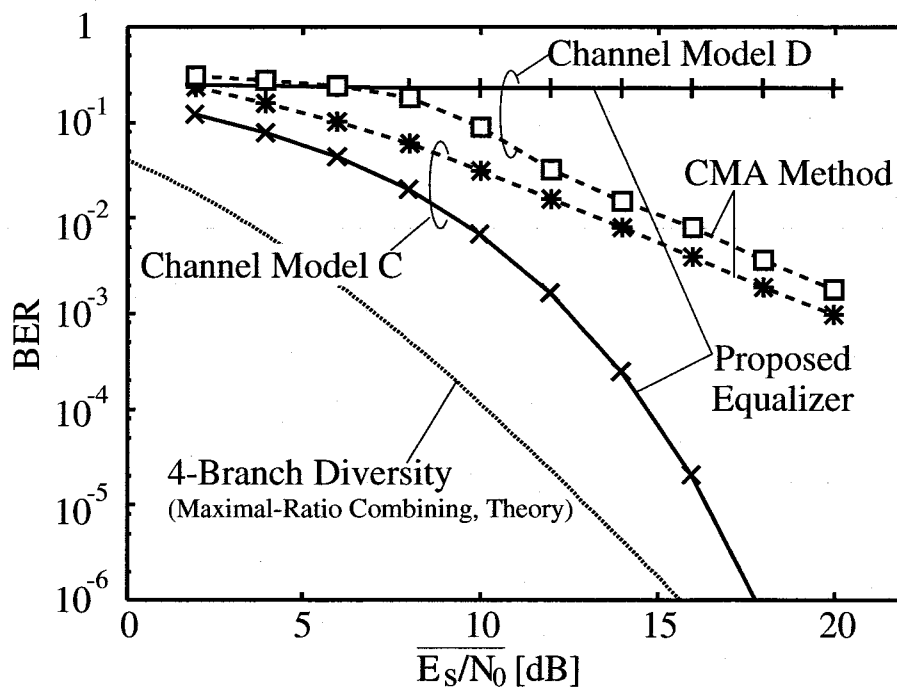
Figure 3.11: BER Performance in Channel Model C and D.

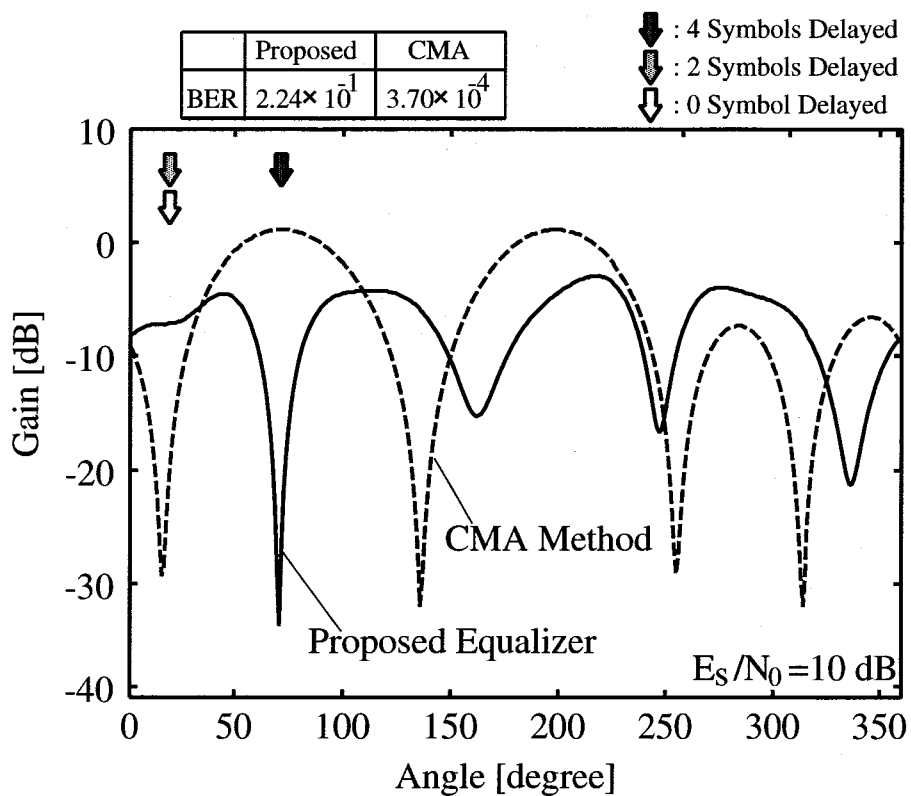|	Proposed	CMA
BER	2.24×10^{-1}	3.70×10^{-4}

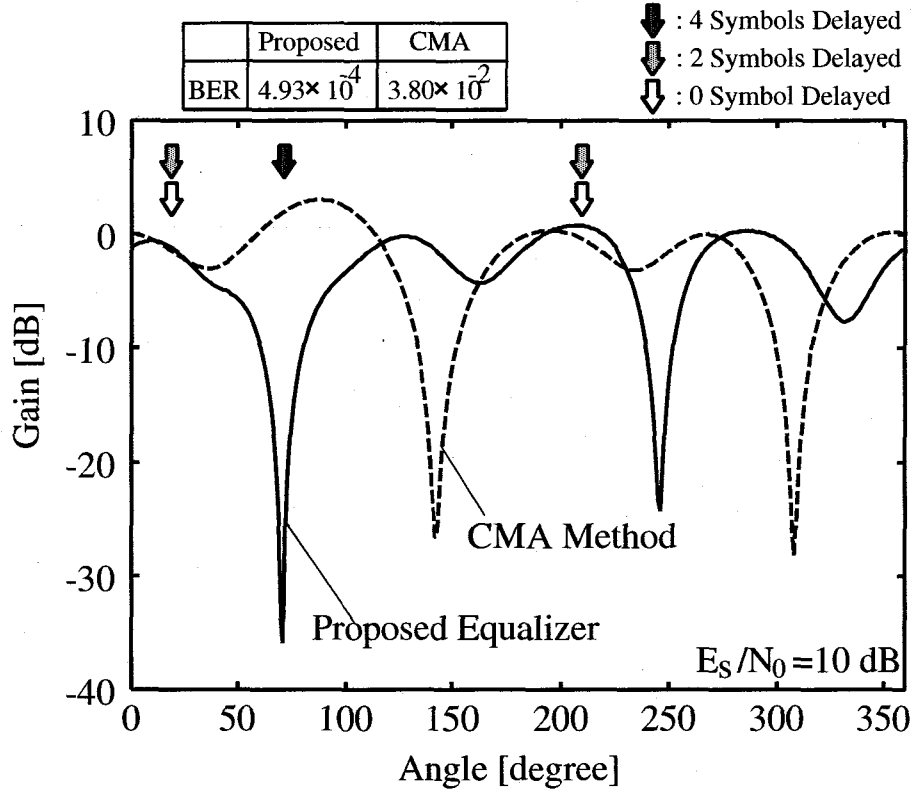Figure 3.12: Antenna Beam Pattern (a).

Figure 3.13: Antenna Beam Pattern (b).

wave of d and f does not become a constant envelope. Therefore, the adaptive antenna array captures the incoming wave e in the CMA method. In contrast, the proposed equalizer always tries to capture the path with the maximum power, namely, the primary wave d in this case. Therefore, the beam is directed toward the primary wave d and the delayed wave f. As a result, the BER is degraded due to the intersymbol interference.

Finally, the difference in operation between the proposed spatial equalizer and the CMA method is analyzed from a viewpoint of the antenna beam pattern. The antenna patters are shown in Figs. 3.12-3.14. Here, the primary wave and the 2- and the 4-symbol delayed waves, which have the same amplitude, are arriving. Also, no fading is taken into account. In Fig. 3.12, where the primary wave and the 2-symbol delayed wave are arriving from the direction of $18°$ while the 4-symbol delayed wave from the direction of $72°$, the beam is oriented in the direction of $72°$ in the CMA method and in the direction of $18°$ in the proposed spatial equalization method. Therefore, the BER by the CMA method is superior to the proposed method. In Fig. 3.13, in addition to the arriving waves in Fig. 3.12, a primary wave and a 2-symbol delayed waves are arriving in the direction of $209°$. In this case, the proposed equalizer forms a null in the direction of $72°$ and beams in the directions of $18°$ and $209°$ so that either the primary waves or the delayed waves are cancelled. That is why the proposed equalizer can achieve a good performance. On the other hand, the BER of the CMA method is degraded since the method tries to combine the signals arriving from three directions to make the envelope of the received signal constant in some computer simulation trials. This means that the CMA method has a fundamental difficulty in the selection of initial values of the weights. In Fig. 3.14, a primary
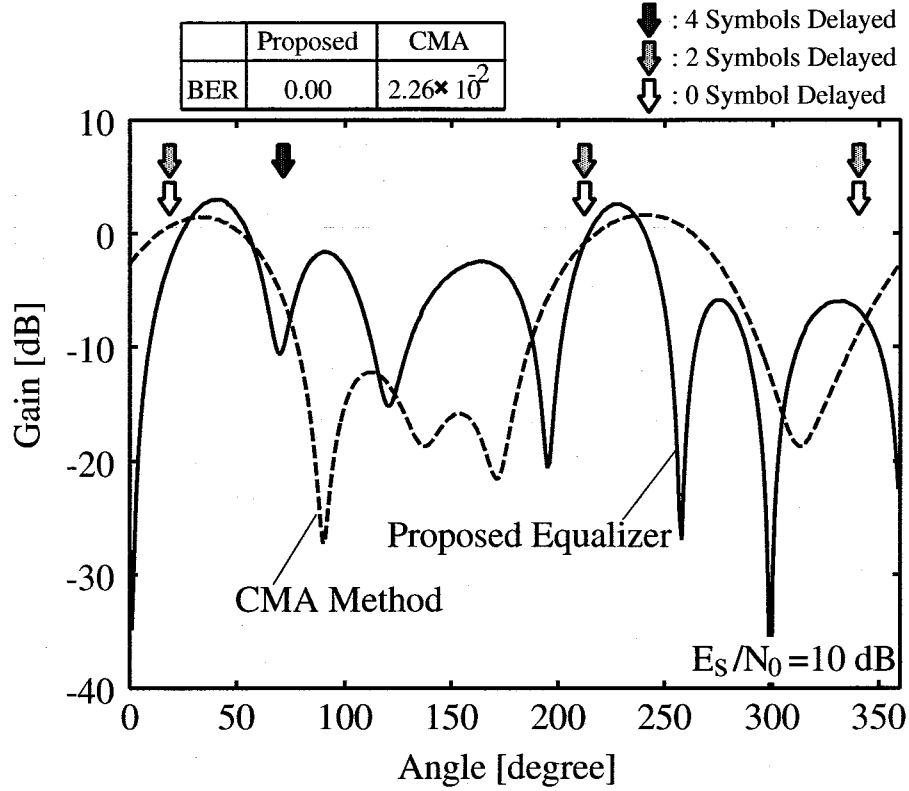
Figure 3.14: Antenna Beam Pattern (c).

wave and a 2-symbol delayed wave are arriving from the direction of 342° in addition to the arrival pattern in Fig. 3.13. In this case, the proposed equalizer forms a null in the direction of 72° and beams in the directions of 18°, 209° and 342° so that either the primary waves or the delayed waves are cancelled as in the previous case. Also, with the beam pattern, the proposed equalizer can achieve a lower BER than the CMA method.

3.4 Pilot-Free Spatial Equalizer

3.4.1 System Configuration

Fig. 3.15 shows the transmitter/receiver structure of the pilot-free spatial equalizer. In the transmitter, data sequence (R_b bit/sec) is first differentially encoded, and then it is converted into QPSK waveform ($R_s(=R_b/2)$ symbol/sec). The baseband signal passes through the LPF, i.e., emission filter, and finally is transmitted from an omnidirectional antenna after up-conversion. In the receiver, the incoming signal is received by an antenna array which has N_{ary} sensors. The received signal undergoes the BPF, the down-converter, the LPF, and the A/D converter. The BPF is used for the suppression of the adjacent channel interference and noise as well as for the extraction of the spectrum around desired signal. The sampling rate of the A/D converter is four times the symbol rate. Next, the received signal is processed in the data signal processing and in the pilot-free signal processing independently. In the data signal processing, the outputs from the matched filter are multiplied by the weights of the
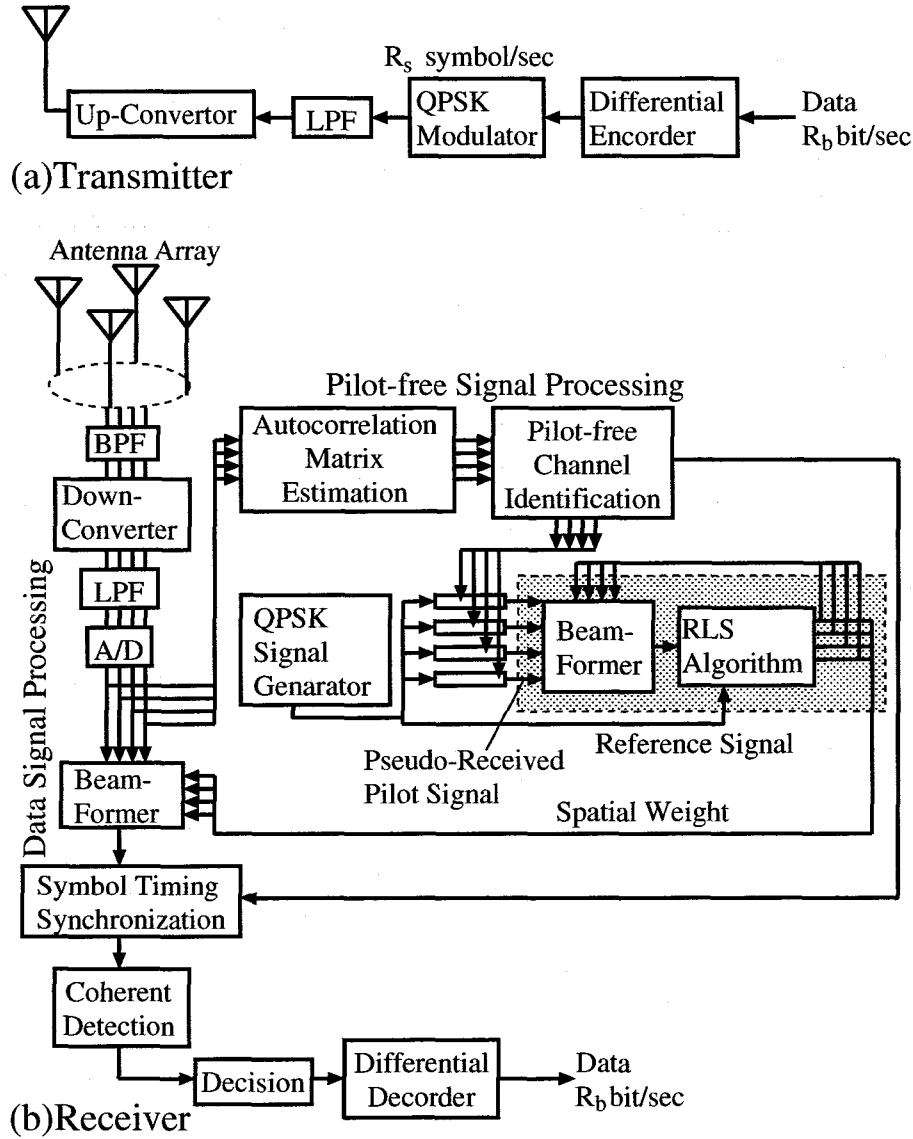
Figure 3.15: Transmitter/Receiver Structure.

adaptive antenna array which are calculated in the pilot-free signal processing. After symbol timing synchronization and coherent demodulation, the data are differentially decoded. In the pilot-free signal processing, the ensemble averaged autocorrelation matrix of the received signal is replaced by the time averaged matrix. Since the autocorrelation matrix is estimated at each sensor, N_{ary} correlation matrices are obtained. Using the correlation matrices, the complex instantaneous impulse response of the channel at each antenna element is estimated by performing second-order statistics-based pilot-free channel identification. Details of the channel identification algorithm are discussed in 3.4.2. With the estimated channel response, the weights of adaptive antenna array are calculated in the same way as the spatial equalizer proposed in section 3.3.

Fig. 3.16 shows the signal frame structure of the pilot-free spatial equalizer. The length of one frame is N (the number of symbols used in calculation of the autocorrelation matrix)
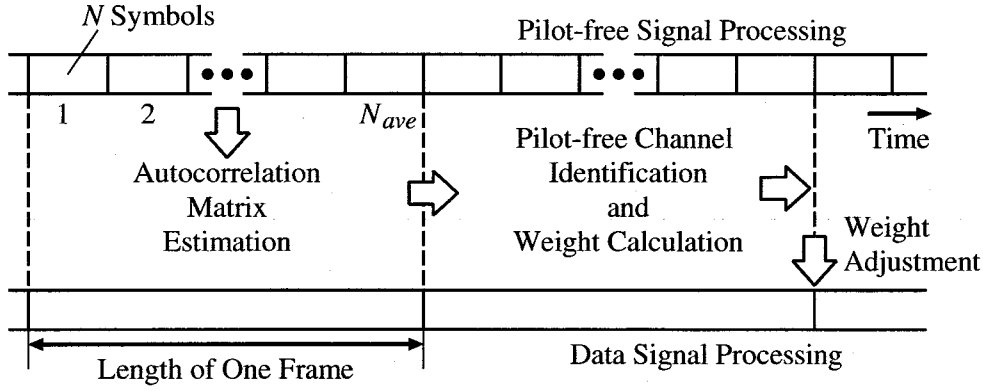
Figure 3.16: Signal Frame Structure.

times N_{ave} (the number of averaging times of autocorrelation matrix estimation) symbols. The autocorrelation matrix of the received signal is estimated using the received signal in the first frame, and during the next frame, the pilot-free channel identification and the calculation of the weights with the RLS algorithm are performed. Finally, at the end of the frame, the weights of the adaptive antenna array are updated.

3.4.2 Pilot-Free Channel Identification

The algorithm described here is mainly based on the method proposed in [26]. However, we have given some modifications to apply it to practical wireless communications situations. In what follows, we assume that the channel at the jth sensor can be modeled as an FIR filter whose impulse response is $h_j(t)$. Note that, $h_j(t)$ includes the effect of the emission filter, the channel response, the antenna response, and matched filter.

Let T, d_n, and $v_j(t)$ denote the symbol duration, the symbol emitted by the digital source at time nT and additive noise at the jth sensor, respectively. The output of the matched filter at time t is given by

$$x_j(t) = \sum_{m=-\infty}^{\infty} d_m h_j(t - mT) + v_j(t). \tag{3.18}$$

For the pilot-free channel identification based on the second-order statistics, several measurements have to be made during sampling period T. This requirement can be satisfied by oversampling the incoming signal which is received by antenna array. Oversampling $x_j(t)$ with a sampling period $\Delta(= t/4)$ constructs a set of $L \times N_{ary}(L = T/\Delta)$ sequences according to $x_n^{(i,j)} = x_j(t_0 + i\Delta + nT)$ for $0 \le i \le L - 1$, $1 \le j \le N_{ary}$. Assuming that the channel can be modeled FIR filter, $h_j(t)$ has finite duration M, therefore, we can write $x_n^{(i,j)}$ in the form,

$$x_n^{(i,j)} = \sum_{m=0}^{M} d_{n-m} h_m^{(i,j)} + v_n^{(i,j)}, \tag{3.19}$$

where

$$v_n^{(i,j)} = v_j(t_0 + i\Delta + nT), \tag{3.20}$$

$$h_n^{(i,j)} = h_j(t_0 + i\Delta + nT). \tag{3.21}$$

Using $h_j^{(i)}(n)$, we can write the discrete-time channel impulse response in the vector form,

$$H = [H_0, \cdots, H_{N_{ary}}]^T, \tag{3.22}$$

$$H_j = [H_j^{(0)}, \cdots, H_j^{(L-1)}]^T, \tag{3.23}$$

$$H_j^{(i)} = [h_0^{(i,j)}, \cdots, h_M^{(i,j)}]^T, \tag{3.24}$$

where $[\cdot]^T$ denotes the transpose. If we gather N successive samples of $x_n^{(i,j)}$, we will have a matrix formulation:

$$X_n^{(i,j)} = \mathcal{H}_N^{(i,j)} D_n + V_n^{(i,j)}, \tag{3.25}$$

where

$$X_n^{(i,j)} = [x_n^{(i,j)}, \cdots, x_{n-N+1}^{(i,j)}]^T, \quad (N \times 1) \tag{3.26}$$

$$D_n = [d_n, \cdots, d_{n-N-M+1}]^T, \quad ((N+M) \times 1) \tag{3.27}$$

$$V_n^{(i,j)} = [v_n^{(i,j)}, \cdots, v_{n-N+1}^{(i,j)}]^T, \quad (N \times 1) \tag{3.28}$$

$$\mathcal{H}_N^{(i,j)} = \begin{bmatrix} h_0^{(i,j)} & \cdots & h_M^{(i,j)} & & 0 \\ & \ddots & & \ddots & \\ 0 & & h_0^{(i,j)} & \cdots & h_M^{(i,j)} \end{bmatrix}. \quad (N \times (N+M)) \tag{3.29}$$

Putting a set of L sequences together will yield

$$X_n^{(j)} = \mathcal{H}_N^{(j)} D_n + V_n^{(j)}, \tag{3.30}$$

where

$$X_n^{(j)} = [X_n^{(0,j)T}, \cdots, X_n^{(L-1,j)T}]^T, \quad (NL \times 1) \tag{3.31}$$

$$V_n^{(j)} = [V_n^{(0,j)T}, \cdots, V_n^{(L-1,j)T}]^T, \quad (NL \times 1) \tag{3.32}$$

$$\mathcal{H}_N^{(j)} = [\mathcal{H}_N^{(0,j)T}, \cdots, \mathcal{H}_N^{(L-1,j)T}]^T. \quad (NL \times (N+M)) \tag{3.33}$$

Furthermore, putting a set of N_{ary} matrices together will yield

$$X_n = \mathcal{H}_N D_n + V_n, \tag{3.34}$$

where

$$X_n = [X_n^{(0)T}, \cdots, X_n^{(N_{ary}-1)T}]^T, \quad (NLN_{ary} \times 1) \tag{3.35}$$

$$V_n = [V_n^{(0)T}, \cdots, V_n^{(N_{ary}-1)T}]^T, \quad (NLN_{ary} \times 1) \tag{3.36}$$

$$\mathcal{H}_N = [\mathcal{H}_N^{(0)T}, \cdots, \mathcal{H}_N^{(N_{ary}-1)T}]^T. \quad (NLN_{ary} \times (N+M)) \tag{3.37}$$

The second-order statistics based pilot-free identification algorithm include subspace decomposition of autocorrelation matrix R_x of vector X_n. R_x can be described as

$$
\begin{aligned}
R_x &= E[X_n X_n^H] \\
&= \mathcal{H}_N R_d \mathcal{H}_N^H + R_v, \quad (NLN_{ary} \times NLN_{ary})
\end{aligned}
\tag{3.38}
$$

where $R_d = E[D_n D_n^H]$ $((N+M)\times(N+M))$ and $R_v = E[V_n V_n^H]$ $(NLN_{ary} \times NLN_{ary})$. R_v denotes the autocorrelation matrix of additive noise vector V_n and is noise part of R_x. This noise part has to be in the shape of (constant) $\times I$ $(NLN_{ary} \times NLN_{ary}$ identity matrix) in order to decompose R_x into subspace. However, in practical wireless communication system, the noise obtained at the matched filter output is no longer white. In this case, pre- and post-multiplying the noise whitening matrix $W_v(= R_v^{-1/2}$ [39] (see Appendix A)) leads to

$$
\begin{aligned}
W_v R_x W_v^H &= W_v \mathcal{H}_N R_d \mathcal{H}_N^H W_v^H + W_v R_v W_v^H \\
&= W_v \mathcal{H}_N R_d \mathcal{H}_N^H W_v^H + \sigma^2 I,
\end{aligned}
\tag{3.39}
$$

where σ^2 denotes a variance of additive noise at the front end of the receiver. Let $\underline{R}_x = W_v R_x W_v^H$ and $\underline{\mathcal{H}}_N = W_v \mathcal{H}_N$, then we have

$$
\underline{R}_x = \underline{\mathcal{H}}_N R_d \underline{\mathcal{H}}_N^H + \sigma^2 I.
\tag{3.40}
$$

This is a desired form.

Let $\lambda_0 \geq \lambda_1 \geq \cdots \geq \lambda_{NL-1}$ denote the eigenvalues of whitened correlation matrix $\underline{R}_x$, and $\nu_0 \geq \nu_1 \geq \cdots \geq \nu_{NL-1}$ dente the eigenvalues of the matrix $\underline{\mathcal{H}}_N R_d \underline{\mathcal{H}}_N^H$. Since we assume $\underline{\mathcal{H}}_N$ is full column rank and R_d is full-rank, the matrix $\underline{\mathcal{H}}_N R_d \underline{\mathcal{H}}_N^H$ has rank $M + N$. This implies that the $NL-M-N$ smallest eigenvalues $\nu_i = 0$. Correspondingly, the smallest eigenvalue of the correlation matrix $\underline{R}_x$ is equal to σ^2 with multiplicity $NL-M-N$, as shown by

$$
\lambda_i = \begin{cases} \nu_i + \sigma^2, & 0 \leq i \leq M + N - 1 \\ \sigma^2. & M + N \leq i \leq NL - 1 \end{cases}
\tag{3.41}
$$

Let $\underline{G}_0, \cdots, \underline{G}_{NL-M-N-1}$ denote unite-norm eigenvectors associated with the eigenvalues $\lambda_{M+N}, \cdots, \lambda_{NL-1}$. Furthermore, let $G = [G_0, \cdots, G_{NL-N-M-1}]$ $(NL\times(NL-N-M))$. All G_i satisfy the relation

$$
\underline{R}_x \underline{G}_i = \sigma^2 \underline{G}_i. \quad 0 \leq i \leq NL - N - M - 1
\tag{3.42}
$$

Using Eq. (3.40), we can rewrite Eq. (3.42) as

$$
\underline{\mathcal{H}}_N R_d \underline{\mathcal{H}}_N^H \underline{G}_i = 0, \quad 0 \leq i \leq NL - N - M - 1
\tag{3.43}
$$

Since $\underline{\mathcal{H}}_N$ is assumed to be of full column rank and the matrix R_d is full-rank, it follows from Eq. (3.43) that

$$
\underline{\mathcal{H}}_N^H \underline{G}_i = 0. \quad 0 \leq i \leq NL - N - M - 1
\tag{3.44}
$$

Substituting $\underline{\mathcal{H}}_N = W_v \mathcal{H}_N$ for Eq. (3.44), we have

$$
G_i^H \mathcal{H}_N = 0, \quad 0 \leq i \leq NL - N - M - 1
\tag{3.45}
$$

where $G_i = W_v^H \underline{G}_i$. Eq. (3.45) implies that G_i is orthogonal to the channel impulse response matrix.

In practice, we can not get real ensemble averaged autocorrelation matrix R_x. We have to base our analysis on time averaged correlation matrix $\hat{R}_x$ instead. $\hat{R}_x$ is described by

$$\hat{R}_x = \sum_{i=0}^{N_{ave}} X_{n+iN} X_{n+iN}^H. \tag{3.46}$$

Strictly speaking, the left side of Eq. (3.45) unequal to zero since only estimates $\hat{G}_i$ of the eigenvectors are available, however, Eq. (3.45) can be solved in least squares sense. The cost function is defined as

$$q(H) = \sum_{i=0}^{NL-N-M-1} |\hat{G}_i^H \mathcal{H}_N|^2, \tag{3.47}$$

where H is the discrete-time channel impulse response defined in Eqs. (3.22), (3.23). As a matter of convenience, it is preferable that the right side of Eq. (3.47) is expressed in terms of H. On that account, we separate the elements of the estimated eigenvectors $\hat{G}_i$ into L components, as shown by

$$\hat{G}_i^T = [\hat{G}_{i0}^T, \hat{G}_{i2}^T, \cdots, \hat{G}_{i(L-1)}^T], \tag{3.48}$$

where $\hat{G}_{ij}^T$ $(0 \leq j \leq L-1)$ are vectors of length N. Furthermore, we define the $ML \times (N+M)$ matrix $\hat{g}_i$ as

$$\hat{g}_i = \begin{bmatrix} \hat{G}_{i0}^T & & 0 \\ & \ddots & \\ 0 & & \hat{G}_{i0}^T \\ & \vdots & \\ \hat{G}_{i(L-1)}^T & & 0 \\ & \ddots & \\ 0 & & \hat{G}_{i(L-1)}^T \end{bmatrix}. \tag{3.49}$$

Since $\hat{G}_i^H \mathcal{H}_N = H^H \hat{g}_i$, we can rewrite Eq. (3.47) as

$$q(H) = H^H Q H, \quad Q = \sum_{i=0}^{NL-M-N-1} \hat{g}_i \hat{g}_i^H. \tag{3.50}$$

According to constraints on H, there are some schemes for the decision of H. We adopted quadratic constraint, that is, minimize $q(H)$ subject to $|H| = 1$. The solution is the unit-norm eigenvector associated with the smallest eigenvalue of matrix Q.

3.4.3 Computer Simulation

Fig. 3.17 shows the channel model discussed in this section. This is a static two ray multipath channel model where there are one primary wave and a 4-symbol delayed wave. The power of these two incoming signals is the same. For the simplicity of the discussion, no fading is taken into account.

System parameters used in the computer simulations are shown in table3.2. The pilot-free spatial equalizer adopts a root Nyquist filter with roll off factor of 0.5 as the LPF in the transmitter and receiver. The window width N is chosen to be 15 and the length of FIR filter
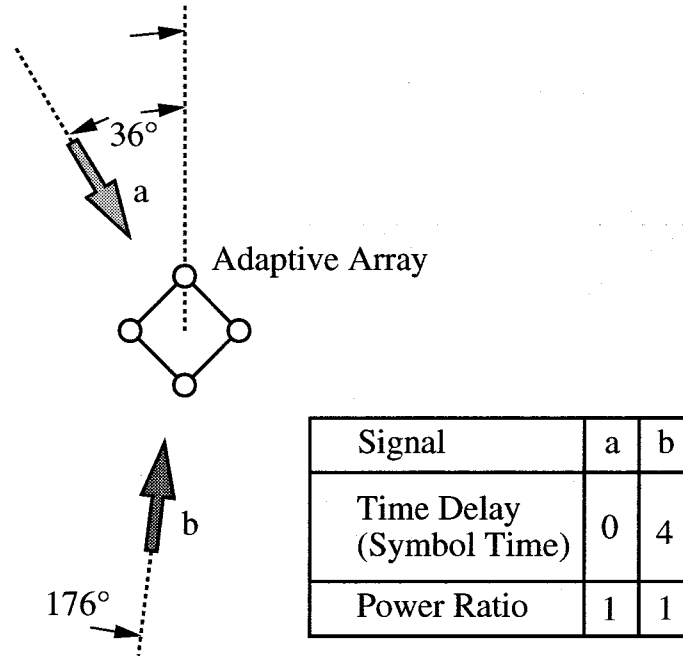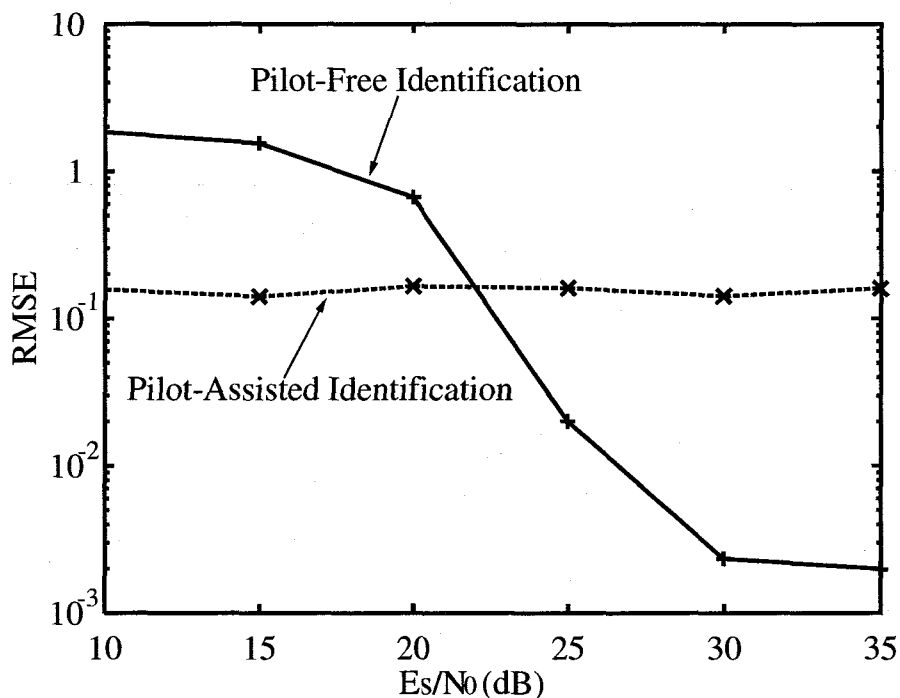
Figure 3.17: Channel Model.

Table 3.2: System Parameters.

# of sensors N_{ary}	4
Symbol rate R_s	100 Msymbol/sec
Mod./Demod. Scheme	DQPSK
Oversampling factor N_{smp}	4
Carrier frequency f_c	60 GHz
Roll-off factor α	0.5
Window width N	15 symbols
Frame Length	4080 symbols
Repetitions of the RLS algorithm	50

(the channel) to be 9. The number of averaging times of correlation matrix is equal to 272, namely, the length of one frame becomes 4080 symbols, and in the estimation of the correlation matrix, the time averaging is performed over 4080 symbols. The number of repetitions of the RLS algorithm is chosen to be 50.

Fig. 3.18 shows the root mean-squared-error (RMSE) of the pilot-free channel identification method versus the (E_s/N_0). The RMSE of the pilot-assisted method proposed in section 3.3 is also plotted in the same figure. Denoting $f_j(k)$ and $\hat{f}_j^l(k)$ as the true and the estimated impulse responses of the channel of at the jth antenna element in the lth trial, respectively, the RMSE is defined as

$$RMSE = \frac{1}{\sum_{i=0}^{N_{ary}-1}||f_i(k)||}\sqrt{\frac{1}{N_{trial}}\sum_{l=0}^{N_{trial}-1}\sum_{j=0}^{N_{ary}-1}||\hat{f}_j^l(k) - f_j(k)||^2}, \qquad (3.51)$$

Figure 3.18: Estimation Error vs. E_s/N_0.

where $||\cdot||$ and N_{trial} denote the Euclidean norm and the number of trials (100 in this simulation). The RMSE of the pilot-assisted method does not depend on E_s/N_0. This is because the noise is almost negligibly small in this E_s/N_0 region, and the autocorrelation property of the M-sequence limits the estimation. On the other hand, the RMSE of the pilot-free estimator decreases suddenly around $E_s/N_0 = 20$ dB. Therefore the performance of the pilot-free system could be superior to that of the pilot-assisted method when E_s/N_0 becomes over around 23 dB.

Fig. 3.19 shows the BER performance in the channel model. For the comparison purpose, the BER performances of the pilot-assisted spatial equalizer and the CMA method are also plotted in the same figure. The pilot-assisted spatial equalizer can achieve the best performance among the three spatial equalizers, however, it requires a known pilot signal. The CMA method, which also works in a pilot-free manner, suffers from slow rate of convergence, since the sample size is too small for the CMA method. This is the reason why the BER of the CMA method improves slowly as the E_s/N_0 increases. The BER of the pilot-free spatial equalizer decreases suddenly around $E_s/N_0 = 20$ dB, while the performance is poor at low E_s/N_0. This agree with what we have seen in Fig. 3.18. Since the pilot-free spatial equalizer employs the same weights calculation method as the pilot-assisted method, the degradation of the BER performance of the pilot-free spatial equalizer will be mainly caused by the error in the channel impulse response estimation.

3.5 Summary

In this chapter, in order to avoid two-step procedure of weights calculation and to make it easy to extend to a spatial and temporal equalization, we have proposed spatial equalization
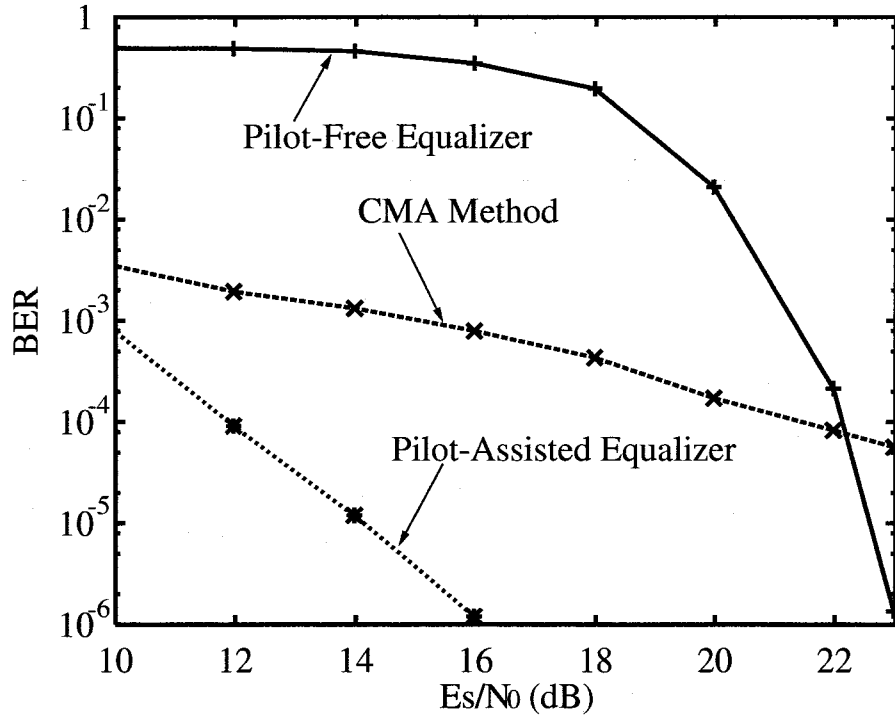
Figure 3.19: BER Performance.

methods, where the weights of the adaptive antenna array are controlled only by the estimated channel impulse response at each sensor. As for the channel estimation method, we have proposed two estimation methods, i.e., a suppressed SS pilot signal assisted method and a pilot-free channel identification method. With the suppressed SS pilot signal, the spatial equalizer can successfully estimate the channel impulse response with sufficient accuracy, and can outperform the conventional spatial equalizer, such as a CMA method. With the pilot-free channel identification method, though the performance is degraded especially when the E_s/N_0 is low, it is clearly shown that the second-order statistics based pilot-free channel identification method is applicable to practical wireless communications systems.

Chapter 4

A Spatial and Temporal Equalization Method with Reduced Number of Weights

4.1 Introduction

In this chapter, we propose a spatial and temporal equalization method with reduced number of weights, utilizing a cascade configuration of an adaptive antenna array and a DFE [36]. Taking advantage of the different features of the adaptive antenna array and the DFE, the equalization functionality is split into spatial processing and temporal processing. To be concrete, 'incoming signals with larger time delays (beyond the filter length of the DFE) are cancelled at the adaptive antenna array.' This makes it possible to reduce the number of weights in the DFE. The weights of both the adaptive antenna array and the DFE are separately calculated using estimated channel impulse response at each sensor.

We show the performance of the proposed system in multipath fading channels often encountered in indoor wireless environments, and discuss the attainable BER, antenna patterns, and the computational complexity in comparison with other equalization methods, such as spatial equalization and temporal equalization.

4.2 Design Criteria

So far, a considerable number of studies have been made on spatial and temporal equalization, and a lot of the equalization methods have been proposed [41]- [50]. However, though the equalization methods can achieve good performance, they require high computational complexity. This is because almost all the methods employ an adaptive TDL array [46], which has temporal filter at each antenna element, or maximum likelihood sequence estimation (MLSE) [36] approach in weights calculation. Attaching greater importance to computational complexity, we consider a configuration of spatial and temporal equalizer with less computational cost, such that an adaptive antenna array without temporal filter is followed by a DFE. The configuration itself is similar to that of the conventional method proposed in [51], where a diversity system and a DFE are combined. However, the conventional method requires that received signals on

different antenna elements are statistically independent, because the antenna array in the conventional system is based on a diversity system. On the other hand, the spatial equalizer in our system is based on a beamformer, therefore, the proposed system can achieve good performance regardless of correlation among the received signals. Moreover, since both the adaptive antenna array and the DFE are capable of equalization and have different features, we could further reduce the number of weights by taking advantage of the features. The adaptive antenna array can form various kinds of beam patterns by changing the weights, and this makes it possible to equalize a distorted received signal. Therefore, the complexity of the adaptive antenna array does not depend on the time delay of the received signal. Since the larger time delay results in the lower correlation between the primary signal and the delayed signal, large time delay of the received signal is preferable for the adaptive antenna array. In this sense, the adaptive antenna array is suited for high-speed wireless communications systems. However, the adaptive antenna array also has a disadvantage that it cannot sufficiently suppress undesired wave for some DoA patterns. On the other hand, the performance of the DFE does not depend on the DoA patterns. However, the DFE has to have enough number of taps [36] to equalize a delayed signal which has maximum time delay. This means that the complexity of the DFE is determined by the maximum time delay of the incoming signals. Based on the discussions above, we take fundamental strategies that the equalization functionality is split into spatial processing and temporal processing, and that incoming signals with larger time delays should be cancelled by the adaptive antenna array. These strategies make it possible to further reduce the weights in the DFE [52], [53].

4.3   System Configuration

Fig. 4.1 shows the transmitter/receiver structure of the proposed spatial and temporal equalizer. In the proposed method, the same frame format and the channel estimation method as in [34] are employed, therefore, only processings in the receiver are explained.

In the traffic channel processing, the outputs from the matched filters are multiplied by the weights of the adaptive antenna array, which are calculated in the pilot channel processing. After symbol timing synchronization and equalization with the DFE which has N_{ftap} taps in the feed-forward (FF) filter and N_{btap} taps in the feed-back (FB) filter, the data are recovered.

In the pilot channel processing, the complex instantaneous channel impulse response at each antenna element is first estimated by correlating the received pilot signal. The estimated channel impulse response is used to calculate the impulse response for the reference signal generation. Details of the reference signal generation are discussed in Section 4.4 Next, a QPSK signal is generated in the receiver and is fed into the filter whose tap coefficients are the same as the estimated channel impulse response, and as a result, the output of the filter becomes a pseudo-received pilot signal (without data signal). Note that, in our approach, the pilot signal is sent as a PN code which is superposed on the data signal, therefore, the received pilot signal itself can not be obtained as a training signal for weight calculation. On the other hand, the generated QPSK signal is also fed into the filter whose tap weights are the same as the impulse response for the reference signal generation. Using the output of this filter as a reference signal and the pseudo-received pilot signal, the weights of antenna elements are calculated by the RLS algorithm [20].
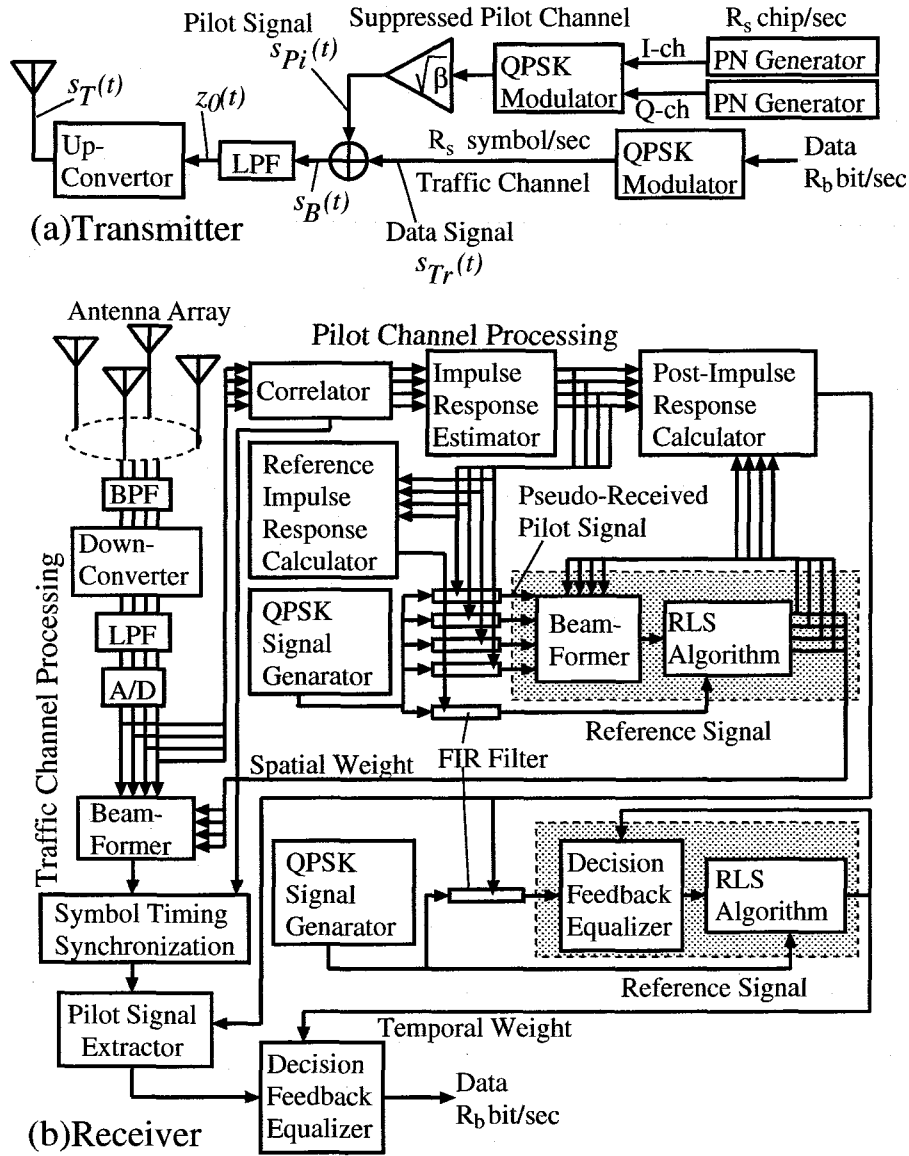
Figure 4.1: Transmitter/Receiver Structure.

Now that the estimated channel impulse response and the weights of the adaptive antenna array elements are available, we can calculate the tap weights of the DFE by the RLS algorithm in the same manner as the beam-weights calculation.

Finally, we summarize the flow of signal processing in the receiver in Fig. 4.2. In the figure, the hatched procedures show a series of signal processing: the receiver first extracts pilot signals from received signals and then estimates the channel impulse response using the signals. During the next frame, the receiver calculates the weights of the adaptive antenna array and the DFE (see Fig. 4.2 a). Further, at the end of the frame, the weights are updated and then are used for the processing of the traffic channel (see Fig. 4.2 b).
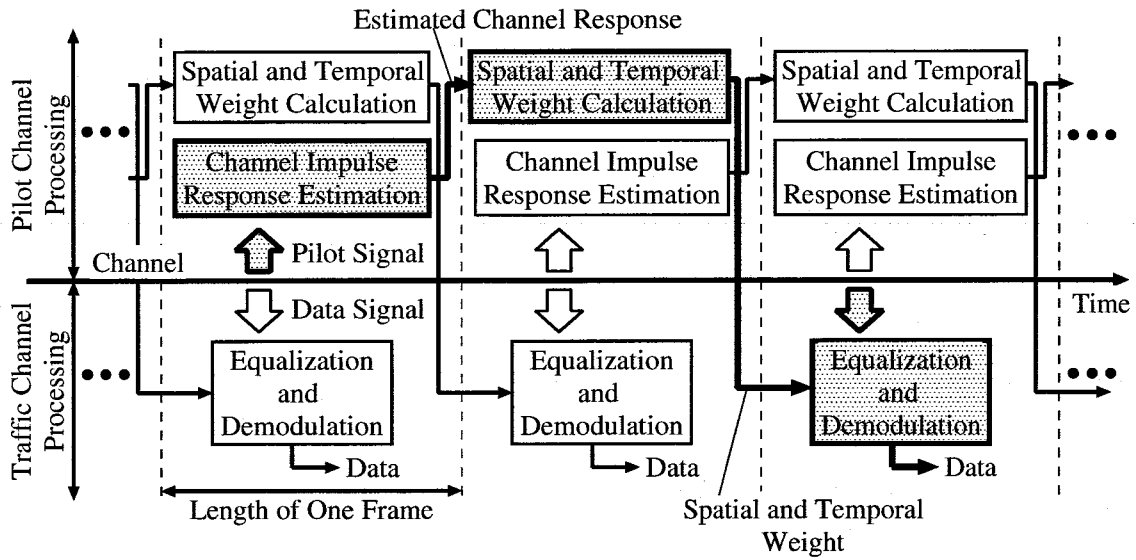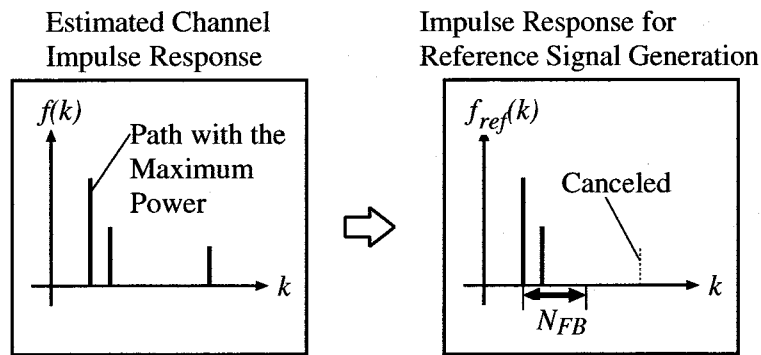
Figure 4.2: Flow of Signal Processing.

Figure 4.3: Impulse Response for Reference Signal Generation.

4.4   Weights Calculation Method

The impulse response for the reference signal generation is calculated from the N_{ary} estimated channel responses. From a statistical point of view, there is no difference among the estimated channel responses, therefore, the response at the $1st$ antenna element $f_1(k)$ is employed as the response for the reference generation. However, considering the effect of fading, the amplitude is chosen to be the average of the estimated responses among the antenna elements. In the end, the impulse response for the reference signal generation $f_{ref}(k)$ can be written as

$$f_{ref}(k) = \frac{1}{N_{ary}}(\sum_{l=1}^{N_{ary}} |f_l(k)|)\frac{f_1(k)}{|f_1(k)|}, \quad (0 \le k \le N_{FB}) \tag{4.1}$$

where N_{FB} denotes the length of the FB filter in the DFE, and $f_{ref}(k)$ is equal to zero for $k > N_{FB}$. In the proposed system, the incoming signal whose delay time exceeds the length of FB filter is canceled at the spatial processing (see Fig. 4.3).

Table 4.1: System Parameters.

	Proposed	Spatial	Temporal
Number of sensors N_{ary}	4	4	1
Number of FF taps N_{ftap}	5	0	10
Number of FB taps N_{btap}	4	0	9
Symbol rate R_s	100 Msymbol/sec		
Mod./Demod. Scheme	QPSK		
Oversampling factor N_{smp}	4		
Carrier frequency f_c	60 GHz		
Roll-off factor α	0.5		
Period of the M-sequence P	255 symbols		
Repetitions of the RLS algorithm N_{cal_S}, N_{cal_T}	50		

The reference signal $x'_{ref}(k)$ can be written as

$$x'_{ref}(k) = d'(k) * f_{ref}(k), \tag{4.2}$$

and finally, with this reference signal $x'_{ref}(k)$ and the pseudo-received pilot signal $x'_l(k)$, the weights of the adaptive antenna array are calculated by the RLS algorithm.

4.5 Computer Simulation

4.5.1 Channel Model

Computer simulations are conducted to evaluate the performance of the proposed spatial and temporal equalizer in comparison with a temporal equalizer (DFE [2]), and a spatial equalizer proposed in section 3.3. Parameters used in all the computer simulations are summarized in Table 4.1. We have assumed that the proposed spatial and temporal equalizer and the spatial equalizer employ a circular antenna array with 4 sensors. The proposed system also employs a DFE which has 9taps (5taps in the FF filter and 4taps in the FB filter).

The number of repetitions of the RLS algorithm in both the spatial processing N_{cal_S} and the temporal processing N_{cal_T} are chosen to be 50. In the spatial equalizer, the same antenna array as the proposed system is employed, while the equalizer has no temporal processing. The number of repetitions of the RLS algorithm N_{cal_S} is also the same as the proposed system. On the other hand, the temporal equalizer employs an omnidirectional antenna and a DFE which has 19taps (10taps in the FF filter and 9taps in the FB filter). The same number of repetitions of the RLS algorithm N_{cal_T} is also employed. Since the temporal equalizer employs an omnidirectional antenna, and the spatial and the proposed equalizer have four antenna elements, in the following figures, the curves of the BER performance of the temporal equalizer will be shifted by 6 dB. In all the systems, we adopt a root Nyquist filter with roll-off factor α of 0.5 as the LPF in the transmitter and receiver. Also, we adopt the symbol rate R_s of 100 Msymbol/sec, the oversampling factor N_{smp} of 4, the period of M-sequence P of 255 symbols, and the carrier frequency f_c of 60 GHz. Taking account of an indoor environment, we set the Doppler shift to 150 Hz.
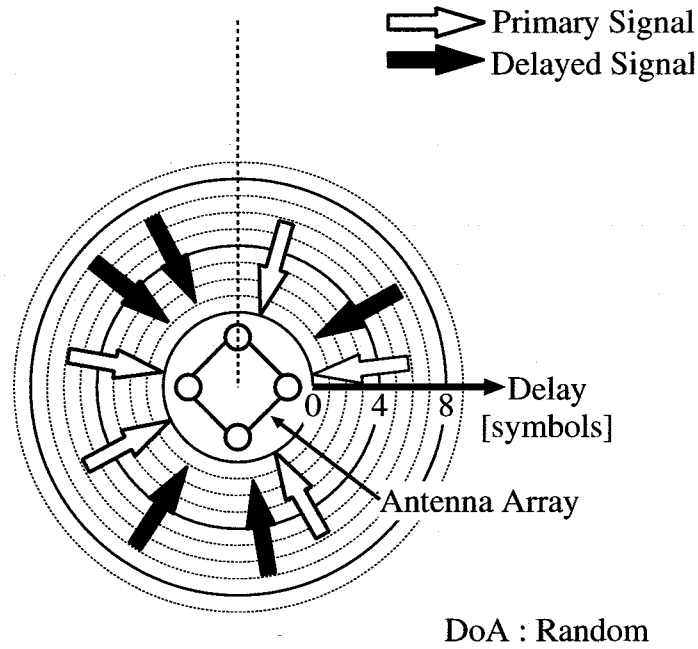
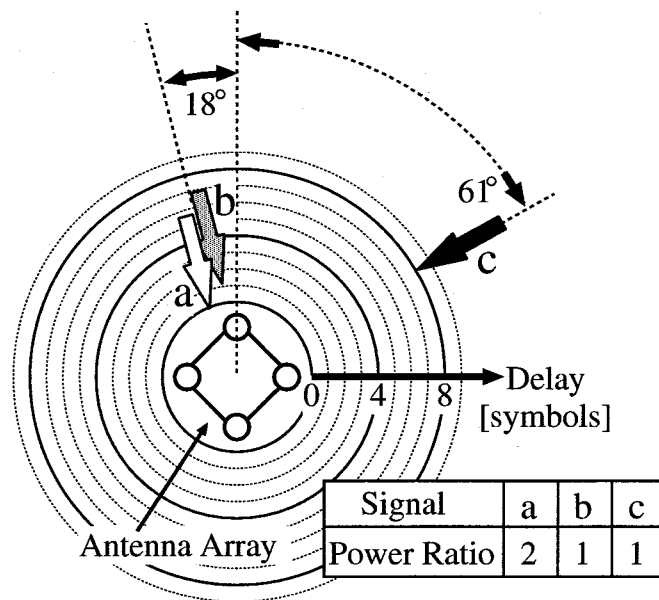Figure 4.4: Channel Model A. (Frequency Selective Fading Channel.)

Figure 4.5: Channel Model B. (Static 3-ray Multipath Channel.)

Fig. 4.4 also shows the frequency selective fading channel model discussed, where there are 5 preceding signals and 5 one-symbol delayed signals. The power ratios of these 10 incoming signals are also the same. DoA of each incoming signal is randomly determined and it changes every frame timing.

Fig. 4.5 shows the static 3-ray multipath channel model. There is a preceding signal in the same direction as a two-symbol delayed signal, and there is one more incoming signal which
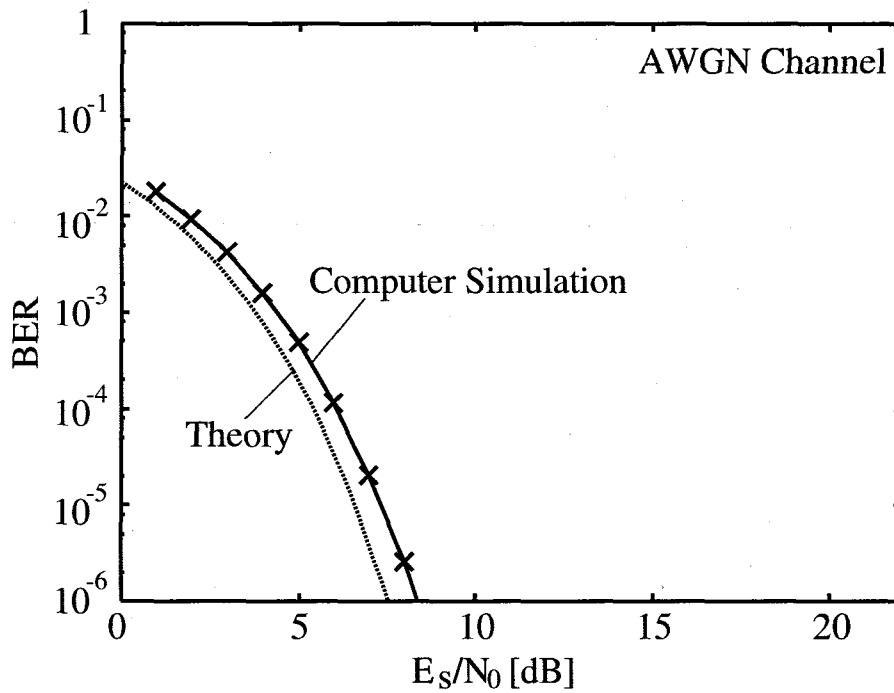
Figure 4.6: BER Performance in AWGN Channel.

has a large (eight-symbol) delay time. We discuss the attained performance based on the channel model A among a temporal equalizer, the spatial equalizer, and the proposed spatial and temporal equalizer.

4.5.2 Bit Error Rate Performance

Fig. 4.6 shows the BER versus E_s/N_0 in an AWGN channel. We can recognize about 1 dB degradation from the theoretical line. This may be because of the insertion of the pilot channel, and the error in the channel impulse response estimation or in the spatial and temporal weights calculation. The effect of the four times over sampling also may be the cause of the degradation. However, both of the first two degradation sources, i.e., the insertion of the pilot channel and the error in the channel identification, severely affect the BER performance. Also, the two degradation sources have a trade-off relationship. Since we have optimized the power of the pilot signal so as to maximize the performance, the influence caused by the two sources will be almost the same degree.

Fig. 4.7 shows the BER performance in the channel model A. The BER performance of the spatial equalizer and the temporal equalizer is also plotted in the same figure. The BER of the temporal equalizer improves gradually as $\overline{E_s/N_0}$ increases, but the performance is the worst among the three equalizers. The spatial equalizer can achieve the fairly good performance, however, we can recognize the BER floor for $\overline{E_s/N_0} > 15$ dB. Since DoAs in this channel model are randomly determined every frame timing, the spatial equalizer sometimes can not equalize the distorted received signal. Namely, the burst errors occur in certain DoA patterns. This is the reason for the BER floor. On the other hand, the proposed system can achieve the best performance among the three equalizers and the gain of 4-branch maximal-ratio combining
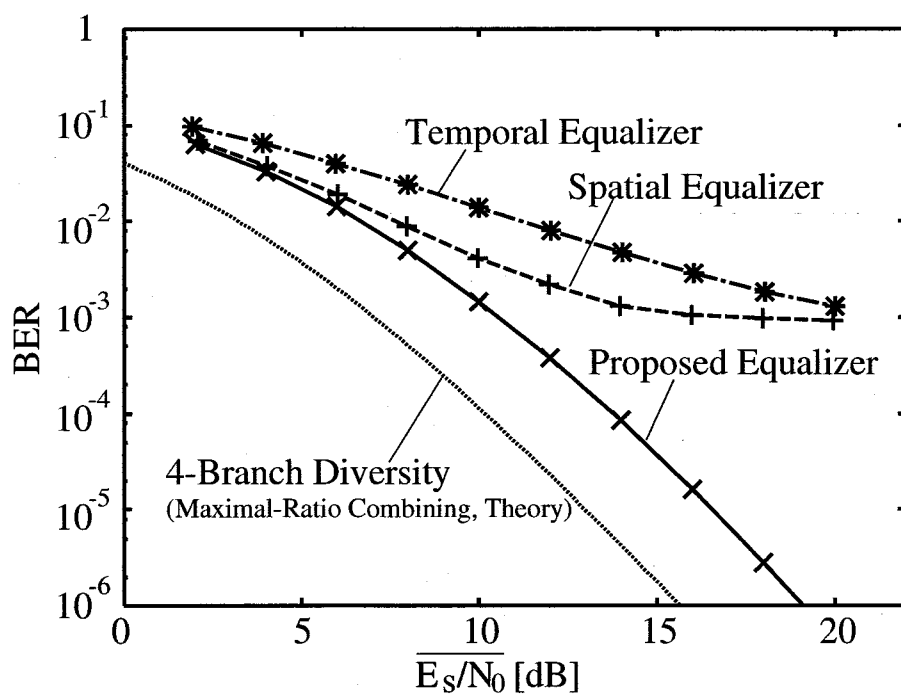
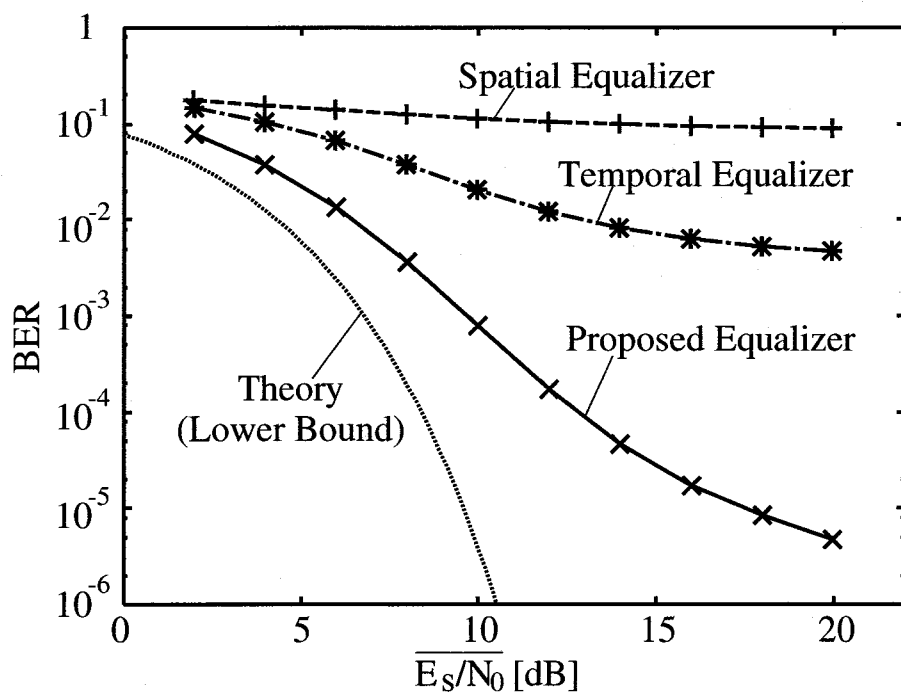Figure 4.7: BER Performance in Channel Model A.

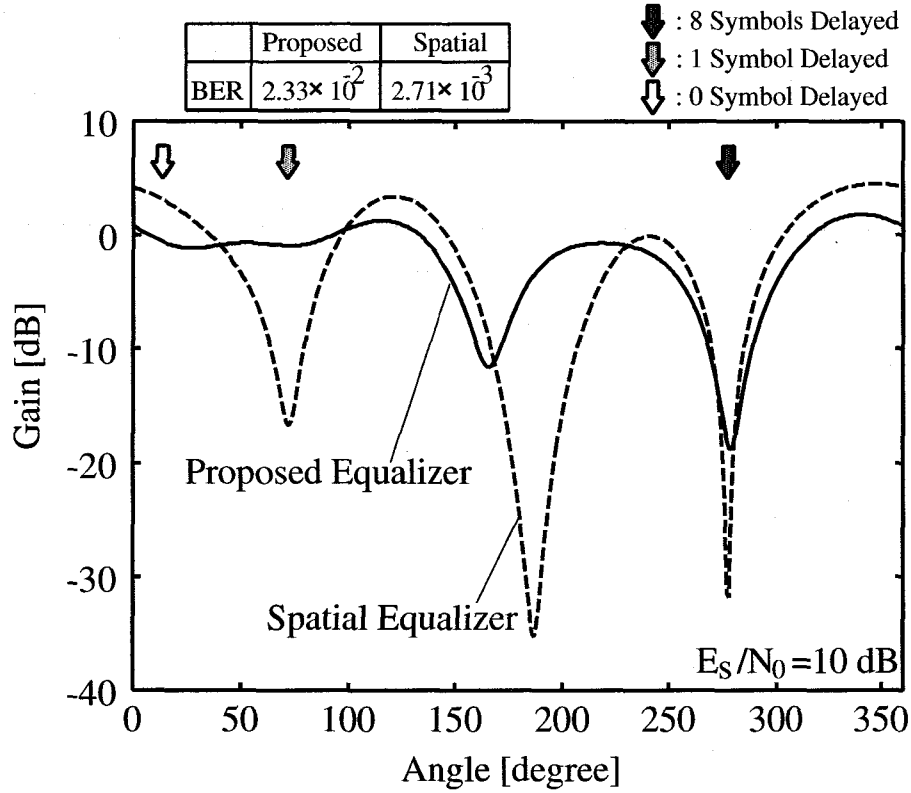Figure 4.8: BER Performance in Channel Model B.

Figure 4.9: Antenna Beam Pattern (a).

diversity. In addition, no error floor can be recognized. This means that the burst errors, which have been observed in the spatial equalizer case, do not occur in any DoA patterns. It can be concluded, therefore, the equalization of the proposed system does not care DoA patterns.

Fig. 4.8 shows the BER performance in the channel model B. The performance of the spatial equalizer is the worst among the three equalizers. The spatial equalizer forms its beam as capturing the path with the maximum power, therefore, it tries to catch the *signal a* . However, since the *signal a* is in the same direction as the delayed signal (*signal b*), the received signal suffers from intersymbol interference. This is the reason for the poor performance of the spatial equalizer. The performance of the temporal equalizer also improves gradually as E_s/N_0 increases in this channel model. However, the proposed system can achieve much better performance. In this channel model, the proposed system cancels the *signal c*, which has large time delay, at the spatial processing. Accordingly, all the temporal processing has to do is to cancel the *signal b*.

4.5.3 Antenna Patterns

Here, the difference in operation between the proposed spatial and temporal equalizer and the spatial equalizer is analyzed from the antenna patterns. Figs. 4.9, 4.10 and 4.11 show the antenna patterns. In all the figures, the primary signal and the 1- and 8-symbol delayed signals are arriving, and the power ratio of these 3 signals is 2 : 1 : 1.

In Fig. 4.9, the primary signal is arriving from the direction of 18° and the 1- and 8-symbol delayed signals are arriving from the direction of 72° and 270°, respectively. In this case, both

	Proposed	Spatial
BER	4.93×10^{-4}	1.36×10^{-1}

↓ : 8 Symbols Delayed
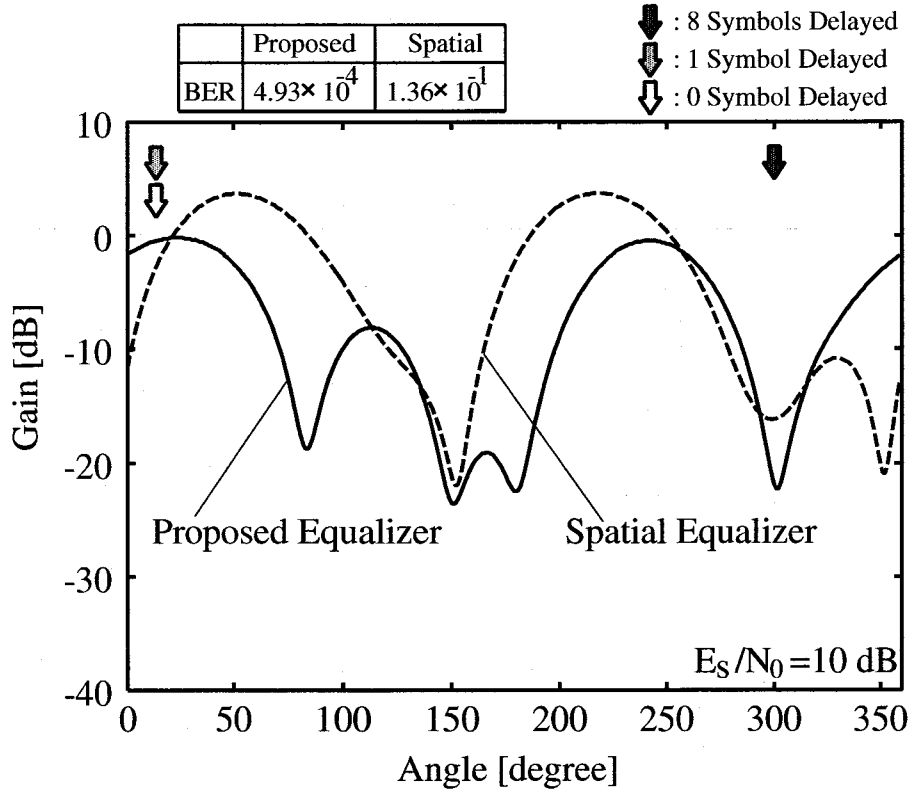↓ : 1 Symbol Delayed
⇩ : 0 Symbol Delayed

Figure 4.10: Antenna Beam Pattern (b).

of the equalizers are likely to work well, however, the BER of the proposed equalizer is worse than that of the spatial equalizer. This is mainly because the proposed equalizer gives smaller gain for the primary signal than the spatial equalizer does.

In Fig. 4.10, the primary signal and the 1-symbol delayed signal are arriving from the direction of 18°, and the 8-symbol delayed signal is arriving from the direction of 299° (This is the same channel model as the channel model B(Fig. 4.5)). As described above, the spatial equalizer controls the beam in the direction of 18°, therefore, the BER is poor. However, the proposed system controls the null in the direction of 299°, and equalizes the primary signal which is collapsed only by the 1-symbol delayed signal at the temporal processing.

In Fig. 4.11, the primary signal and the 1- and 8-symbol delayed signals are arriving from the direction of 45°, 225° and 299°, respectively. The primary signal and the delayed signals are not in the same or near direction, therefore, it is expected that the BER of the spatial equalizing method will be good. However, in practice, the spatial equalizer can not extract only the primary signal and the error rate is poor. This is a matter of the limitation of the degrees of freedom in forming beams. Adaptive antenna array can form various beampatterns, however, this does not mean that it can make arbitrary beampattern. Namely, if a beam is controlled in one direction, it may results in forming another beam toward another direction. Setting coordinate as in Fig. 4.12, the beampattern $R(\theta)$ can be written as

$$R(\theta) = | \sum_{l=1}^{N_{ary}} \exp[j\cos(\frac{\pi}{2}l - \theta)]w_l|^2, \tag{4.3}$$

	Proposed	Spatial
BER	0.00	1.21×10^{-1}

⬇ : 8 Symbols Delayed
⬇ : 1 Symbol Delayed
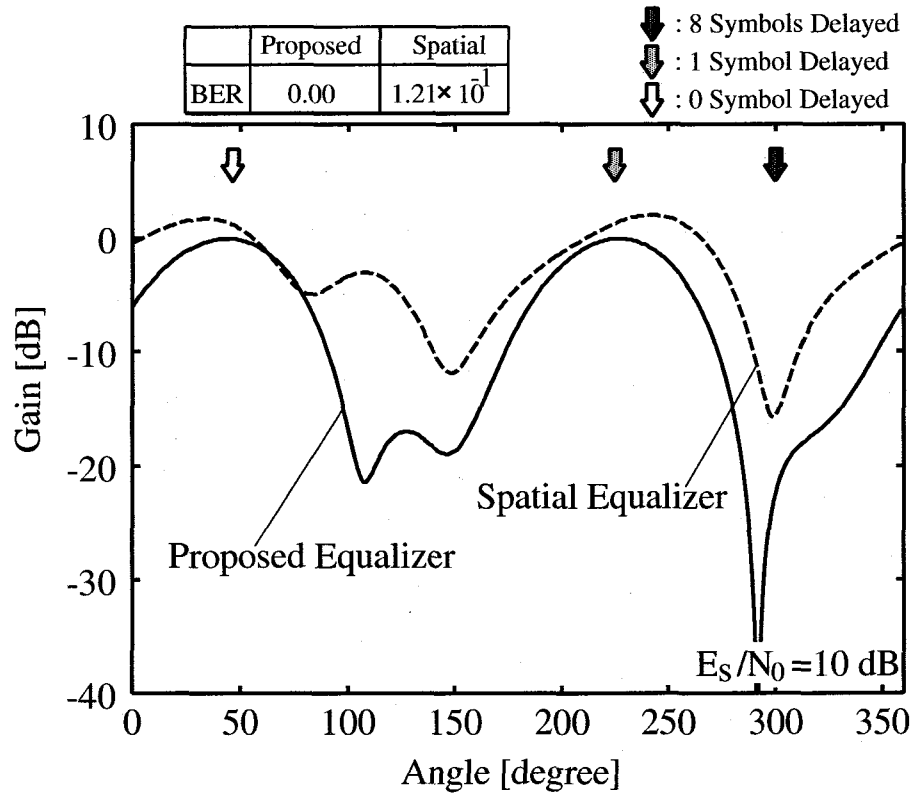⇩ : 0 Symbol Delayed

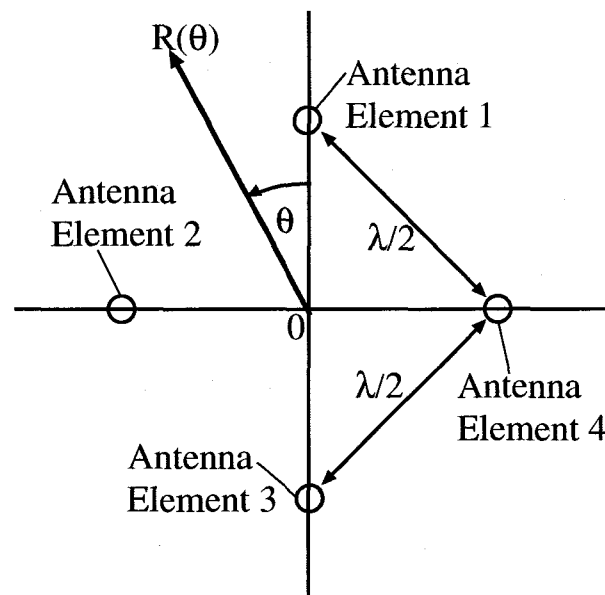Figure 4.11: Antenna Pattern (c).

Figure 4.12: Antenna Arrangement.

where w_l denotes the weight corresponding to the lth antenna element. From Eq. (4.3), it turns out that the antenna array can not have such a beampattern that $R(\pi/4) = 1$ and $R(5\pi/4) = 0$. Therefore, the weights of the spatial equalizer do not converge well. This is the reason of the poor BER performance of the spatial equalizer. However, the proposed system works properly, that is, the delayed signal with large time delay is cancelled at the spatial processing.

4.5.4 Computational Cost

We show the number of multiplications in the weights calculation algorithm as a computational cost. In the following, N_{tap} denotes the total number of taps in the DFE, namely, $N_{tap} = N_{ftap} + N_{btap}$. For the proposed system, the number of multiplication in the weight calculation algorithm is

$$N_{cal\_S} \times (7N_{ary}^2 + 12N_{ary}) + N_{cal\_T} \times (7N_{tap}^2 + 12N_{tap}) = 41,750 \ (times),$$

for the spatial equalizer,

$$N_{cal\_S} \times (7N_{ary}^2 + 12N_{ary}) = 8,000 \ (times),$$

and for the temporal equalizer (DFE),

$$N_{cal\_T} \times (7N_{tap}^2 + 12N_{tap}) = 137,750 \ (times).$$

The spatial equalizer requires the least computational complexity, but it suffers from break down of the equalization for certain DoA patterns. The computational complexity of the temporal equalizer depends on the maximum time delay of the incoming signal which we must equalize. Therefore, the temporal equalizer may be not suited for high speed communications. The proposed spatial and temporal equalizer not only can achieve an excellent BER performance but also requires a relatively low computational cost.

4.6 Summary

In this chapter, we have proposed a spatial and temporal equalization method with reduced number of weights and evaluated the performance comparing with that of the spatial equalizer presented in chapter 3. and the DFE. Here, our fundamental criterion is 'delayed incoming signals with large time delays should be canceled by the spatial processing', which makes it possible to decrease the computational complexity. The criterion will not give the spatial and temporal equalizer the best performance, however, if we regard the computational complexity as important, the criterion could be a good choice. In addition, the proposed equalizer uses only estimated channel impulse response to adjust the weights of the spatial and temporal equalizer, therefore, it requires no information on DoA. We have shown the attainable BER performance in an AWGN channel, a frequency selective fading channel, and a static 3-ray multipath channel. Moreover, we have analyzed the operation of the spatial processing of the proposed system from the viewpoint of antenna patterns. We have also shown the computational complexity in terms of the number of multiplications in the total weight calculation. From all the results, it can be concluded that the proposed system can achieve the best and stable performance among the three equalization methods with a low computational complexity.

Chapter 5

A Versatile Spatial and Temporal Equalization Method for Various Direction-of-Arrival Patterns

5.1 Introduction

This chapter proposes a versatile spatial and temporal equalization method for various kinds of channel models, where the DoA patterns are randomly determined, with a cascade configuration of an adaptive antenna array and a DFE.

The spatial and temporal equalizer with the cascade configuration can be realized in low computational complexity, however, if it tries to capture only the path with the maximum power, the weights may be trapped by a local minimum during the adaptation of MMSE based adaptive algorithm, since the error performance surface becomes a fourth-order function of the weights, and possibly has two minima. In order to avoid the wrong trap, the proposed equalizer calculates the weights of the adaptive antenna array and the DFE separately, and the adaptive antenna array selects a path or paths to capture depending on channel conditions.

5.2 Design Criteria

Generally, the performance of a wireless communications system which employs an adaptive antenna array largely depends on DoA patterns of channels. However, considering wireless LAN environments, where users freely install both base and mobile stations, it is necessary for spatial and temporal equalizers to achieve robustness to the DoA patterns.

Although, so far, only an adaptive TDL array [40] depicted in Fig. 5.1 is the spatial and temporal equalizer which is capable of achieving such a robustness, and it is possible to realize an optimum receiver with the configuration [46], the adaptive TDL array requires quite a few number of weights, and hence prohibitive computational complexity. This means that the adaptive TDL array is not suited for high-speed wireless communications systems, such as wireless LANs. In this chapter, we, therefore, consider a cascade configuration of a spatial and temporal equalizer such that an adaptive antenna array without temporal filter is followed by a DFE as shown in Fig. 5.2. The cascade configuration requires smaller number of weights [47]-
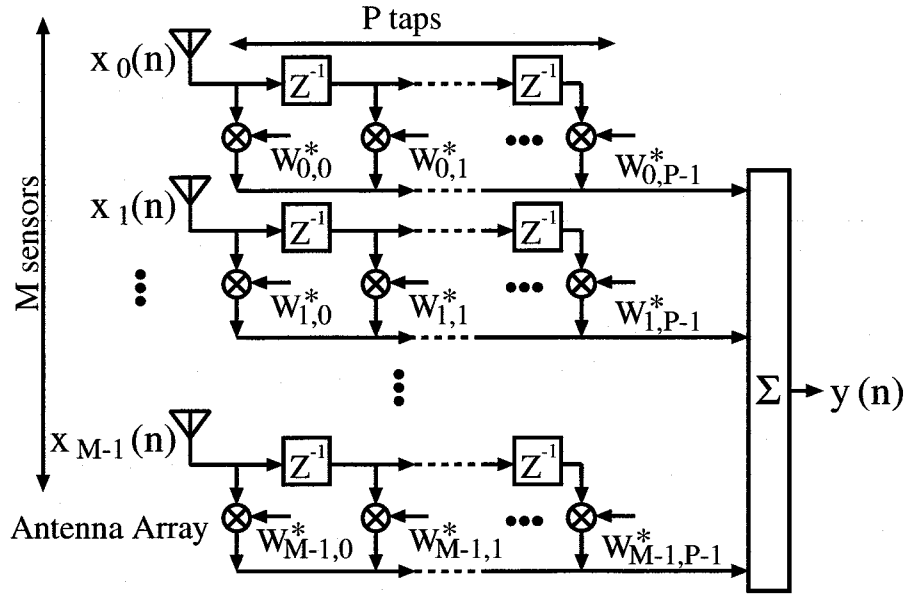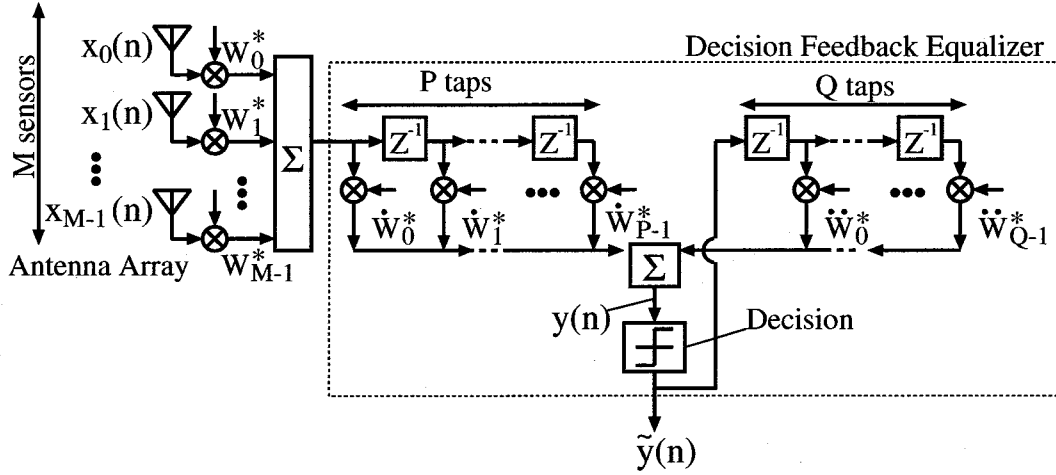
Figure 5.1: Adaptive TDL Array.

Figure 5.2: Cascade Configuration.

[50] than the adaptive TDL array, however, it needs to pay a price for the simplicity when it tries to capture a path with the maximum power using a MMSE based adaptive algorithm. Here, we show the "price" from a viewpoint of error performance surface in comparison with adaptive TDL array and discuss the method of settlement.

5.2.1   Error Performance Surface of Adaptive TDL Array

When input signals of the adaptive TDL array depicted in Fig. 5.1 at time n are $x_0(n), \ldots, x_{M-1}(n)$, the output $y(n)$ is represented by

$$y(n) = \sum_{m=0}^{M-1} \sum_{p=0}^{P-1} w_{m,p}^* x_m(n-p), \tag{5.1}$$

where M, P and $w_{m,p}$ are the number of sensors, the length of the TDL and the weights of the adaptive TDL array. Defining the error signal $e(n)$ as

$$
\begin{aligned}
e(n) &= d(n) - y(n) \\
&= d(n) - \sum_{m=0}^{M-1} \sum_{p=0}^{P-1} w_{m,p}^* x_m(n-p),
\end{aligned}
\tag{5.2}
$$

where $d(n)$ denotes the desired signal, the cost function J for the adaptive TDL array of Fig. 5.1 can be expressed as follows:

$$
\begin{aligned}
J &= E[e(n)e^*(n)] \\
&= E[|d(n)|^2] \\
&\quad - \sum_{m=0}^{M-1} \sum_{p=0}^{P-1} w_{m,p}^* E[x_m(n-p)d^*(n)] - \sum_{m=0}^{M-1} \sum_{p=0}^{P-1} w_{m,p} E[x_m^*(n-p)d(n)] \\
&\quad + \sum_{m=0}^{M-1} \sum_{p=0}^{P-1} \sum_{k=0}^{M-1} \sum_{i=0}^{P-1} w_{m,p}^* w_{k,i} E[x_m(n-p)x_k^*(n-i)].
\end{aligned}
\tag{5.3}
$$

Eq. (5.3) states that the cost function J of the adaptive TDL array is a second-order function of the weights, and has a bowl-shaped MP+1 dimensional surface with MP degrees of freedom represented by the weights. The surface has a unique minimum, therefore, the weights of the adaptive TDL array can be calculated using MMSE based adaptive algorithms, such as RLS or LMS algorithms.

5.2.2 Error Performance Surface of Spatial and Temporal Equalizer with Cascade Configuration

Then, we analyze the spatial and temporal equalizer with cascade configuration shown in Fig. 5.2 in the same manner as the adaptive TDL array. If the inputs of the spatial and temporal equalizer at time n are $x_0(n), \ldots, x_{M-1}(n)$, the output $y(n)$ can be written as

$$
y(n) = \sum_{m=0}^{M-1} \sum_{p=0}^{P-1} w_m^* \dot{w}_p^* x_m(n-p) + \sum_{q=0}^{Q-1} \ddot{w}_q^* \tilde{y}(n-q-1),
\tag{5.4}
$$

where M, P, Q, w_m, $\dot{w}_p$, $\ddot{w}_q$ and $\tilde{y}(n)$ denote the number of sensors, the length of the FF filter in the DFE, the length of the FB filter, the weights of adaptive antenna array, the weights of the FF filter, the weights of the FB filter and the detected signal. Using the error signal $e(n)$ defined as

$$
e(n) = d(n) - \left\{ \sum_{m=0}^{M-1} \sum_{p=0}^{P-1} w_m^* \dot{w}_p^* x_m(n-p) + \sum_{q=0}^{Q-1} \ddot{w}_q^* \tilde{y}(n-q-1) \right\},
\tag{5.5}
$$

the cost function of the spatial and temporal equalizer with cascade configuration of Fig. 5.2 can be represented by

$$
\begin{aligned}
J &= E[|d(n) - y(n)|^2] \\
&= E[|d(n)|^2] \\
&\quad - \sum_{q=0}^{Q-1} \{ \ddot{w}_q^* E[\tilde{y}(n-q-1)d^*(n)] + \ddot{w}_q E[\tilde{y}^*(n-q-1)d(n)] \}
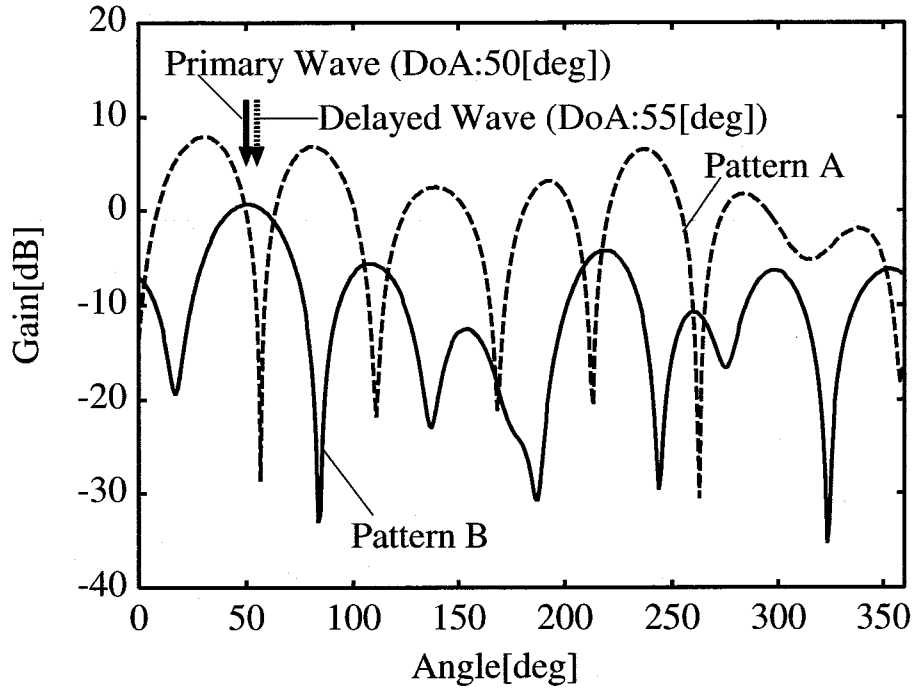\end{aligned}
$$

Figure 5.3: Example of Antenna Beam Pattern.

$$
\begin{aligned}
-\; &\sum_{m=0}^{M-1}\sum_{p=0}^{P-1}\{w_m^*\ddot{w}_p^* E[x_m(n-p)d^*(n)] + w_m\ddot{w}_p E[x_m^*(n-p)d(n)]\} \\
+\; &\sum_{q=0}^{Q-1}\sum_{k=0}^{Q-1}\ddot{w}_q^*\ddot{w}_k E[\ddot{y}(n-q-1)\ddot{y}^*(n-k-1)] \\
+\; &\sum_{m=0}^{M-1}\sum_{p=0}^{P-1}\sum_{q=0}^{Q-1}\{w_m^*\ddot{w}_p^*\ddot{w}_q E[x_m(n-p)\ddot{y}^*(n-q-1)] \\
&\qquad\qquad +w_m\ddot{w}_p\ddot{w}_q^* E[x_m^*(n-p)\ddot{y}(n-q-1)]\} \\
+\; &\sum_{m=0}^{M-1}\sum_{p=0}^{P-1}\sum_{k=0}^{M-1}\sum_{i=0}^{P-1}\{w_m^*\ddot{w}_p^* w_k\ddot{w}_i E[x_m(n-p)x_k^*(n-i)]\}.
\end{aligned}
\tag{5.6}
$$

Eq. (5.6) states that the cost function of the spatial and temporal equalizer with cascade configuration J is a fourth-order function of the weights, and possibly has two local minima. If we use MMSE based adaptive algorithms in order to calculate the weights, the weights may be trapped by a local minimum during the adaptation. This is the unique problem of the spatial and temporal equalizer with the cascade configuration.

5.2.3   Practical Considerations

From a viewpoint of practical operation of the spatial and temporal equalizer, the local minima can be seen when a desired and a undersized (delayed) waves, each of them has small angular spread, come from almost the same direction. Fig. 5.3 shows examples of the antenna beam patterns (pattern A and B) of the spatial and temporal equalizer with cascade configuration when a desired wave with no angular spread comes from 50°, while a undesired wave also with

no angular spread comes from 55°. Pattern A has a null point at the undesired wave, however, it also has high sidelobe level. Since the thermal noise is white in space, the high sidelobe level results in the degradation of the SNR at the output of the adaptive antenna array, which can not be recovered with the equalization of the DFE. On the other hand, pattern B does not suffer from the degradation of SNR, though pattern B can not cancel the undesired wave. The undesired component included in the output of the adaptive antenna array can be canceled at the DFE, therefore, the equalizer can achieve good performance with pattern B [54]- [60]. In this case, pattern A could be a local minimum of the cost function J and pattern B may be the global or local minimum of which value of the cost is smaller than pattern A.

This example suggests that we could guide the weights to the global minimum by adequately selecting a path (or paths) to capture with the adaptive antenna array depending on channel conditions. Moreover, with the path selection, the weights of the adaptive antenna array and the DFE can be calculated separately, therefore, we can employ usual MMSE adaptive algorithm for the weights calculation. In addition, since it is easy to apply a pipeline processing for such separated weights calculations, the separated processing is quite suitable for high-speed wireless communications systems [61].

5.3 System Configuration

Fig. 5.4 shows the receiver structure of the proposed spatial and temporal equalizer. Incoming waves are received by an antenna array with M sensors, then, the signals are processed in the data signal processing section and in the pilot signal processing section independently. In the data signal processing section, the outputs from the matched filters are multiplied by the weights of the adaptive antenna array, which are calculated in the pilot signal processing section. After symbol timing synchronization and the equalization with the DFE, which has P taps in the FF filter and Q taps in the FB filter, data are recovered. In the pilot signal processing section, the complex instantaneous channel impulse response at each sensor is first estimated by correlating the received pilot signal. Then, using the estimated channel response, the equalizer selects a path (or paths) to capture with the adaptive antenna array. Details of the weight calculation method and the path selection algorithm are discussed in section 5.4, but the weights of the adaptive antenna array are calculated by the RLS algorithm. The weights of DFE are also determined in the same manner as the beam-weights calculation.

5.4 Weight Calculation Method

5.4.1 Selective Reception with Adaptive Antenna Array

Generally, an adaptive antenna array based on MMSE criterion algorithm captures only one path which is synchronized with the reference signal, however, with the cascade configuration of Fig. 5.4, the adaptive antenna array needs to capture not only the path with the maximum power but also all the paths around the path with the maximum power in order to avoid the degradation of SNR. Note that the purpose of the selective reception is not increasing the total power of the received signal, since the proposed equalizer employs DFE, which is capable of not combining diversity but selection diversity. Such a selective reception with the adaptive
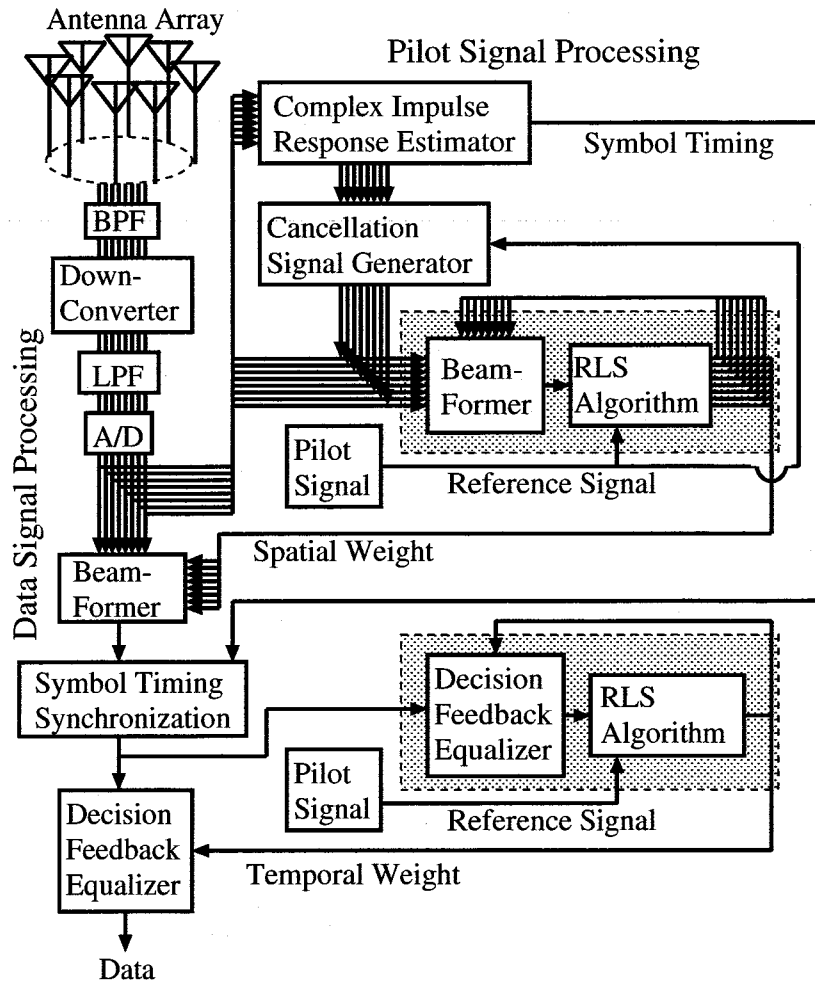
Figure 5.4: Configuration of the Proposed System.

antenna array can be realized by controlling the reference signal in the MMSE based weight calculation [50]. In the method, the output signal of a transversal filter, whose input is the known pilot signal, is used as the reference signal, and the weights of both the adaptive antenna array and the transversal filter are simultaneously calculated by MMSE based adaptive algorithm. With the method, the adaptive antenna array can capture any paths, however, the method requires additional weights, namely the weights of the transversal filter, to be determined, which results in an increase of the computational complexity. In this section, we propose a selective reception method with the adaptive antenna array, which is realized by controlling not the reference signal but the received pilot signal.

Fig. 5.5 shows the principle of the proposed selective reception method with the adaptive antenna array. In the figure, (A) shows the channel impulse response and the DoA pattern. The paths a, b, and c in the response correspond to the incoming waves a, b, and c respectively. If we use the received pilot signal as it is to calculate the weights of the adaptive antenna array synchronizing with the path with the maximum power a, the adaptive antenna array forms a null toward the path c, which has almost the same DoA as the path a. This results in the degradation of SNR because of the high sidelobe level. In the proposed method, to capture
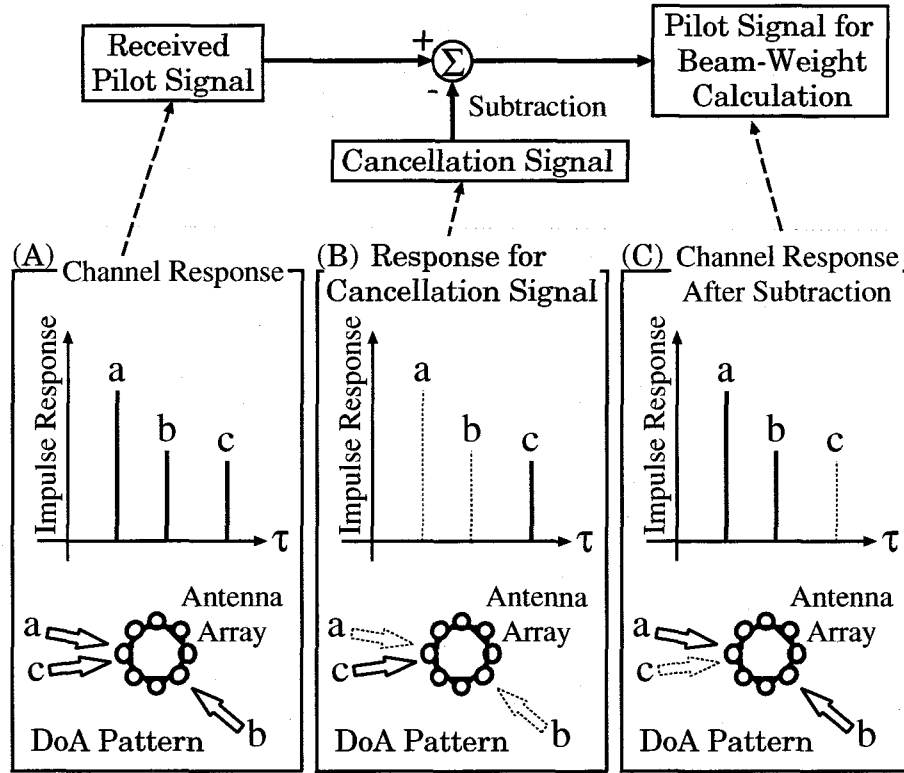
Figure 5.5: Selective Reception with Adaptive Antenna Array.

both the path a and c, the equalizer generates a signal for cancellation using the response shown in Fig. 5.5 (B). By subtracting the cancellation signal from the received pilot signal, we'll have the signal which is equivalent to the received pilot signal passed through the channel shown in Fig. 5.5 (C). With the equivalent received pilot signal, the adaptive antenna array can capture both the path a and c, while giving the maximum gain to the path a (the path with the maximum power).

5.4.2 Procedure of Weights Calculation

Fig. 5.6 shows the frame format and the weights calculation procedure in the proposed method. Each frame consists of a pilot signal, which is composed of PN sequence with L symbols long, and a data signal. Using the pilot signals of three consecutive frames, the weights of the adaptive antenna array and the DFE are calculated as in the followings:

-1st. frame: The complex instantaneous channel impulse response at each sensors is first estimated by correlating the received pilot signal. Using the estimated response, the path(s) to capture is(are) selected. Details of the path selection method are discussed in 5.4.3. Also, the estimated response is used for the frame synchronization.

-2nd. frame: If the path to capture is only the path with the maximum power ($path_{max}$), the received pilot signal is used for the calculation of the weights of the adaptive antenna array as it is. Otherwise, the received pilot signal which is subtracted by the corresponding
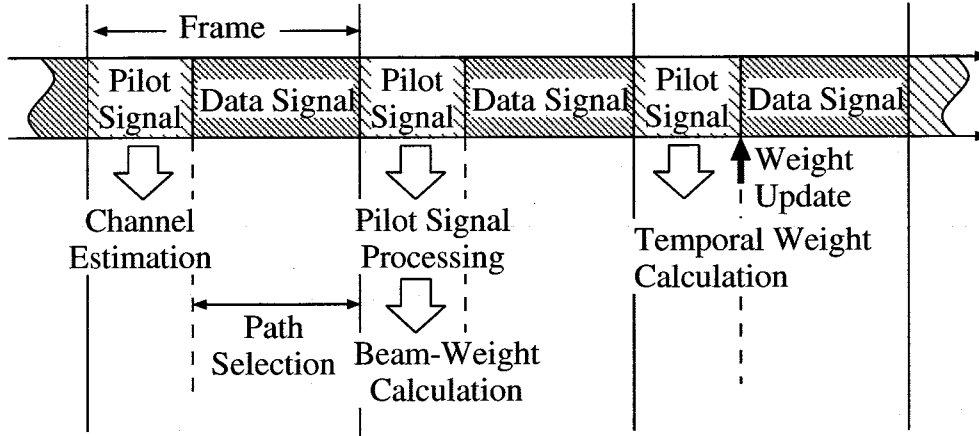
Figure 5.6: Frame Format and Weight Calculation.

components of the path to capture excluding the $path_{max}$ will be used for the weights calculation. Here, we employ the RLS algorithm [2] as the MMSE based adaptive algorithm, and the known pilot signal is used for the reference signal.

-3rd. frame: Using the received pilot signal and the weights of the adaptive antenna array, the weights of the DFE are calculated by the RLS algorithm. The known pilot signal is also used as the reference signal. All the weights are updated at the end of the pilot signal of this frame.

5.4.3   Path Selection Algorithm

The proposed equalizer selects a path or paths to capture with the adaptive antenna array depending on the channel conditions, and the channel conditions are judged from the estimated channel impulse response. In the followings we show the classification of the channel conditions, and discuss how to select the path(s) for the each channel condition.

Small Angular Spread of Each Incoming Wave: In this case, DoAs of incoming waves can be estimated from phase differences of the estimated channel response at each sensors. According to DoA patterns, the channel conditions can be further classified into the following two situations;

-DoA of the $Path_{max}$ $\neq$ DoAs of the other paths: The adaptive antenna array can capture only the $Path_{max}$ without high sidelobe level (and hence the degradation of the SNR), therefore, the equalizer selects the $Path_{max}$ as the path to capture with the adaptive antenna array.

-DoA of the $Path_{max}$ $\cong$ DoAs of the other paths: The equalizer selects both the $Path_{max}$ and the path(s) around the $Path_{max}$ in order to avoid the degradation of the SNR. The residual ISI component(s) will be equalized by the latter DFE.

Large Angular Spread of Each Incoming Wave: In this case, DoAs of incoming waves cannot be estimated from the channel impulse response, however, the adaptive antenna
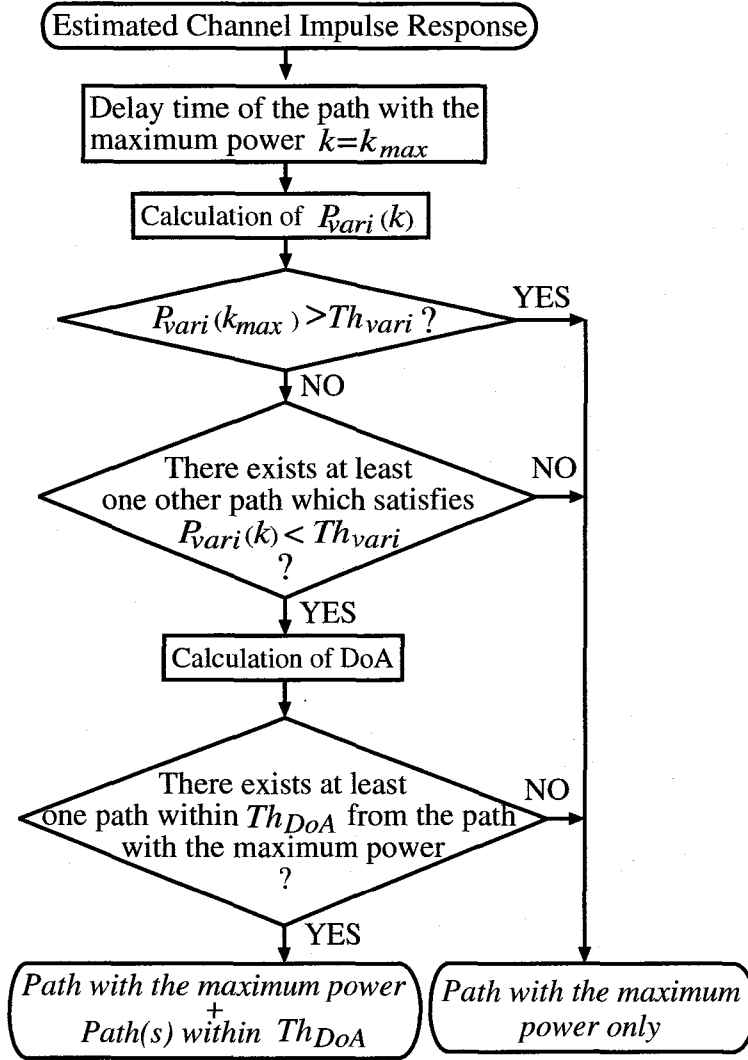
Figure 5.7: Path Selection Algorithm.

array operates as a diversity system [54] because of low correlation of the received signals among the sensors. This means that the adaptive antenna array can eliminate the undesired waves not by forming nulls but by combining them as they disappear. Therefore, the equalizer can select only the $Path_{max}$ as the path to capture regardless of DoA patterns.

Fig. 5.7 shows the proposed path selection algorithm based on the discussion above. The equalizer first determines the delay time k_{max} of the $Path_{max}$ from the estimated channel response. Then, it calculates the normalized variation of the instantaneous amplitude of the estimated channel response P_{vari}, which is defined as

$$P_{vari}(k) = \frac{1}{M}\sum_{m=1}^{M}\frac{\{|f_m(k)| - \overline{|f(k)|}\}^2}{\overline{|f(k)|}^2}, \tag{5.7}$$

$$\overline{|f(k)|} = \frac{1}{M}\sum_{m=1}^{M}|f_m(k)|, \tag{5.8}$$

Table 5.1: System Parameters.

	Proposed Equalizer	Adaptive TDL Array
Antenna Array	Equi-Spaced Circular Array (8 Sensors)	
Filter Length	FF: 9 taps FB: 8 taps	9 (or 3) taps
Total # of Weights	25 taps	72 (or 24) taps
Symbol Rate	100 Msymbol/sec	
Carrier Frequency	60 GHz	
Mod./Demod. Scheme	QPSK	
Pulse Shaping	Root-Nyquist Filter (Roll-off Factor = 0.5)	
Pilot Signal	M Sequence(L=255 symbols)	
Oversampling Factor	4	
RLS Repetitions	Spatial N_{cal_S}: 200 Temporal N_{cal_T}: 200	N_{cal_TDL}: 20 (or 200)

where $f_m(k)$ denotes the estimated channel impulse response on the mth antenna sensor at time k. Since the large angular spread results in low correlation of the received signals among the sensors, we can tell the angular spread of each path by comparing the $P_{vari}(k)$ with a threshold Th_{vari}. If the angular spread of the $Path_{max}$ is large, the adaptive antenna array can extract only the $Path_{max}$ regardless of DoA pattern, therefore, the $Path_{max}$ is selected as the path to capture. In this case, the adaptive antenna array operates as the diversity system. Else if the angular spread of all the other paths is large, the $Path_{max}$ is selected likewise as the path to capture, since the adaptive antenna array can cancel out the paths without high sidelobe level. Only when the $Path_{max}$ and any one of the other paths have small angular spread, the proposed equalizer calculates the DoAs of the paths. And if any one of the paths (except for the $Path_{max}$) exists within the threshold of Th_{DoA} from the $Path_{max}$, all the paths around the $Path_{max}$ are selected, otherwise, only the $Path_{max}$

5.5 Computer Simulation

Computer simulations are conducted to evaluate the performance of the proposed spatial and temporal equalizer in comparison with adaptive TDL arrays.

5.5.1 System Parameter

System parameters used in all the computer simulations are summarized in Table 5.1.

Assume that the proposed spatial and temporal equalizer is applied to the indoor wireless LAN system, the carrier frequency and the symbol rate are set to be 60 GHz and 100 Msymbol/sec, respectively. Both the proposed system and the adaptive TDL array have an equi-spaced circular array with 8 sensors, whose sensor spacing is half of the carrier wavelength. Generally, in order to withstand timing jitter, a fractional-spaced filter is employed as the FF filter in the DFE,
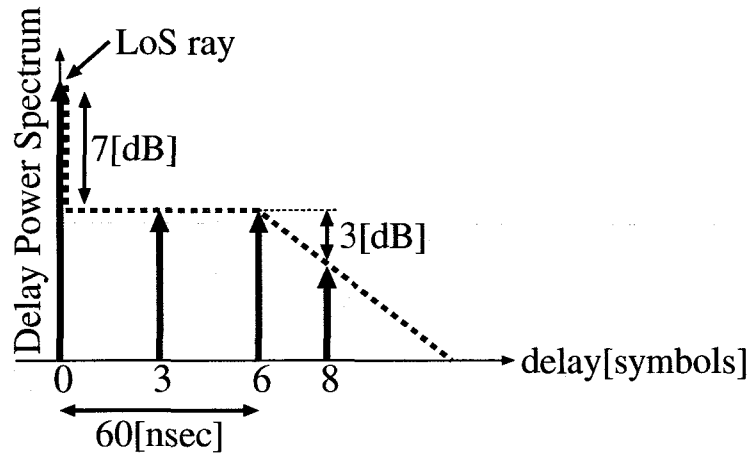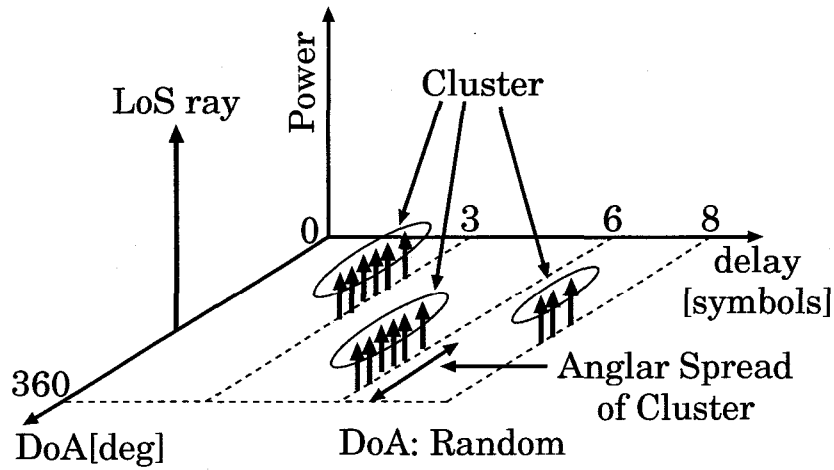
Figure 5.8: Delay Power Spectrum.

Figure 5.9: Space-Time Channel Model A and B.

however, we have employed a symbol-spaced DFE for the simplicity. Furthermore, assuming that the maximum time delay of the incoming waves is 8 symbols time, we have set the number of taps in the FF filter and FB filter to be 9 and 8 taps respectively. On the other hand, we assume two adaptive TDL arrays, which have totally 72 or 24 taps. The number of RLS repetitions of the proposed system, the ATDLA with 24taps and the ATDLA with 72taps are set to be 200, 200 and 20, so that the computational complexity of all the systems is the same amount.

5.5.2 Space-Time Channel Model

In agreement with measurements reported in [62], we use delay power spectrum (DPS) of a line-of-sight (LoS) channel defined in Fig. 5.8. In the figure, the dotted line shows the model of the DPS proposed in [62], and the arrows show the model used in these simulations. Moreover, we assume the spatial properties of the channel as depicted in Fig. 5.9 (channel model A), where delayed incoming rays form clusters which have observed in [63]. In the case of no LoS
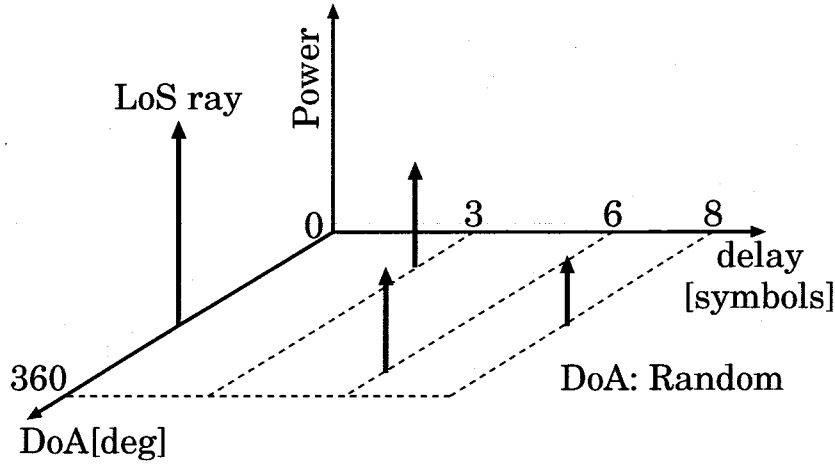
Figure 5.10: Space-Time Channel Model C.

channel (channel model B), the LoS ray in Fig. 5.9 is omitted. DoAs of the LoS ray and the clusters follow a uniform distribution of $[0{:}360)°$, whereas distribution of the individual clusters is assumed to be a uniform distribution of $[{-}45{:}45]°$, which corresponds to standard deviation of $26°$. Note that the DoAs of all the incoming waves are changed at every frame timing with following the distributions. In order to evaluate the performance when angular spread of the incoming waves is quite small, we further assume a channel, where the angular spread is zero, as channel model C. Taking account of an indoor environment, we have chosen the Doppler spectrum of flat and the maximum Doppler shift of 150 Hz.

5.5.3 Optimum Threshold Setting

In the beamforming criterion selection algorithm, the proposed system has two thresholds, that is, the threshold of the normalized variation of the estimated channel response Th_{vari} and the DoA Th_{DoA}. In order to determine the thresholds, we evaluate the BER of the proposed system in channel model A and B by computer simulations. In these simulations, the $(\overline{E_s/N_0})$ is set to be 12 dB.
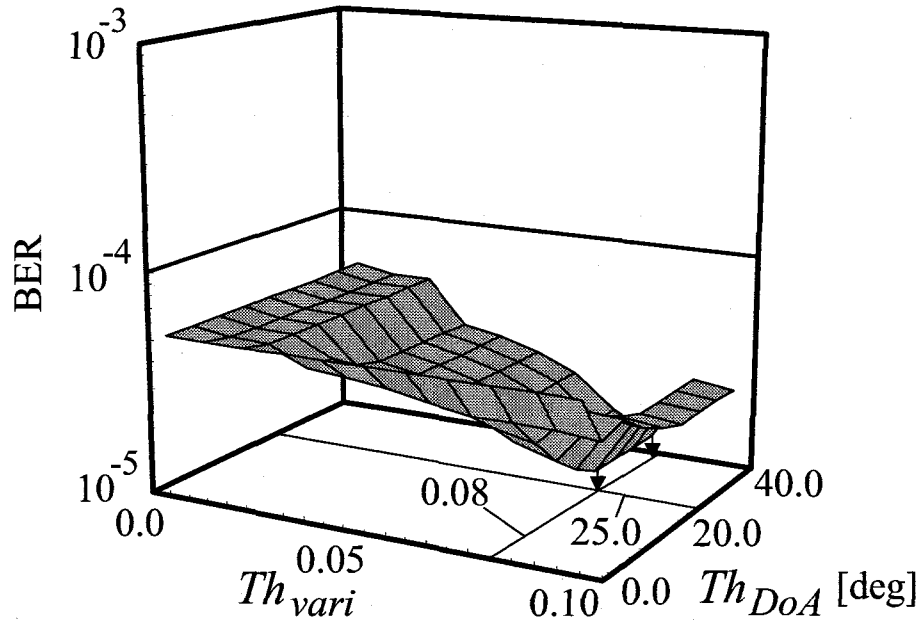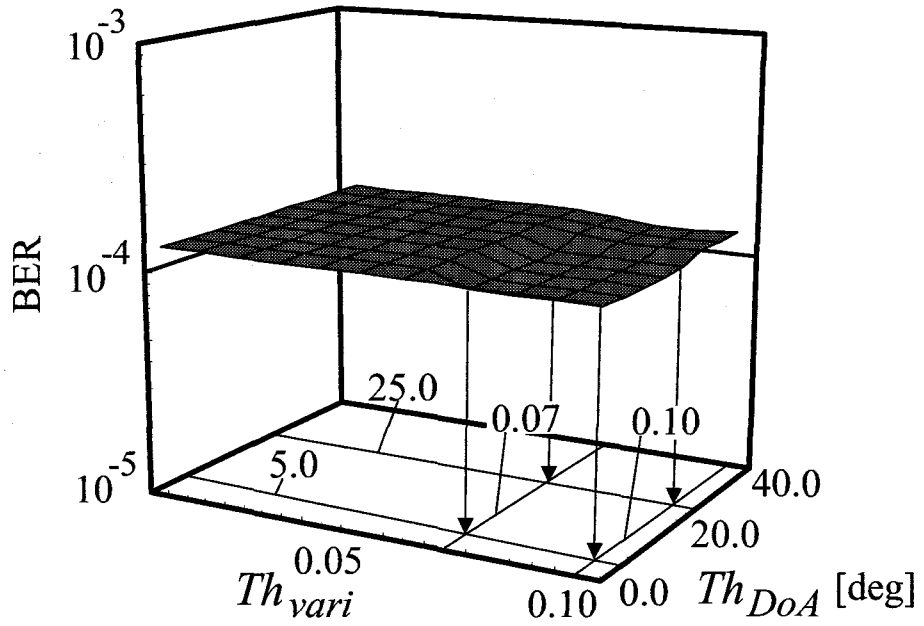
Figs. 5.11 and 5.12 show the BER in channel model A and B, when the thresholds are changed. In both of the channel models, the proposed system can achieve the best performance with the threshold of $Th_{vari} = 0.08$ and $Th_{DoA} = 25.0°$. In all the following simulations, we use the values as the thresholds.

5.5.4 Bit Error Rate Performance

Fig. 5.13 shows the computer simulation results of the BER versus the (E_s/N_0) in an AWGN channel. Also, the theoretical BER in AWGN channel [2], which is given by

$$BER = \frac{1}{2}erfc\left(\sqrt{N_{ary} \cdot \gamma_s/2}\right),\qquad(5.9)$$

where $erfc(\cdot)$ and γ_s denote the complementary error function and E_s/N_0, respectively, is also depicted in the same figure. Since the adaptive antenna array can coherently combine the

Figure 5.11: BER vs. Th_{vari} and Th_{DoA}. (Channel Model A.)

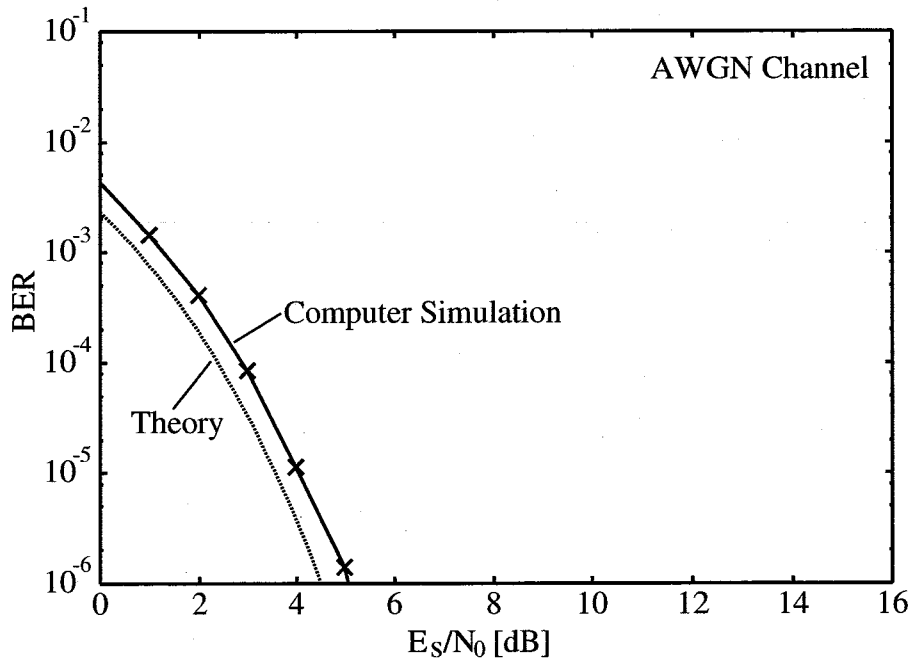Figure 5.12: BER vs. Th_{vari} and Th_{DoA}. (Channel Model B.)

Figure 5.13: BER Performance in AWGN Channel.

received signals, the E_s/N_0 is multiplied by the number of sensors, namely 8. We can recognize about 0.5 dB degradation from the theoretical line. This could be because of the error in the channel impulse response estimation or in the spatial and temporal weights calculation. The effect of the four times over sampling also could be the cause of the degradation.

Figs. 5.14-5.16 show the BER performance of the proposed system in the channel model A, B and C, respectively. For comparison purpose, the performances of the adaptive TDL array with 72 and 24 taps, and the cascade configuration without the proposed path selection algorithm are also plotted in the same figures. In the channel model C, we can show the theoretical lower bound of the BER for the proposed system. This is because the LoS path is always the $Path_{max}$ in the model, and the temporal processing in the proposed equalizer cannot utilize the power of the delayed paths.

In the channel model A, the proposed equalizer can achieve the best performance among the four systems. Especially, the comparison between the BERs of the cascade configuration with and without the path selection algorithm proves that the selection algorithm gives a considerable improvement of the performance to the equalizer. The reason why the performance of the adaptive TDL array with 72 taps is worse than that with 24 taps in the low E_s/N_0 region is that the weights of the adaptive TDL array with 72 taps do not converge well due to large number of the weights.

In the channel model B, the BERs of all the systems are almost the same, however, the inclinations of the BER performance curves of the adaptive TDL arrays are larger than that of the proposed equalizer. The operation of the temporal processing in the adaptive TDL array is capable of the combining diversity, while the temporal processing in the proposed system is essentially the selection diversity, therefore, the adaptive TDL array can achieve larger diversity gain than the proposed system. In the channel model, the adaptive antenna array can cancel
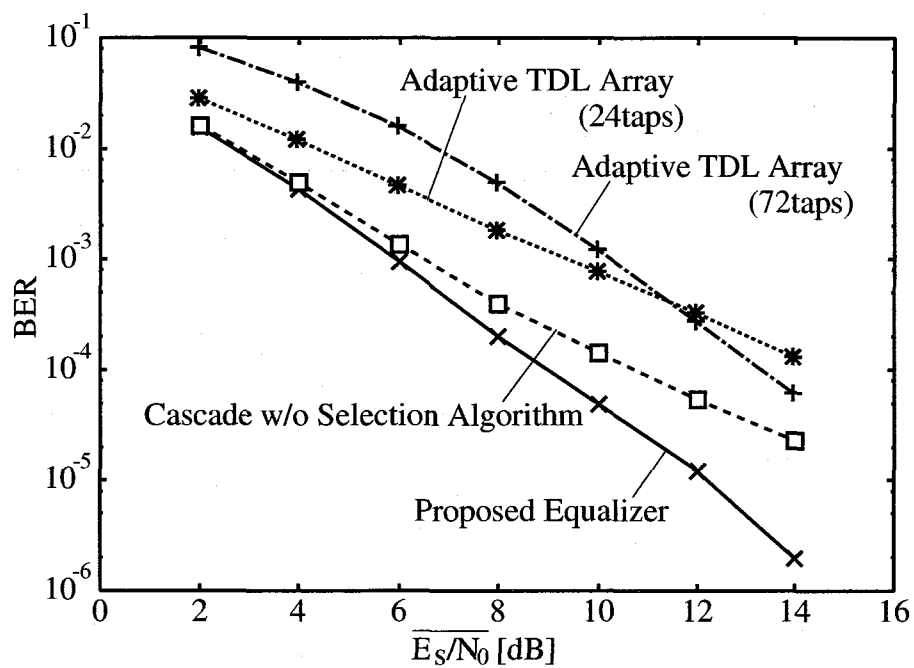
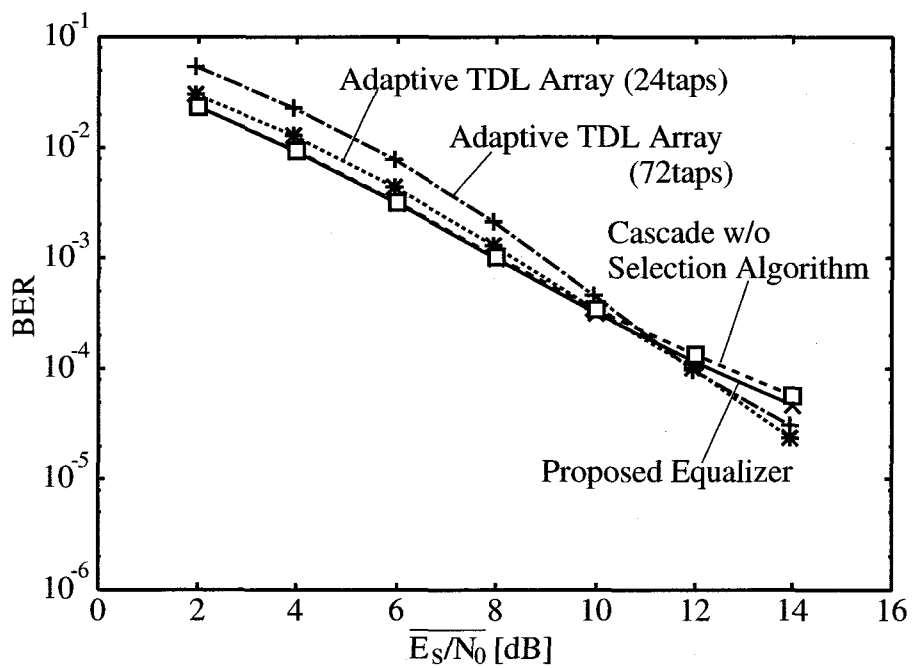Figure 5.14: BER Performance in Channel Model A.

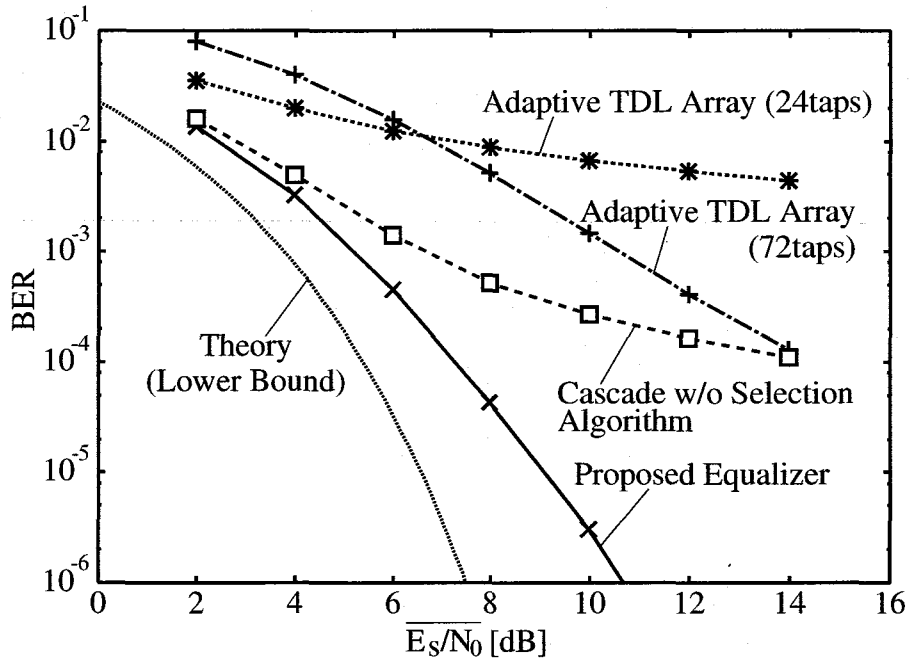Figure 5.15: BER Performance in Channel Model B.
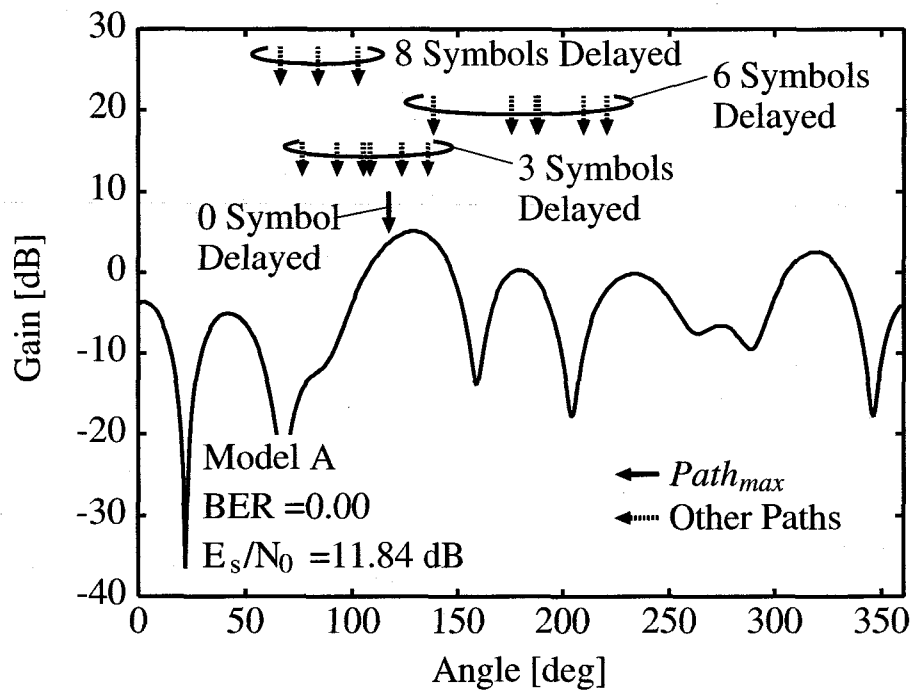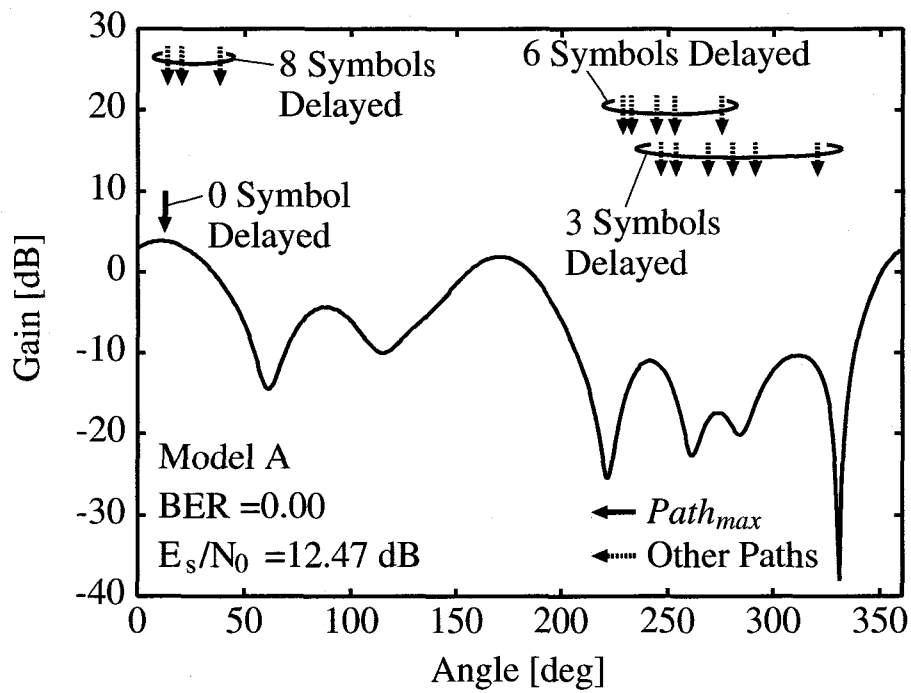
Figure 5.16: BER Performance in Channel Model C.

the undesired paths without suffering from the high sidelobe level, since all the paths have some angular spread. This is the reason for the small difference of the performance between the cascade configuration with and without the selection algorithm.

In the channel model C, the BER performance of the adaptive TDL array with 24taps is the worst among the four systems. This means that the length of temporal filter of 3taps is not enough for the channel, and that even spatial and temporal equalizer, which can utilize both the spatial and temporal information of the received signal, has to employ temporal filter with enough temporal aperture, if the incoming waves have small angular spread. In the BER curve of the cascade configuration without the selection algorithm, we can recognize the BER floor, which is caused by the SNR degradation because of the high sidelobe level. On the other hand, the proposed equalizer can achieve a good performance, though the channel model is severe for the adaptive antenna array. The reason for the degradation from the theoretical lower bound of the BER could be the consumption of the degree-of-freedom of the adaptive antenna array by forming nulls toward the delayed waves, or the Doppler shift.

5.5.5   Antenna Beam Pattern

Here, we analyze the operation of the proposed path selection algorithm from a viewpoint of antenna beam pattern. Figs. 5.17-5.22 respectively show the beam patterns of the proposed system in channel model A, B and C, when the $Path_{max}$ or all the paths around the $Path_{max}$ is (or are) selected for the path to capture. The BERs of the frame are also shown in the same figures.

In Figs. 5.17 and 5.19, though the desired wave (the $Path_{max}$) comes from almost the same direction as the undesired clusters, no bit error occurs with selecting only the $Path_{max}$. This

Figure 5.17: Antenna Beam Pattern in Channel Model A, Path to Capture: $Path_{max}$.

Figure 5.18: Antenna Beam Pattern in Channel Model A, Path to Capture: All the Paths around $Path_{max}$.
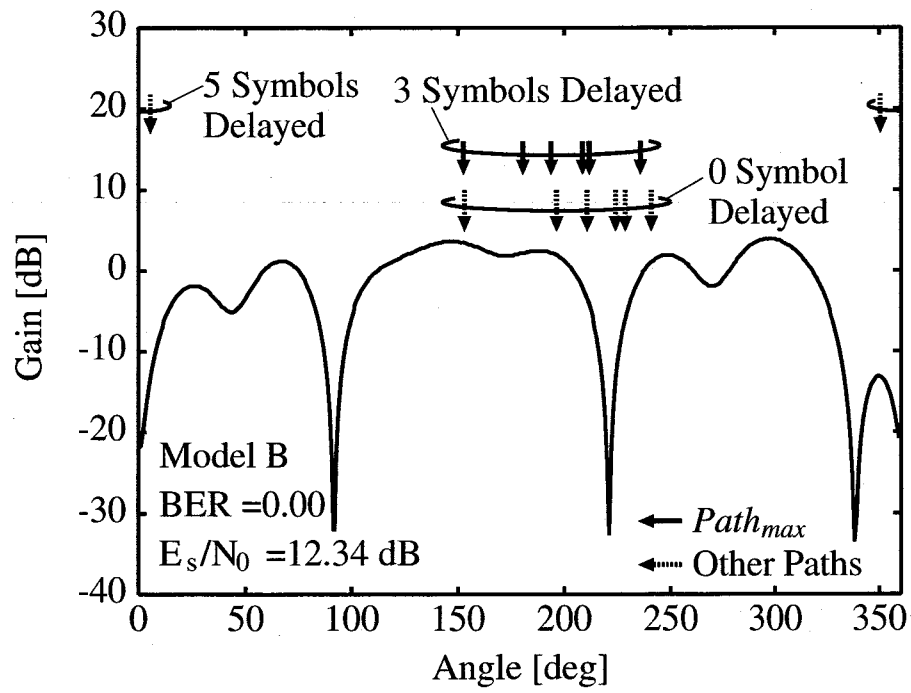
Figure 5.19: Antenna Beam Pattern in Channel Model B, Path to Capture: $Path_{max}$.
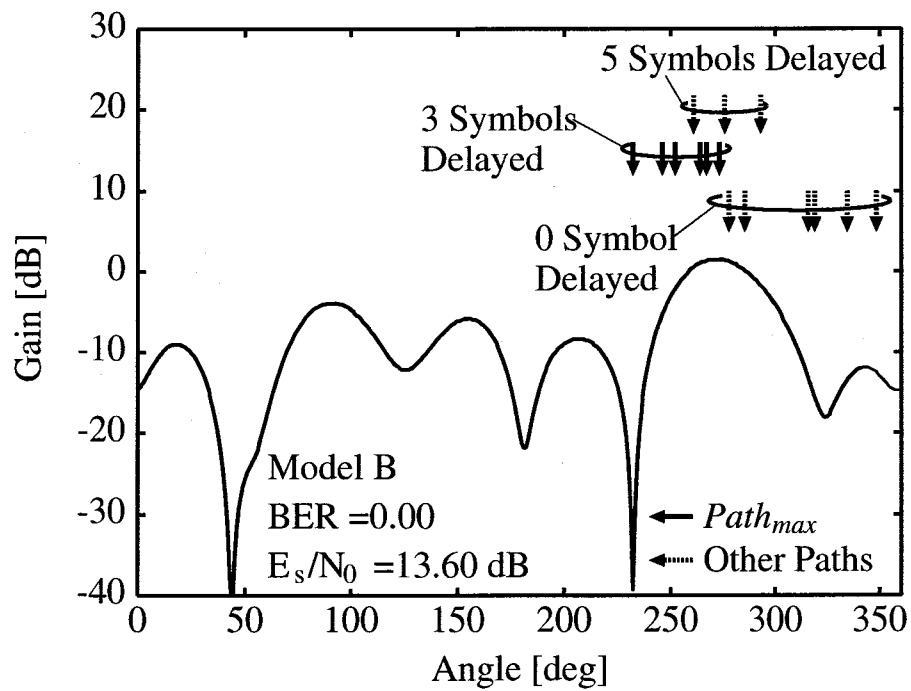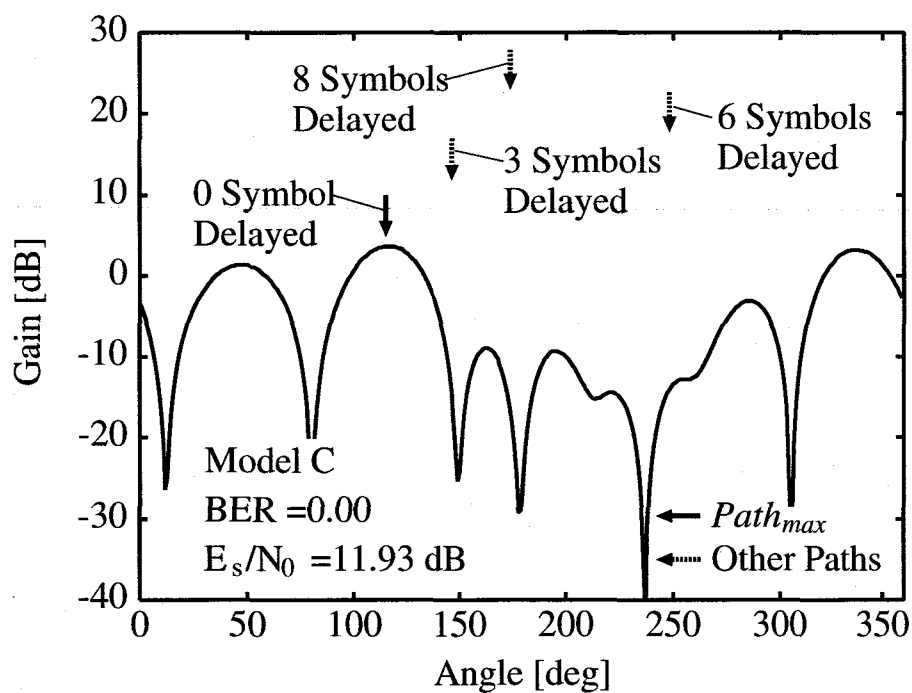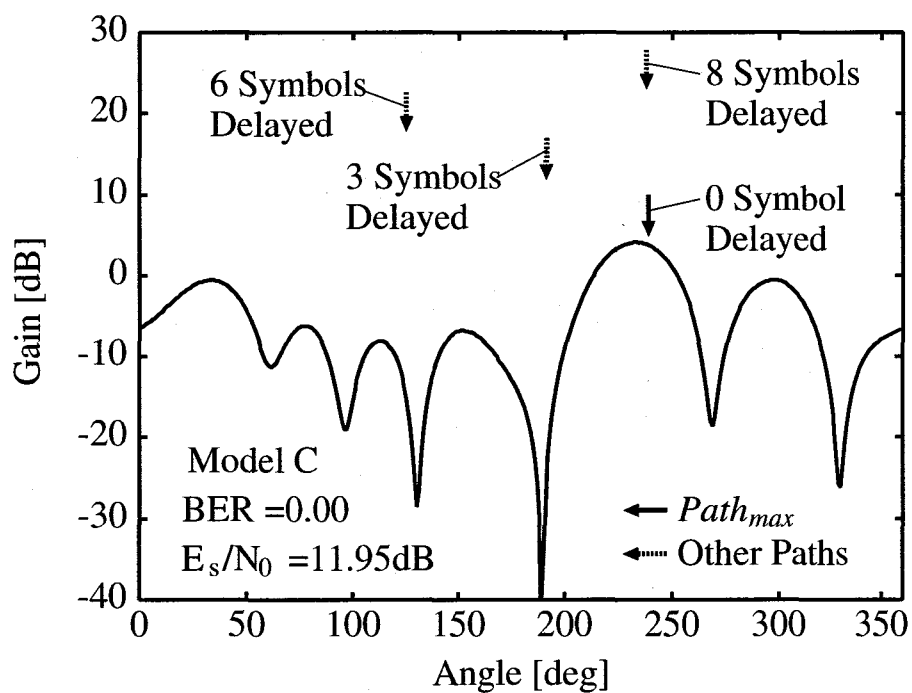

Figure 5.20: Antenna Beam Pattern in Channel Model B, Path to Capture: All the Paths around $Path_{max}$.

Figure 5.21: Antenna Beam Pattern in Channel Model C, Path to Capture: $Path_{max}$.

Figure 5.22: Antenna Beam Pattern in Channel Model C, Path to Capture: All the Paths around $Path_{max}$.

is because, the undesired clusters having large angular spread, the adaptive antenna array can combine the undesired components as to disappear. Moreover, there is no distinct null toward the undesired wave which should be cancelled in Figs. 5.17- 5.20, whereas nulls are steered toward the undesired waves in Figs. 5.21 and 5.22. These results support that the adaptive antenna array operates as a diversity system when the incoming waves have large angular spread. We can also see that the proposed system selects all the paths around the $Path_{max}$ when both the $Path_{max}$ and the ISI paths have small (or no) angular spread and the paths have almost the same DoA.

From all the results, it can be concluded that the proposed equalizer can successfully select a path (or paths) to capture by the adaptive antenna array depending on the channel conditions.

5.5.6 Computational Cost

The signal processing in the proposed system includes "channel estimation", "weights calculation of the adaptive antenna array" and "weights calculation of the DFE" on the pilot signal reception, and "selection of the path to capture" on the data signal reception. However, we exclude the "channel estimation" from the evaluation of the computational cost, since it can be performed by an application specific integrated circuit (ASIC), such as a sliding correlator, parallel with the other digital signal processings. Here, note that the purpose of the computational complexity reduction is not to decrease the power consumption but to make the proposed equalizer realizable with practical digital signal processing devices. Also, the processing of the "selection of the path to capture", which includes the calculation of the $P_{vari}(k)$s and the DoAs, will not be a bottle-neck, since the proposed equalizer have only to finish the processing within the data signal period, which is far longer than pilot signal period. Based on the discussion above, we evaluate a computational cost which is required in one RLS iteration on the pilot signal reception. At present, most DSPs can simultaneously operate multiplications, addition/subtraction, and data transfer between registers [36], therefore, we employ the number of multiplications as an index of the computational cost.

The maximum number of multiplications $C_{proposed}$ of the proposed system is given by

$$C_{proposed} = 7M^2 + 12M + 4MK + 7R^2 + 12R, \qquad (5.10)$$

where M is the number of sensors, R the total weight number of DFE, K the maximum number of paths to capture. Here, in the RLS algorithm, the number of multiplications per one iteration of the system which has totally N weights is given by $7N^2 + 12N$ [36]. On the other hand, the number of multiplications C_{ATDLA} of the adaptive TDL array is obtained by

$$C_{ATDLA} = 7(MR)^2 + 12MR, \qquad (5.11)$$

where M and R denote the number of sensors and the length of the TDL respectively.

Substituting the parameters used in the computer simulation (proposed equalizer:$M = 8$, $R = 17$, $K = 4$, adaptive TDL array:$M = 8$, $R = 9$), we have the number of multiplications shown in table 5.2. The required processing speeds of digital signal processing device are also shown in the table. From the table, we can see that the number of multiplications of the proposed equalizer is fewer than one tenth of that of the adaptive TDL array, and that the proposed equalizer can be realized with the expected processing speed of the DSP in 2010, i.e., 1,000,000 MIPS, while attaining the bit rate of 200 Mbit/sec.

Table 5.2: Number of Multiplications.

	# of Multi. (Normalized)	Required Processing Speed
Proposed Equalizer	2,899 (1)	300,000 MIPS
Adaptive TDL Array	37,152 (12.8)	3700,000 MIPS

MIPS : Million Instructions Per Second

5.6 Summary

In this chapter, we have proposed a versatile spatial and temporal equalization method for various DoA patterns, where the cascade configuration of an adaptive antenna array and a DFE is employed and all of the weights are calculated by an MMSE based adaptive algorithm. In the proposed method, in order to avoid wrong trap by a local minimum, the weights of the adaptive antenna array and the DFE are calculated separately, and the adaptive antenna array selects a path or paths to capture depending on channel conditions. We have shown the BER performance in the three space-time channel models, which are based on measurement reports. Also, the computational complexity of the proposed system is evaluated in terms of the number of multiplications in one RLS iteration. From the results, it can be concluded that the proposed system can achieve good performance in various kinds of channels and be realizable with the expected processing speed of DSP in 2010, while attaining the bit rate of 200 Mbit/sec.

In this chapter, we have assumed only the existence of ISI, however, with a few modifications, the proposed system can achieve CCI cancellation ability (see Appendix B).

Chapter 6

Conclusions

This dissertation has presented spatial and temporal equalization methods for high-speed wireless communications systems, which are based on the study conducted by the author during the doctoral course. The main results obtained in this dissertation are summarized as follows:

1. Fundamentals of array signal processing has been presented by showing three applications of the array processing; DoA estimation, beamforming, and pilot-free channel identification. Array signal processing is defined as a processing of spatially sampled signals. In wireless communications systems, the spatial sampling can be performed by antenna array. Although array signal processing, in other words, spatial signal processing, and conventional temporal signal processing arise in entirely different application areas, there is analogy between them.

2. In order to avoid two-step procedure of weights calculation and to make it easy to extend to a spatial and temporal equalization, we have proposed spatial equalization methods, where the weights of the adaptive antenna array are controlled only by the estimated channel impulse response at each sensor. As for the channel estimation, we have proposed two estimation methods, i.e., a suppressed SS pilot signal assisted method and a pilot-free channel identification method. With the suppressed SS pilot signal, the spatial equalizer can successfully estimate the channel impulse response with sufficient accuracy, and can outperform the conventional spatial equalizer, such as a CMA method. With the pilot-free channel identification method, though the performance is degraded especially when the E_s/N_0 is low, it is clearly shown that the second-order statistics based pilot-free channel identification method is applicable to practical wireless communications systems.

3. A spatial and temporal equalization method with reduced number of weights has been proposed and the performance has been evaluated comparing with that of the spatial equalizer presented in chapter 3. and the DFE. Here, the fundamental criterion is 'delayed incoming signals with large time delays should be canceled by the spatial processing', which makes it possible to decrease the computational complexity. The criterion will not give the spatial and temporal equalizer the best performance, however, if we regard the computational complexity as important, the criterion could be a good choice. In addition, the proposed equalizer uses only estimated channel impulse response to adjust the weights of the spatial and temporal equalizer, therefore, it requires no information on DoA. We

have shown the attainable BER performance in an AWGN channel, a frequency selective fading channel, and a static 3-ray multipath channel. Moreover, we have analyzed the operation of the spatial processing of the proposed system from the viewpoint of antenna patterns. We have also shown the computational complexity in terms of the number of multiplications in the total weight calculation. From all the results obtained here, it can be said that the proposed system can achieve the best and stable performance among the three equalization methods with a low computational complexity.

4. We have proposed a versatile spatial and temporal equalization method for various DoA patterns, where the cascade configuration of an adaptive antenna array and a DFE is employed and all of the weights are calculated by an MMSE based adaptive algorithm. In the method, in order to avoid wrong trap by a local minimum, the weights of the adaptive antenna array and the DFE are calculated separately, and the adaptive antenna array selects a path or paths to capture depending on channel conditions. We have shown the BER performance in the three space-time channel models, which are based on measurement reports. Also, the computational complexity of the proposed system is evaluated in terms of the number of multiplications in one RLS iteration. From the results, we have clearly shown that the proposed equalizer can achieve good performance in various kinds of channels and be realizable with the expected processing speed of DSP in the year 2010, while attaining the bit rate of 200 Mbit/sec. We have assumed only the existence of ISI, however, with a few modifications, the proposed system can achieve CCI cancellation ability.

From all the results, it can be concluded that the proposed equalization methods can realize a high-speed wireless communications system, when the transmission rate will exceed 100 Mbit/sec in 2010.

Appendix A

Autocorrelation Matrix of Filtered Noise

This appendix shows the autocorrelation matrix R_v of additive noise which has passed through the matched filer.

Since $R_v = E[V_n V_n^H]$ (V_n is defined in Eqs. (3.28), (3.32), (3.36)), you can easily verify that the (p,q) component of R_v is $E[v_{p-N\alpha-NL\beta+n-1}^{(\alpha,\beta)} v_{q-N\gamma-NL\delta+n-1}^{(\gamma,\delta)*}]$ where α, β, γ, and δ denote the integer parts of $(p-NL\beta)/N$, $p/(NL)$, $(q-NL\delta)/N$, and $q/(NL)$, respectively. Therefore, I will calculate the value of $E[v_p^{(i,j)} v_q^{(k,l)*}]$.

Let $s_n^{(i,j)} = s_j(t_0 + i\Delta + nT)$ denote the discrete time impulse response of the matched filter which is the length of K symbols and $w_n^{(i)} = w(t_0 + i\Delta + nT)$ additive white noise whose variance is equal to σ^2. Also define

$$
\mathcal{S}_N^{(i)} = \begin{bmatrix} s_0^{(i)} & \cdots & s_M^{(i)} & & 0 \\ & \ddots & & \ddots & \\ 0 & & s_0^{(i)} & \cdots & s_M^{(i)} \end{bmatrix}. \tag{A.1}
$$
$$
(N \times (N + M))
$$

I assume that the additive noise is white at the input of the matched filter. Let $w_j(t_0 + i\Delta + nT)$ denotes the white noise at the $j$the antenna element and $s(t_0 + i\Delta + nT)$ denotes the impulse response of the matched filter. The components of R_v can be calculated as followings:

$$
E[v_p^{(i,j)} v_q^{(k,l)*}]
$$
$$
= E[v_j(t_0 + i\Delta + pT)v_l^*(t_0 + k\Delta + qT)]
$$
$$
= E[\sum_{a=-\infty}^{\infty} w_j(a\Delta)s(t_0 + i\Delta + pT - a\Delta)
$$
$$
\cdot \sum_{b=-\infty}^{\infty} w_l^*(b\Delta)s^*(t_0 + k\Delta + qT - b\Delta)]
$$
$$
= \sum_{a=-\infty}^{\infty} \sum_{b=-\infty}^{\infty} s(t_0 + i\Delta + pT - a\Delta)
$$
$$
\cdot s^*(t_0 + k\Delta + qT - b\Delta)E[w_j(a\Delta)w_l^*(b\Delta)]
$$
$$
= \sigma^2 \sum_{a=-\infty}^{\infty} s(i\Delta + pT - a\Delta)s^*(j\Delta + qT - a\Delta),
$$

81

where σ^2 denotes the variance of white noise. Though it is a matter of course, the components of R_v depends only on the impulse response of matched filter. In general, since we have the knowledge of the matched filter, we can calculate the noise autocorrelation matrix R_v, a prior.

Appendix B

CCI and ISI Cancellation Method

The proposed system in Chapter 5. can operate in the environment, where CCIs exist, with a few modifications. Here, we show how to modify the proposed system in order to cancel both CCIs and ISIs.

In the proposed system, the adaptive antenna array only can eliminate the CCIs, therefore, if a $Path_{max}$ and CCIs, which have small angular spread, are in the same direction, it is impossible to capture the $Path_{max}$ with suppressing the CCIs. This means that the equalizer have to take the CCIs' DoA patterns consideration on determining the path to capture with the adaptive antenna array. Moreover, the adaptive antenna array can not always capture the $Path_{max}$. In order to know the information about the CCIs, such as delay times, DoA patterns, and angular spreads, we modify the frame format as depicted in Fig. B.1. In the figure, the "Configuration 1" shows the frame format employed in the system presented in chapter 5, and the "Configuration 2" the format after the modification for the CCI cancellation. Also, "Pilot Signal 1" is a common pilot signal among users, and "Pilot Signal 2" is a unique pilot signal to the users. Using the "Pilot Signal 1", the equalizer can estimate the channel impulse response, which includes both the desired waves (with ISIs) and the CCIs, and utilizing the "Pilot Signal 2", it can have the response without the CCIs likewise. (The "Pilot Signal 2" is also used for the weights calculation by RLS algorithm.) With the additional channel information about the CCIs, the proposed equalizer determine the time k_max, which appeared in the path selection algorithm presented in chapter 5, as shown in Fig. B.2 before executing the algorithm.

The equalizer first calculates the angular spreads of the CCIs. If they all exceed a threshold,

Configuration 1: | Pilot Signal | Data Signal |

⇩ Modification

Configuration 2: | Pilot Signal 1 | Pilot Signal 2 | Data Signal |

Unique Pilot Signal
Common Pilot Signal

Figure B.1: Modified Frame Format.

83

Figure B.2: Determination of Time k_{max}.

the equalizer set the delay time of the $Path_{max}$ to be the k_{max}. Otherwise, the equalizer searches angular spreads of the desired paths and differences of DoAs between the desired paths and the CCIs in descending order of the power of the desired paths. The time of the path, which first satisfies a condition that the angular spread is large or that the angular spread is small and the difference of the DoAs is large, is chosen for the time k_{max}. After the determination of the k_{max}, the path selection algorithm is executed to determine the path to capture.

In this way, the proposed equalizer can cancel both the ISIs and the CCIs in principle.

Abbreviations

ASIC	application specific integrated circuit
AWGN	additive white Gaussian noise
A/D	analog-to-digital
BER	bit error rate
BPF	band pass filter
CCI	co-channel interference
CMA	constant modulus algorithm
CNR	carrier to noise power ratio
DFE	decision feedback equalizer
DoA	direction of arrival
DPS	delay power spectrum
DSL	digital subscriber line
DSP	digital signal processor
E_s/N_0	the ratio of the energy per symbol to the noise power density
FB	feed-back
FF	feed-forward
FFT	fast Fourier transform
FIR	finite impulse response
FTTH	Fiber to the Home
HOS	higher-order statistics
IF	intermediate frequency
ISI	inter-symbol interference
IT	information and communication technology
I-ch	inphase channel
LAN	local area network
LMS	least mean square
LoS	line-of-sight
LPF	low pass filter
MIPS	million instructions per second
MLSE	maximum likelihood sequence estimation
MMSE	minimum mean-squared-error
M-	maximum length shift resister
OFDM	orthogonal frequency division multiplexing

PAM	pulse amplitude modulation
PC	personal computer
PN	pseudo noise
QPSK	quadrature phase shift keying
Q-ch	quadrature channel
RF	radio frequency
RLS	recursive least square
RMSE	root mean-squared-error
SIMO	single-input multiple-output
SISO	single-input single-output
SNR	signal to noise power ratio
SS	spread spectrum
TDL	tapped-delay-line

Bibliography

[1] Ministry of Public Management, Home Affairs, Posts and Telecommunications, Japan, *2001 WHITE PAPER Information and Communications in Japan*, (2001).

[2] J. G. Proakis, *Digital Communications, Third Edition*, McGraw-Hill (1995).

[3] S. Guerin, "Indoor Wideband and Narrowband Propagation Measurements around 60.5 GHz in an Empty and Furnished Room," in *proc. VTC'96*, pp. 160-164. (Apr. 1996).

[4] H. Xu, V. Kukshya, T. S. Rappaport, "Spatial and Temporal Characterization of 60 GHz Indoor Channels," in *proc. VTC2000*, vol. 1, pp. 6-13, (Sept. 2000).

[5] R. Prasad and B. C. van Lieshout, "Cochannel Interference Probability for Micro- and Picocellular Systems at 60 GHz," *Electronics Letters*, pp. 1909-1910, (Oct. 1993).

[6] B. D. Van Veen and K. M. Buckley, "Beamforming: A Versatile Approach to Spatial Filtering," *IEEE ASSP Magazine*, pp. 4-24 (Apr. 1988).

[7] S. Haykin, *Adaptive Filter Theory, Second Edition*, Prentice Hall (1991).

[8] S. J. Orfanidis, *Optimum Signal Processing: An Introduction, Second Edition*, McGraw-Hill (1988).

[9] R. Roy and T. Kailath, "ESPRIT-Estimation of Signal Parameters Via Rotational Invariance Techniques," *IEEE Trans. Acoust., Speech, and Signal Processing*, vol. 37, No. 7, pp. 984-995, (July 1989).

[10] R. O. Schmidt, "Multiple Emitter Location and Signal Parameter Estimation," *IEEE Trans. Antennas and Propagation*, vol.AP-34, No. 3, pp. 276-280, (Mar. 1986).

[11] G. Xu and T. Kailath, "Direction-of-Arrival Estimation via Exploitation of Cyclostationarity -A Combination of Temporal and Spatial Processing," *IEEE Trans. Signal Processing*, vol.40, No. 7, pp. 1775-1786, (July 1992).

[12] T. J. Shan, M. wax, and T. Kailath, "On Spatial Smoothing for Direction-of-Arrival Estimation of Coherent Signals," *IEEE Trans. Acoust., Speech, and Signal Processing*, vol.ASSP-33, No. 4, pp. 806-811, (Aug. 1985).

[13] W. A. Gardner, "Simplification of MUSIC and ESPRIT by Exploitation of Cyclostationarity," *Proc. of IEEE*, vol.76, No. 7, pp. 845-847, (July 1988).

[14] A. van der Veen, M. C. Vanderveen, and A. Paulraj, "Joint Angle and Delay Estimation Using Shift-Invariance Techniques," *IEEE trans. Signal Processing*, vol.46, No. 2, pp. 405-418, (Feb. 1998).

[15] A. V. Oppenheim, R. W. Schafer, and J. R. Buck, *Discrete-Time Signal Processing, Second Edition*, Prentice Hall (1999).

[16] R. T. Compton, Jr., *Adaptive Antennas Concepts and Performance*, Prentice Hall (1988).

[17] S. P. Applebaum, "Adaptive Arrays," *IEEE Trans. Antenna and Propagation*, pp. 585-598 (Sept. 1976).

[18] H. Krim and M. Viberg, "Two Decades of Array Signal Processing Research," *IEEE Signal Processing Magazine*, pp. 67-94 (July 1996).

[19] S. Haykin, J. P. Reilly, V.Kezys, and E.Vertatschitsch, "Some Aspects of Array Signal Processing," *IEE Proc.*, pp. 1-26 (Feb. 1992).

[20] S. Haykin, *Adaptive Filter Theory, Third Edition*, Prentice Hall (1996).

[21] L. Tong, and S. Perreau, "Multichannel Blind Identification: from Subspace to Maximum Likelihood Method," *Proc. IEEE*, vol. 86, no. 10, pp. 1951-1968 (Oct. 1998).

[22] Y. Sato, "Two Extensional Applications of the Zero-Forcing Equalization Method," *IEEE Trans. Commun.*, vol.COM-23, pp. 684-687, (1975).

[23] L.Tong, G.Xu, and T.Kailath, "Blind Channel Identification Based on Second-Order Statistics : A Time Domain Approach," *IEEE Trans. Inform. Theory*, vol.41, pp. 340-349, (Mar. 1994).

[24] L.Tong, G.Xu, B.Hassibi,and T.Kailath, "Blind Channel Identification Based on Second-Order Statistics : A Frequency Domain Approach," *IEEE Trans. Inform. Theory*, vol.40, pp. 340-349, (Mar. 1994).

[25] W. Gardner, *Cyclostationarity in Communications and Signal Processing*, IEEE Press, (1993).

[26] E.Moulines, P.Duhamel, J.F.Cardoso, and S.Mayrargue, "Subspace Methods for the Blind Identification of Multichannel FIR Filters," *IEEE Trans. Signal Processing*, vol.43, pp. 516-525, (Feb. 1995).

[27] G.Xu, H.Liu, L.Tong, and T.Kailath, "A Least Squares Approach to Blind Channel Identification," *IEEE Trans. Signal Processing*, vol.43, pp. 2982-2993, (Dec. 1995).

[28] H.Zeng, and L.Tong, "Connections between the Least-Squares and Subspace Approaches to Blind Channel Estimation," *IEEE Trans. Signal Processing*, vol.44, pp. 1593-1596, (June 1996).

[29] K.Abed-Meraim, E.Moulines, and P.Loubaton, "Prediction Error Method for Second-Order Blind Identification," *IEEE Trans. Signal Processing*, vol.45, pp. 694-705, (Mar. 1997).

[30] L.Tong, Q.Zhao, "Joint Order Detection and Blind Channel Estimation by Least Squares Smoothing," *IEEE Trans. Signal Processing*, vol.47, pp. 2345-2355, (Sept. 1999).

[31] A.P.Liavas, P.A.Regalia, and J.P.Delmas, "Blind Channel Approximation : Effective Channel Order Determination," *IEEE Trans. Signal Processing*, vol.47, pp. 3336-3344, (Dec. 1999).

[32] A. V. Oppenheim and R. W. Schafer, *Digital Signal Processing*, Prentice Hall (1975).

[33] T. Kailath, *Linear Systems*, Prentice Hall (1980).

[34] K. Hayashi, N. Murashima, S. Hara, S. Sampei, and N. Morinaga, "A Beamforming Method Using Suppressed Pilot Signal," *IEICE Trans. Commun.*, vol.J81-B-I no.11, pp. 661-670 (Nov. 1998).

[35] K. Hayashi and S. Hara, "A New Beamforming Method Using Second Order Statistics-Based Blind Channel Identification," *in proc. WPMC*, pp. 364-369 (Nov. 1998).

[36] S. Sampei, Applications of Digital Wireless Technologies to Global Wireless Communications, Prentice Hall, (1997).

[37] J. R. Treichler and B. G. Agee, "A New Approach to Multipath Correction of Constant Modulus Signals," *IEEE Trans. Acoust., Speech, and Signal Processing*, vol.ASSP-31, pp. 459-472 (Apr. 1983).

[38] A. A. M. Saleh and R. A. Valenzuela, "A Statistical Model for Indoor Multipath Propagation," *IEEE J. Selct. Areas Commun.*, vol.SAC-5, no. 2, pp. 128-137 (Feb. 1987).

[39] G. H. Golub and C. F. V. Loan, *Matrix Computations, Third Edition*, Johns Hopkins (1996).

[40] R. Kohono, "Spatial and Temporal Communication Theory Using Adaptive Antenna Array," *IEEE Personal Communications*, pp. 28-35 (Feb. 1988).

[41] A. J. Paulraj and B. C. Ng, "Space-Time Modems for Wireless Personal Communications," *IEEE Personal Communications*, pp. 36-49 (Feb. 1988).

[42] G. E. Bottomley and K. Jamal, "Adaptive Arrays and MLSE Equalization," *Proc. VTC*, vol. 1, pp.50-54, (July 1995).

[43] S. N. Diggavi and A. Paulraj, "Performance of Multisensor Adaptive MLSE in Fading Channels," *Proc. VTC*, vol. 3, pp.2148-52, (May 1997).

[44] Y. Doi, T. Ohgane, and E. Ogawa, "ISI and CCI Canceller Combining the Adaptive Array Antennas and the Viterbi Equalizer in a Digital Mobile Radio," *Proc. VTC*, pp.81-85, (Apr. 1996).

[45] B. C. Ng, J. T. Chen, and A. Paulraj, "Space-Time Processing for Fast Fading Channels with Co-Channel Interference," *Proc. VTC*, pp.1491-95, (Apr. 1996).

[46] I. Yoshii and R. Kohno, "Adaptive Spatial and Temporal Optimal Receiver Using Adaptive Array Antenna," *IEICE Trans. Commun.*, vol. J82-A, no. 6, pp. 885-892, (June 1999).

[47] K. Fukawa, "Spatio-Temporal Equalization in High Speed Digital Mobile Communications -A Cascading Connection of Adaptive Array and MLSE for Combining of Long Delay Components-," *Proc. 1997 IEICE Autumn Conference*, B-5-52, (Sept. 1997).

[48] Y. Saito, K. Kitagawa, S. Futagi, and M. Uesugi, "A Study of a Split Channel Estimation Scheme for the Spatial and Temporal Equalizer," *Technical Report of the IEICE*, RCS99-183, pp.25-30, (Jan. 2000).

[49] S. Tomisato, N. Miki, and T. Matsumoto, "Signal Transmission Performance of a Joint Spatial and Temporal Equalizer using Separated Spatial and Temporal Signal Processing for Mobile Radio Communications," *Technical Report of the IEICE*, RCS2000-2, pp.7-12, (Apr. 2000).

[50] M. L. Leou, C. C. Yeh, H. J. Li, "A Novel Hybrid of Adaptive Array and Equalizer for Mobile Communications," *IEEE Trans. Veh. Technol.*, vol. 49, No. 1, pp.1-10, (Jan. 2000).

[51] P. Balaban, and J. Salz, "Dual Diversity Combining and Equalization in Digital Cellular Mobile Radio," *IEEE Trans. Veh. Technol.*, vol. 40, no. 2, pp.342-354, (May 1991).

[52] K. Hayashi and S. Hara, "A New Spatio-Temporal Equalization Method without DoA Information," *proc. PIMRC'99*, pp. 780-784, (Sept. 1999).

[53] K. Hayashi and S. Hara, "A New Spatio-Temporal Equalization Method Based on Estimated Channel Impulse Response," *IEEE Trans. Veh. Technol.*, vol. 50, pp. 1250-1259, (Sept. 2001).

[54] K. Hayashi and S. Hara, "A New Spatio-Temporal Equalization Method Using Estimated Channel Impulse Response," *proc. VTC2000*, vol. 3, pp. 2477-2481, (May 2000).

[55] K. Hayashi and S. Hara, "An Adaptive Spatio-Temporal Equalization Method Based on Estimated Channel Impulse Response," *Proc. 2000 IEICE Autumn Conference*, B-5-52, (Sept. 2000).

[56] K. Hayashi and S. Hara, "A Spatio-Temporal Equalization Method Based on Estimated Channel Impulse Response," *Technical Report of the IEICE*, RCS2000-253, pp.55-62, (Mar. 2001).

[57] K. Hayashi and S. Hara, "A Spatio-Temporal Equalization Method for Indoor Wireless LAN System," *Proc. 2001 IEICE Spring Conference*, B-5-243, (Mar. 2001).

[58] K. Hayashi and S. Hara, "A Spatio-Temporal Equalization Method for 60 GHz Indoor Wireless Local Area Networks," in *proc. PIMRC2001*, (Sept. 2001).

[59] K. Hayashi and S. Hara, "A Spatio-Temporal Equalization Method for Indoor Wireless LANs with Beamforming Criterion Selection," *proc. VTC2001 Fall*, (Oct. 2001).

[60] K. Hayashi and S. Hara, "A Spatio-Temporal Equalization Method Using an Adaptive Antenna Array and a Decision Feedback Equalizer," *Technical Report of the IEICE*, RCS2001-138, pp.57-62, (Oct. 2001).

[61] K. Hayashi and S. Hara, "A Spatio-Temporal Equalization Method with Cascade Configuration of an Adaptive Antenna Array and a Decision Feedback Equalizer," *IEICE Trans. Commun.*, Accepted for publication.

[62] P. F. M. Smulders, *Broadband Wireless LANs: A Feasibility Study,* Ph.D. Thesis, Eindhoven University of Technology, Eindhoven, The Netherlands, (1995).

[63] Q. H. Spencer, B. D. Jeffs, M. A. Jensen, and A. L. Swindlehurst, "Modeling the Statistical Time and Angle of Arrival Characteristics of an Indoor Multipath Channel," *IEEE J. Select. Areas Commun.*, vol. 3, pp. 347-360, (Mar. 2000).

List of Publications by the Author

1. Papers

   (a) Kazunori Hayashi, Nobuyuki Murashima, Shinsuke Hara, Seiichi Sampei, and Norihiko Morinaga, "A Beamforming Method Using Suppressed Pilot Signal," *IEICE Transactions on Communication*, Vol. J81-B-I, No.11, pp661-670, (Nov. 1998). (in Japanese)

   (b) Kazunori Hayashi and Shinsuke Hara, "A New Spatio-Temporal Equalization Method Based on Estimated Channel Response," *IEEE Transactions on Vehicular Technology*, Vol. 50, pp. 1250-1259, (Sept. 2001).

   (c) Kazunori Hayashi, and Shinsuke Hara, "A Spatio-Temporal Equalization Method with Cascade Configuration of an Adaptive Antenna Array and a Decision Feedback Equalizer," *IEICE Transactions on Communication*, (Accepted for Publication).

2. International Conferences

   (a) Kazunori Hayashi and Shinsuke Hara, "A New Beamforming Method Using Second Order Statistics-Based Blind Channel Identification," *Proceedings of the First International Symposium on Wireless Personal Multimedia Communications (WPMC'98)* , pp. 364-369, Yokosuka, Japan, (Nov. 1998).

   (b) Kazunori Hayashi and Shinsuke Hara, "A New Spatio-Temporal Equalization Method without DoA Information," *Proceedings of the 10th International Symposium on Personal, Indoor and Mobile Radio Communications (PIMRC'99)*, pp. 780-784, Osaka, Japan, (Sept. 1999).

   (c) Kazunori Hayashi and Shinsuke Hara, "A New Spatio-Temporal Equalization Method Using Estimated Channel Impulse Response," *Proceedings of IEEE Vehicular Technology Conference (VTC) 2000-Spring*, vol. 3, pp.2477-2481, Tokyo, Japan, (May 2000).

   (d) Toyokazu Kitano, Kazunori Hayashi, Hitoshi Masutani and Shinsuke Hara, "Hardware Design of Filter Bank-Based Narrowband/Wideband Interference Canceller for Overlaid TDMA/CDMA Systems," *Proceedings of IEEE Vehicular Technology Conference (VTC) 2000-Spring*, pp.1095-1099, Tokyo, Japan, (May 2000).

   (e) Kazunori Hayashi and Shinsuke Hara, "A Spatio-Temporal Equalization Method with Beamforming Criterion Selectability," *Proceedings of the 7th Asia-Pacific Conference on Communications(APCC 2001)*, pp. 364-367, Tokyo, Japan (Sept. 2001).

93

(f) Kazunori Hayashi and Shinsuke Hara, "A Spatio-Temporal Equalization Method for 60 GHz Indoor Wireless Local Area Networks," *Proceedings of the 12th International Symposium on Personal, Indoor and Mobile Radio Communications*, D4-4, San Diego, USA, (Sept. 2001).

(g) Kazunori Hayashi and Shinsuke Hara, "A Spatio-Temporal Equalization Method for Indoor Wireless LANs with Beamforming Criterion Selection," *Proceedings of IEEE Vehicular Technology Conference (VTC2001-Fall)*, pp.506-510, Atlantic City, USA, (Oct. 2001).

3. Domestic Conferences

(a) Kazunori Hayashi and Shinsuke Hara, "An Adaptive Spatio-Temporal Equalization Method Based on Estimated Channel Impulse Response," *Proceedings of the 2000 IEICE Autumn Conference*, B-5-52 (Sept. 2000).

(b) Kazunori Hayashi, and Shinsuke Hara, "A Spatio-Temporal Equalization Method for 60 GHz Wireless Local Area Networks," *Technical Report of the IEICE*, RCS2000-253, (Mar. 2001).

(c) Kazunori Hayashi, and Shinsuke Hara, "A Spatio-Temporal Equalization Method for Indoor Wireless LAN System", *Proceedings of the 2001 IEICE Sprint Conference*, B-5-243 (Mar. 2001).

(d) Kazunori Hayashi, and Shinsuke Hara, "A Spatio-Temporal Equalization Method Using an Adaptive Antenna Array and a Decision Feedback Equalizer," *Technical Report of the IEICE*, RCS2001-138, (Oct. 2001).